6-2005

Characterization of a Rotary Flat Tail as a Spoiler and Parametric Analysis of Improving Directional Stability in a Portable UAV

Troy A. Leveron

CHARACTERIZATION OF A ROTARY FLAT TAIL AS A SPOILER AND PARAMETRIC ANALYSIS OF IMPROVING DIRECTIONAL STABILITY IN A PORTABLE UAV

THESIS

Troy A Leveron, Ensign, USNR
AFIT/GAE/ENY/05-J06

DEPARTMENT OF THE AIR FORCE
AIR UNIVERSITY

AIR FORCE INSTITUTE OF TECHNOLOGY

Wright-Patterson Air Force Base, Ohio

AFIT/GAE/ENY/05-J06

CHARACTERIZATION OF A ROTARY FLAT TAIL AS A SPOILER AND PARAMETRIC ANALYSIS OF IMPROVING DIRECTIONAL STABILITY IN A PORTABLE UAV

THESIS

Presented to the Faculty

Department of Aeronautics and Astronautics

Graduate School of Engineering and Management

Air Force Institute of Technology

Air University

Air Education and Training Command

In Partial Fulfillment of the Requirements for the

Degree of Master of Science in Aeronautical Engineering

Troy A. Leveron, B.S.N.A.

Ensign, USNR

May 2005

AFIT/GAE/ENY/05-J06

CHARACTERIZATION OF A ROTARY FLAT TAIL AS A SPOILER AND PARAMETRIC ANALYSIS OF IMPROVING DIRECTIONAL STABILITY IN A PORTABLE UAV

Troy A. Leveron, B.S.N.A.
Ensign, USNR

Approved:

_____	_____
Prof. Mark F. Reeder (Chairman)	date
_____	_____
Lt. Col. Raymond Maple (Member)	date
_____	_____
Prof. Ralph Anthenien (Member)	date

AFIT/GAE/ENY/05-J06

Abstract

The United States Air Force Research Lab, Munitions Directorate, Flight Vehicles, Integration Branch (AFRL/MNAV), has developed a flexible wing micro air vehicle (MAV) to be used with special tactics groups. In keeping with the requirement that this MAV be compact, previous research developed a rotatable tail mechanism which resulted in tail movement similar to that of a bird's tail. In this study the design of this tail was modified to produce a more storable vehicle. The redesign also allowed the tail to deflect upward to large angles, enabling the tail to be used as a spoiler. The aerodynamic affects of adding a vertical stabilizer mechanism to improve the stability of the vehicle and rotatable tail combination was also quantified. Data from these tests confirmed the tail is a plausible method to reduce lift and increase drag, consistent with proper spoiler function. A wide range of angles were used to demonstrate that forces and moments from the flat tail were similar to those of traditional rudder. Directional stability was improved by the stabilizer, and recommendations for further improvements are given.

Acknowledgements

I would first like to express my gratitude to all my instructors past and present. I hope that I have accomplished at least a meager effort in demonstrating the volumes of knowledge you have imparted upon me.

My advisor, Dr. Mark Reeder, deserves great credit. His knowledge, guidance, and enthusiasm furthered my education as well as kept me interested in this research. Under his tutelage I was able to finally bring together the subjects in which I studied at AFIT. For his time and efforts, I am extremely grateful.

Mr. Dwight Gehring did an excellent job setting up and operating the wind tunnel for my research. Without his efforts this thesis would have been impossible.

My parents, who taught me the value of hard work and perseverance, your lessons will always be with me. You were there when I felt there was no light at the end of the tunnel. Your patient listening allowed me to work towards solutions for myself.

Lastly, I wish to thank my Lord God. With out his love and constant intervention I would not be present today.

Troy Andre Leveron

Table of Contents

List of Figures

94.

List of Tables

Table Page

List of Symbols

A	Axial Force (Body Axis)
Y	Side Force (Body Axis)
N	Normal Force (Body Axis)
D	Drag Force (Wind Axis)
S	Side Force (Wind Axis)
L	Lift Force (Wind Axis)
N_1 & N_2	Balance Normal Sensors
S_1 & S_2	Balance Side Sensors
A_1	Balance Axial Sensor
ℓ_1	Balance Roll Moment Sensor
AR	Aspect Ratio
S	Wing Area
C	Wing Root Chord
$\bar{c}$	Wing Mean Chord
Re_c	Reynolds Number at the Chord
L/D	Lift-to-Drag Ratio
M	Mach Number
R	Ideal Gas Constant
CG	Center of Gravity
M.A.C.	Mean Aerodynamic Center
MAV	Micro-Air-Vehicle
2b	Wing Span
$q\infty$	Far Field Dynamic Pressure
$U\infty$	Far Field Velocity
a	Speed of Sound
ℓ	Roll Moment
m	Pitch Moment
n	Yaw Moment
ρ	Air Density
μ	Air Viscosity
α	Angle of Attack ($\alpha = \theta$)
α_{Stall}	Angle of Wing Stall
β	Sideslip Angle
ψ	Yaw Angle ($\psi = -\beta$)
Γ	Wing Dihedral Angle
Φ	Wing Roll Angle
δ_e	Elevon Deflection Angle
δ_r	Rudder Deflection Angle
δ_{rn}	Rotation Angle of Tail
C_L	Lift Coefficient
C_Y	Side Force Coefficient
C_D	Drag Force Coefficient
C_l	Roll Moment Coefficient
C_m	Pitch Moment Coefficient

C_{n}	Yaw Moment Coefficient
$C_{m\alpha}$	Longitudinal Stability Derivative
$C_{n\beta}$	Directional Stability Derivative
$C_{\ell\beta}$	Roll Stability Derivative
lb_f	Pounds Force
lb_m	Pounds Mass
″	Inches
′	Feet
°	Degrees (360° = 2π radians)

CHARACTERIZATION OF A ROTARY FLAT TAIL AS A SPOILER AND PARAMETRIC ANALYSIS OF IMPROVING DIRECTIONAL STABILITY IN A PORTABLE UAV

I. Introduction

Background

In today's ever changing battlefields enemies are using more unconventional means of attack and evasion. This can be seen most clearly in the current global war on terrorism. Increasingly unorthodox approaches must be developed to seek out, monitor, and attack these enemies.

The United States Armed Forces currently employs the Predator and Global Hawk for its long range reconnaissance work. The U.S. also is developing and using smaller UAVs (Unmanned Aerial Vehicles) to fill the need for reconnaissance and battle damage assessment on the company or platoon level (Parga, 2004: 3). The current UAVs for this type of work are: Desert Hawk, Shadow and Dragon Eye. Room does exist for improvements in size and portability of these UAVs.

The United States Air Force Research Lab, Munitions Directorate, Flight Vehicles, Integration Branch (AFRL/MNAV) has produced a flexible wing, portable UAV to study and develop a better, smaller unit UAV for the war on terrorism. This vehicle was studied by Captain DeLuca and Lt. Rivera Parga in their theses. The focus of this study is to build upon the "bird like", flat, rotating tail described by Lt. Rivera Parga. The influence of avian research is not limited to only Lt. Parga's work; this research may

prove to be beneficial to the development of future UAVs. Birds demonstrate considerable tail muscle control, which gives them considerably more degrees of freedom than the two degrees used in this and previous studies.

Today, avian flight is used to improve the understanding of flight. Avian tails are being researched to find different manners to control flight and improve upon current tail designs. Studies conducted by R.G. Hoey and then A. L. Thomas suggest several possibilities of how birds use their tails and how this may develop into use by humans. Their research has uncovered several manners of which birds use their tails.

However, "The study of bird tails is very polarized. One camp of theorists emphasizes the importance of ordinary physics, and the other camp points to the extraordinary tails of male peacocks and barn swallows as examples of sexy fashions overpowering sensible aerodynamics" (Rayner; 1988).

Examples that the researchers who favor the use of bird's tails for control offer strike a resemblance to the use of tails on aircraft. For instance, one author (Horton-Smith in a 1938 text, The Flight of Birds, page 38) states: "A bird, like an airplane, uses rotation of wing and tail. There is no vertical fin in the bird's tail so it has to rely on banking. It is possible that a long tail, when bent to one side, may function as a rudder". Additionally, John H. Storer comments: "The tail of a bird, indeed, has many uses. It can steer in any direction, act as a brake, form a slot behind the wings, or become a part of the bird's lifting surface, supplementing the wings. The swallow-tailed kite twists its tail to steer. It may turn its tail so that either the upper or the lower surfaces will strike the air stream in steering. The sides of the tail may be controlled separately."

Opposing theorists offer: ""The tail of birds virtually has no stabilizing effect. It is, hence not a stabilizing instrument. Only to a limited extent is it used as a steering device. Mostly it is used at low speed as a landing flap" (Nickel & Wohlfahrt, 1994: 25). These same theorists state that a bird achieves stability by varying lift generated by each wing, through flexure, changing angle of attack independently, and sweep. Warrick et al. sum the debate of avian tail use best with the following statement: "Beyond its theoretical capabilities, the precise use of the tail in flying birds has not been thoroughly documented."

However, Warrick et al. then go on to present a histogram, Figure 1, of occurrences of tail elevation, twist, depression, combined twist and depression, and no tail manipulation for a swallow during a series of videotaped prey-capture maneuvers. Though the data is limited to a few hundred maneuvering observations, the data suggests that tail elevation (pitch up) is used only to increase drag in order to stall the flight and initiate a dive. Furthermore, the most common tail orientation during a level turn was a combined tail depression and twist while the most common tail orientation during a climb was depression (pitch down) only. By and large, this set of observations is consistent with comments presented above which favored tail use as a flight control mechanism.

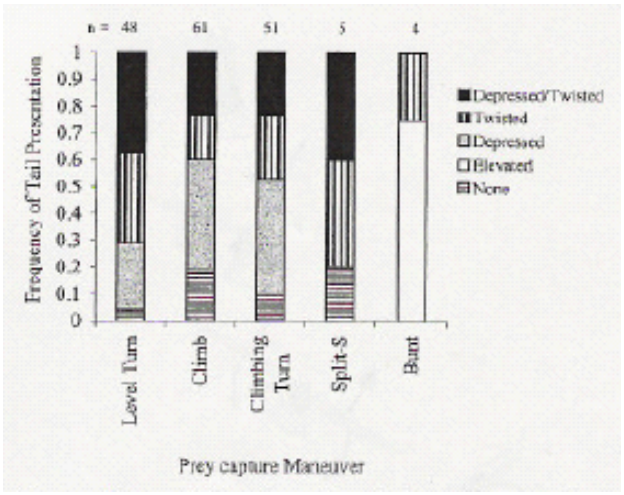

Figure 1. Uses of Bird Tails (Warrick et al, 2002)

In the thesis of Jose Parga, micro air vehicle tails were modeled after studying the tails of various birds. Since modeling a complete bird's tail with its many movements would be almost impossible, a design that resembled a bird's tail in combined rotation was deemed more practical. The result was a bird-like tail that could be used to affect pitch as well as roll. However, problems with stability were encountered with the MAV and vertical-stabilizer-less configuration that birds do not seem to display. In the thesis by Parga it was summarized that the micro air vehicle in question would be able to achieve controllable flight if modifications to the tail were made.

Motivation

In keeping with an inherent goal of micro UAV design, building a smaller vehicle, Lt. Parga removed the V-tail configuration on the AFRL/MNAV micro air vehicle (MAV). It was then replaced with a "rotary" flat tail that was developed after studying the tails of various birds. This rotary tail enabled the tail to move as if it was an elevator and at the same time revolve about the x axis of the aircraft body (Parga, 2004:

10). Having characterized this tail as a plausible means to control flight, Parga's thesis then summarized control effects by measuring changes in the force and moment coefficients. Motivation for the current thesis was found in searching for ways the MAV could become more recoverable. One way to accomplish this is to reduce the horizontal velocity of the vehicle prior to landing by using the tail as an airbrake.

To accomplish this task the tail was envisioned to deflect, as an elevator, to -90^{o}. The tail used by Parga could not accomplish this deflection without reducing the range of positive deflection. A different tail using the same volume coefficient as Lt. Parga's tail designs was constructed. The new tail, however, was completely flat and attached to the MAV in a slightly different way. The configuration change also allowed the tail to fold completely parallel with the top of the MAV, thus improving its compactness for storage or transport, witnessed in Figure 2.

Figure 2. Fully Foldable MAV Tail

Due to Cn_{β} being negative, as evidenced in Lt. Parga's thesis, a stabilizing mechanism was developed. This mechanism consisted of two ventral fins placed on the

lower aft portion of the MAV fuselage. This arrangement gave the added benefit of providing a hard point to attach rear wheels for landing to make the vehicle more recoverable.

Research Objective

a. The primary focus of this study is to use the AFIT open-circuit, low-speed wind tunnel to characterize the behavior of the improved flat tail and stability modifications. To achieve this end state the following data points were gathered:

b. Calculate and compare the lift, drag, and side force coefficients, C_L, C_D, and C_S for the Parga tail vs. the flat tail in a high deflection condition.

c. Calculate and compare the force coefficients, moment coefficients and stability derivatives for larger values of elevation and rotation angles of each tail.

d. Calculate and compare force and moment coefficients of the two tail configurations in various deflection and rotation angles.

e. Add vertical fins and recalculate the stability derivatives of the two tails for this configuration.

II. Literature Review

Introduction

Extensive research into unmanned aerial vehicles (UAVs) during the past few years has led to advancements in the miniaturization of cameras, data transmitting links, navigation systems, thrust generator, lifting surfaces, and control surfaces (Gad-el-Hak, 2001: 419). Miniaturization of lifting surfaces has brought about its own set of challenges.

With chord lengths of micro air vehicle wings becoming smaller, Reynolds numbers also become small. Most MAVs fall with in the Reynolds number range 10^4 – 10^6 (Carmichael, 1981). When Reynolds number falls in the range of 10^4 – $10^{5,}$ challenges are presented because the lifting surfaces experience greater susceptibility to flow separation and lower efficiency (Gad-el-Hak, 2001: 419). The MAV in this study has Reynolds numbers ranging from 0.9 X 10^5 to 1.3 X 10^5 for the velocities tested.

Low Reynolds Number Design

"Within $10^4 < Re < 10^6$ a complex flow phenomena takes place on the upper surface of the airfoil. Separation of the flow will take place before transition to turbulent flow. Flow in this range of Reynolds numbers is laminar and can support only a very small adverse pressure gradient without separation. With any surface roughness on the wings pressure gradients become inherent. Thus, the laminar flow separates and forms a free-shear layer that quickly transforms to turbulent flow. Reattachment of the flow will then occur if sufficient energy is supplied to the wall region by entrainment of the high-speed fluid. A separation bubble will form" (Gad-el-Hak, 2001: 419).

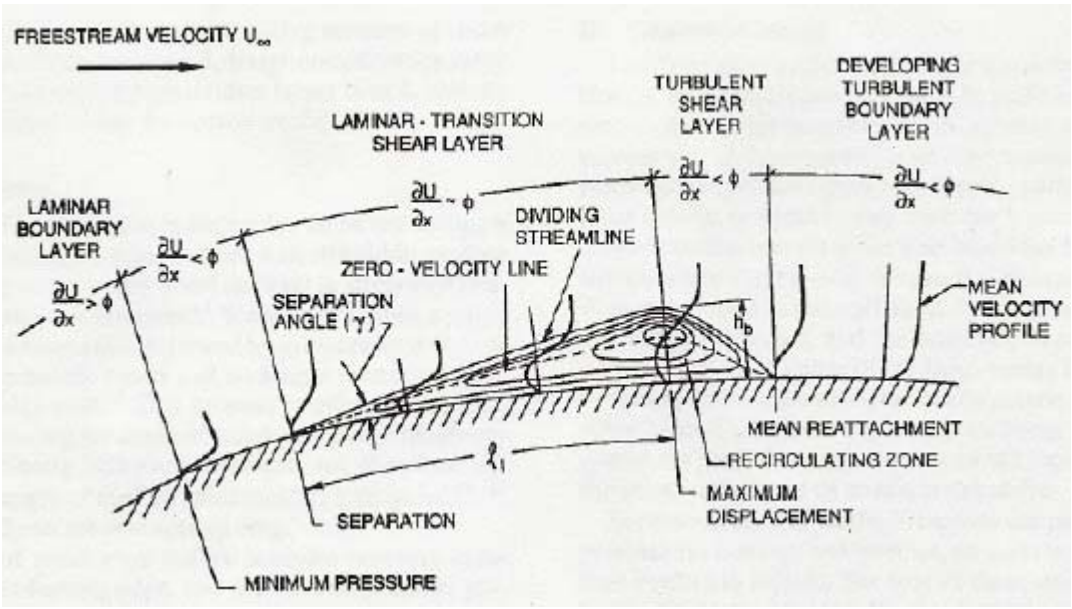

Figure 3. Laminar Separation Bubble (Gad-el-Hak, 2001: 421)

A separation bubble, shown in Figure 3, will serve to de-energize the flow over the wing and result in decreased lifting efficiency. Aerodynamic efficiency of the wing is already low within the range of Reynolds numbers due to viscous forces producing a high drag in the shear layer. According to Nechyba and Ifju, biological aircraft such as bats, insects, and birds are able to mitigate this problem and are able to outperform any manmade miniature flight vehicle.

The optimal situation for MAV designers would be to create a scenario where the size of the separation bubble decreases as the incident angle of attack increases through the stall angle, α_{stall}, at which point the flow enters a turbulent transition state near the trailing edge (Biber et al, 2004:7). Using an aeroelastic wing with the ability to adapt to atmospheric disturbances; researchers with The University of Florida and NASA Langley Research Center have accomplished such a task (Waszak, 2001: 1).

Flexible Wing MAVs

The University of Florida research group is considered to be at the forefront of MAV design with root chords of 6" or smaller. An example of one of the group's vehicles is presented in Figure 4. The group has experienced great success, winning the International Society of Structural and Multidisciplinary Optimization (ISSO) Micro Aerial Vehicle Competition for three years in a row (Waszak and Jenkins, 2001:1). They accomplished the task by using carbon fiber matrix ribs supporting a parachute-latex membrane to make the planar surface of the wing; enabling what is termed as adaptive washout.

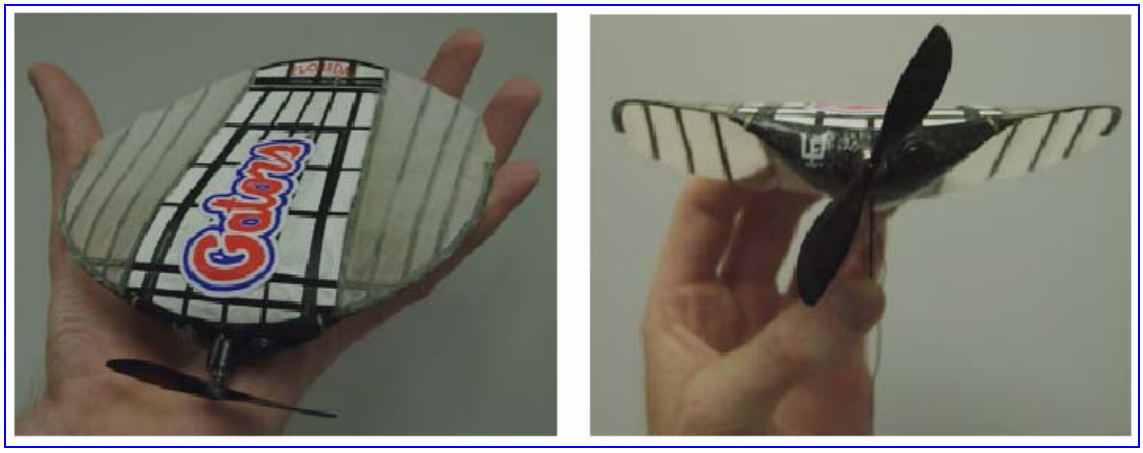

Figure 4. University of Florida's 3.3" Mean Chord, Flexible Wing MAV

In adaptive washout the flexible wings may compensate for changes in speed and altitude by changing angle of attack along the span. This adaptive washout is also seen in sails of sail boats. Here the sail is twisted by wind velocity to extend the wind range of the sail and produce a more constant thrust, even in gusty conditions (Ifju et. al, 2002: 2)

Local flow conditions can be compensated for by the flexible membrane moving or twisting to achieve a more constant lift (Waszak and Jenkins, 2001:2). In other words the severity of negative pressure gradients is reduced. Wind tunnel tests were conducted

by The University of Florida to compare differences in a flexible wing and rigid wing design. Figure 5 shows the improvement in lifting characteristics of a flexible wing design. Additionally the work of Capt. Deluca, Figure 6 and Figure 7, is included for comparison. The plots show that the flexible wing is able to achieve higher L/D and lift coefficient. C_L plots show how a higher angle of attack can be achieved with the flexible wing, demonstrating that separation of flow and the resulting loss of lift is delayed.

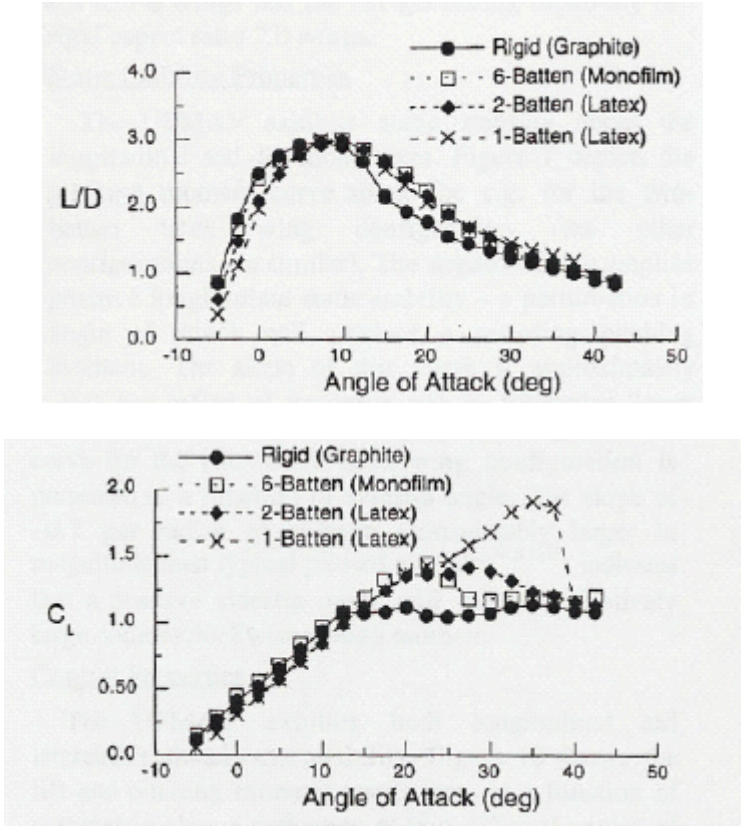

Figure 5. L/D and C_L vs. α for University of Florida MAV (Waszak & Jenkins, 2001: 4)

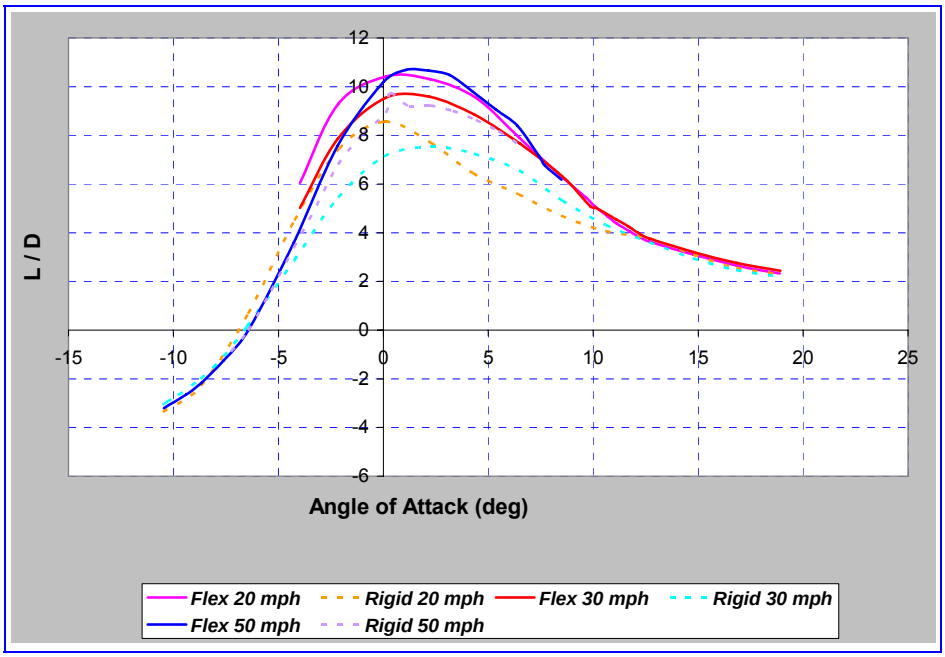

Figure 6. L/D Plot for Rigid and Flexible Wing MAV (DeLuca, 2004: 54)

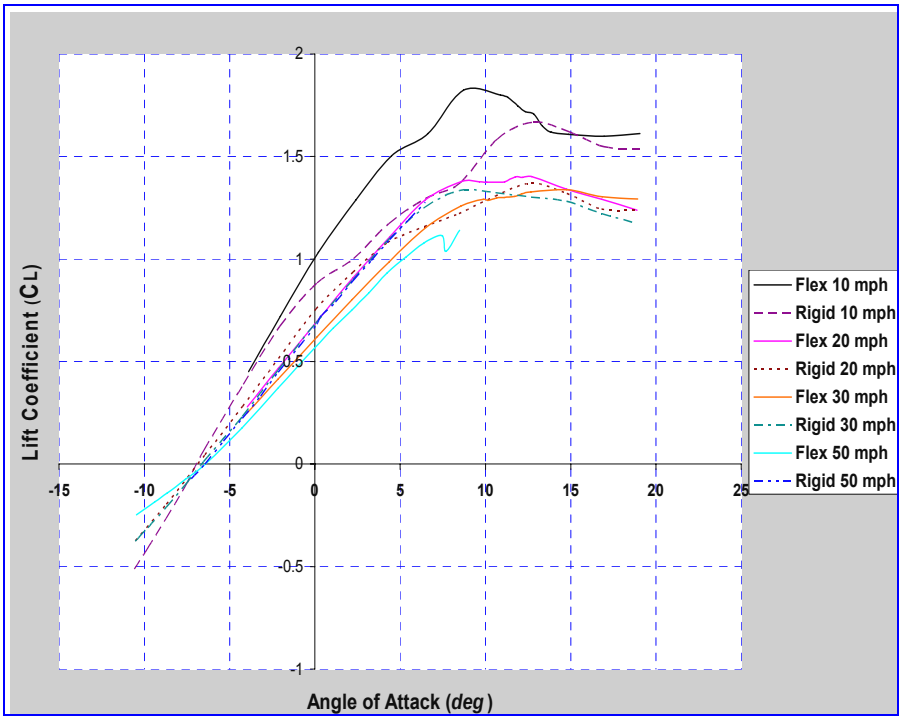

Figure 7. C_L Plot for Rigid and Flexible Wing MAV (DeLuca, 2004: 48)

A second aspect of optimization due to miniaturization of UAVs is the improvement of control surfaces, most notably the tail. The tail is crucial not only for control but for stability. While some aircraft are tailless, most use a conventional T, or cruciform type of configuration for the tail. Small glider enthusiasts have been using a V-tail configuration due to it compact size and combination of control surfaces. The MAV for this study originally had a V-tail with two "ruddervators". This configuration was studied by Deluca.

The idea of a rotatable tail-plane is not a new idea. William Nash patented a design in 1992. Patent Number 5069143 is assigned to a tail plane that can rotate from a horizontal stabilizer to a vertical stabilizer position; additionally, it may rotate about an axis parallel to the y body axis, as a regular control surface would.

In the same year as the patent, Robert G. Hoey conducted research into avian flight by building a remote control raven model. The objectives of his research were to determine if soaring birds are statically stable in the lateral axis, pitch axis, find the source of this stability, and to investigate the method birds used to control turns. Two raven models were built. The first model had drag flaps on the wing to induce yaw and the tail was deflected as an elevator only. The second model retained the drag flaps but the tail was modified to allow tail rotation and elevator deflection. With this second model, different wing plan form shapes as well as tip feather spread and its affects on stability were investigated. In R.G. Hoey's paper, "Research on the Stability and Control of Soaring Birds", no quantitative analysis of the tail was given. Hoey concluded, "The handling qualities were not very comfortable for a human pilot but they are probably completely normal to a raven."

While the use of a bird's tail in flight is highly debated, some research indicates that tails do serve a purpose. A bird bends its tail to one side using it as a rudder (Horton-Smith, 1938; 38). Proponents of birds using their tails for control present evidence that the tail may be used as a lifting surface (Storer, 1948; 38). With any distance between the tail and wings of a bird, the tail can be used to produce a moment, thus it becomes similar to an elevator and/or rudder.

III. Methodology

Introduction

This study used four primary pieces of equipment. The first two pieces are the MAV, provided by AFRL/MNAV, and the two rapid prototyped tails. The AFIT low speed wind tunnel, the third piece of equipment, provided the means to test the tails. Last, the AFIT-1 balance was used to measure the forces of the MAV in the wind tunnel.

MAV and Tail Description

The original MAV, shown in Figure 8, is constructed of a carbon fiber matrix used for the entire fuselage and tail. The wings, however, use the carbon fiber for the forward ¼ of the chord. From this ¼ chord position, carbon fiber ribs are then used to support a parachute type material. (DeLuca, 2004:16) This structure is rigid in upward bending, but is flexible in downward bending. This allows the wings to be wrapped under the body, increasing compactness for storage. Properties of the original MAV and tail are given in Table 1.

Table 1. Original MAV and Tail Dimensions

Wing	
Root Chord	6"
Span	24"
Area	93.5 in^2
Aspect Ratio	6.16
Mean Aerodynamic Chord	4.2"
Leading edge thickness	0.025"
Parachute Material Thickness	0.005"
Tail	
Mean Chord	2.35"
Span	6.3"
Area	14.8 in^2
Aspect Ratio	2.7
Thickness	0.03"
Horizontal Tail Volume Coeff.	0.54

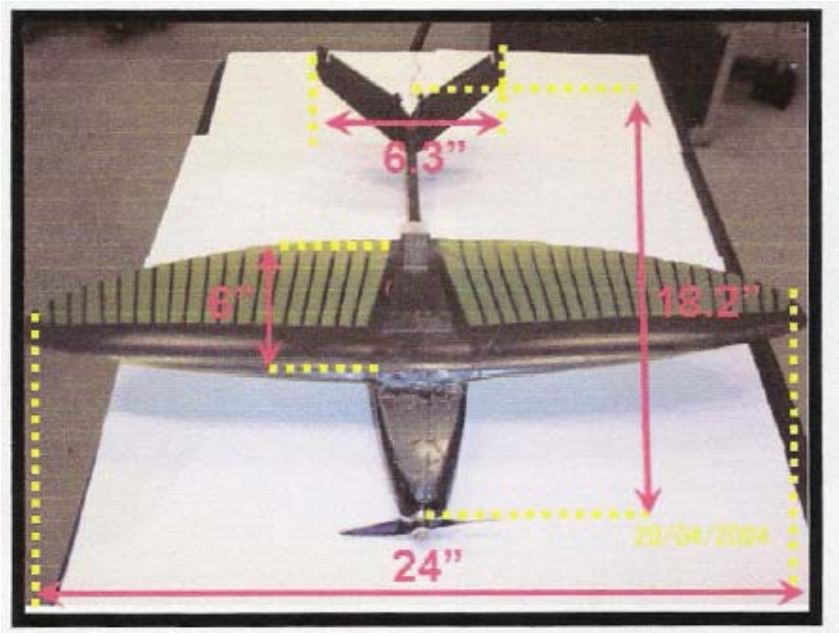

Figure 8. Original MAV Selected Dimensions (Parga, 2004: 51)

To conduct the research done for Parga's thesis the V-tail, shown in Figure 8 was removed and a rotatable tail mechanism, Figure 9, installed. The same actuators as the V-tail design were used, although they were repositioned. Removing the old tail and attaching the new tail gave an overall length of approximately 14.08 inches vs. 18.2 inches of the original design wing dimensions remained the same. When folded, the full vehicle length was less than 10 inches.

Figure 9. Foldable Rotatable Tail MAV

The rotatable mechanism allows the tail to be rotated around the "x" body axis for roll control as well as to be deflected for pitch control. The rotation mechanism was drawn in Solid Works™ and produced on a Stratasys 3300 rapid prototype machine.

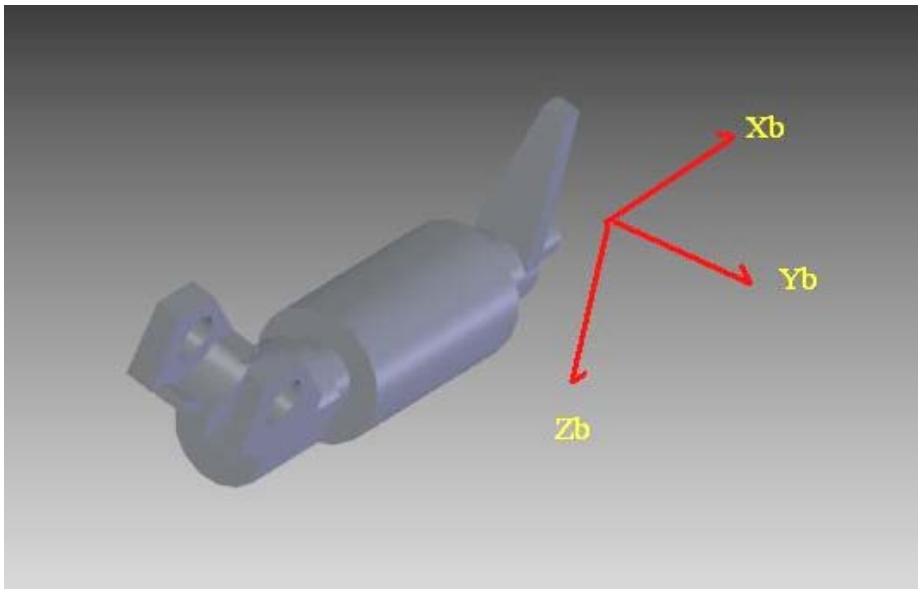

Figure 10. Rotation Mechanism

A control rod attached to a rack runs axially through the piece pictured in Figure 10. The geared rack moves fore and aft along the x body axis, depending upon the

control command given. A gear positioned on the rotation mechanism and attached to the tail is meshed with the rack. As the rack, seen in Figure 11, is actuated, the gear rotates causing a deflection in the tail. The control horn near the top of Figure 10 is attached to the servo that controls rotation. The control horn's main function is to allow more leverage and rotation angle. Actuating the servo results in a rotation of the entire rotation mechanism and tail. Inside the fuselage the piece in Figure 10 is installed into a yoke that constrains all movements except rotation in the "x" body axis. Figure 12 shows the internal configuration and control actuation attachments of the MAV.

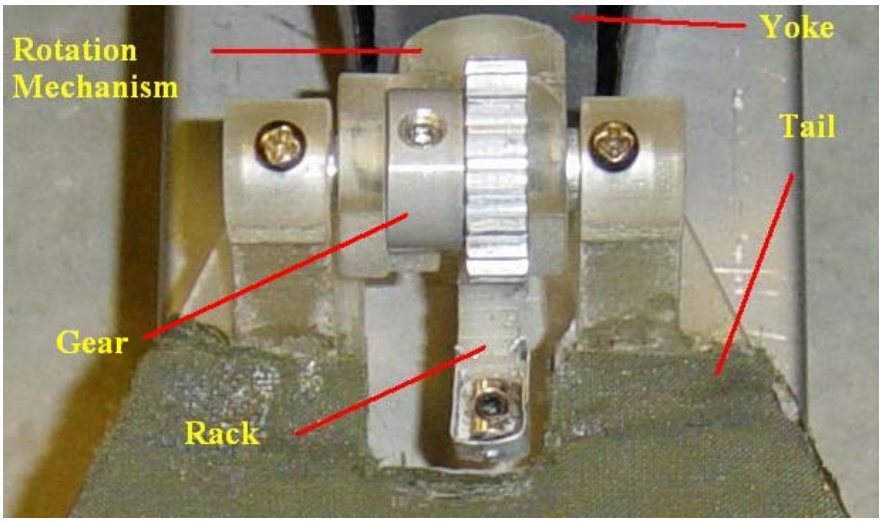

Figure 11. Rotatable Tail Attachment

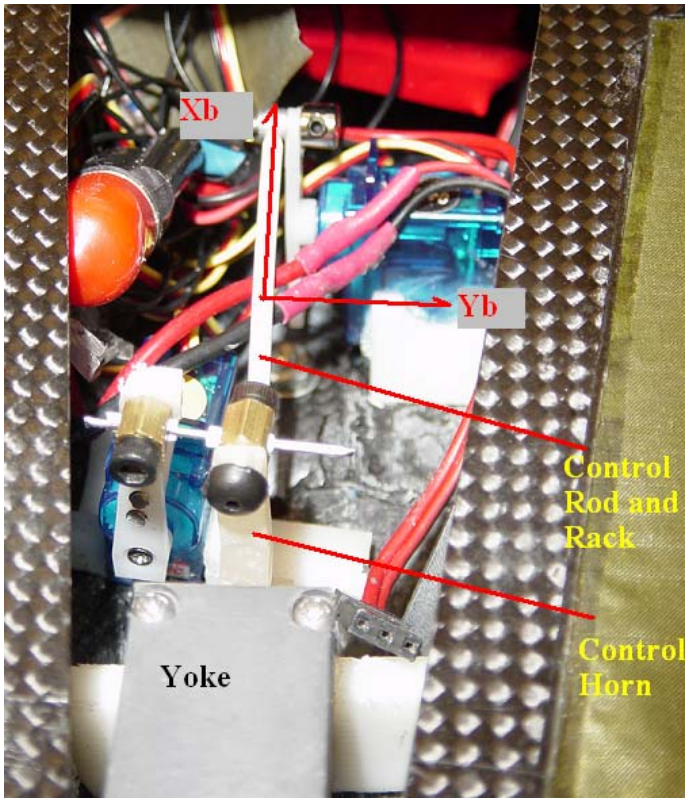

Figure 12. Internal Layout of Rotatable Tail

The MAV tested in this study differs slightly from the one in Lt. Parga's study. A new rotation mechanism was printed out for the new rapid prototype machine. The new machine allows for tighter tolerances and a stronger part. A second benefit of the new mechanism is the allowance for increased rotation angles over the one tested previously. This was desirable as this study sought to investigate such angles. Additionally, the servos were replaced with a higher torque servo; to reduce some of the tail movement due to wind forces during tests.

In some tests conducted in this study vertical stabilizers were attached to the model to improve problems with directional stability as uncovered in Lt. Parga's work. The stabilizer was placed at the aft end of the aircraft, just forward of the tail mechanism. Two screws were already located on the model to hold the tail yoke in place. The screws

provided an excellent attaching point. The location chosen could double as an excellent position for landing gear supports. To examine this, two holes were drilled in the stabilizers and landing gear axils and wheels were attached for later tests.

Figure 13. Stabilizer

The stabilizers, Figure 13, were designed by considering the second tail configuration in Parga's thesis which had vertical stabilizers. Results from Parga showed that the vertical stabilizers improved directional stability to the point that $C_{n\beta}$ was positive. Stabilizer area was increased over that of the Parga model due to their placement and loss of moment arm. The increase in this area was weighted against the length attainable with out interfering with tail operation.

Table 2. Stabilizer Properties

Length	2.75"
Height	1.5"
Width	2.125"
Area	7.13 in^2
Weight	0.040 kg

The tail used by Lt. Parga and labeled as "Tail 1" in his tests was also used in the tests for this study. It will be referred to as Tail 1 in this study. The use of this tail provided a baseline for comparison to this earlier work. Tail 1 was designed using Solid

Works^{TM}, printed with a rapid prototype machine, and covered with a polyester fabric (Parga, 2004: 54). Table 3 shows the properties of this tail.

Table 3. Geometric Properties of Tail 1

Area	9.42 in^2
Chord	4.66"
Span	4.375"
Thickness	0.07"
Aspect Ratio	2.02
Taper Ratio	0.3755
Tail Volume Coefficient	0.2

Parga stated that the total estimated time for construction of this tail to be 9 hours. The second tail used in this study consumed a similar amount of time. This tail will henceforth be referred to as Tail 3 since the name Tail 2 was used in Parga's thesis for the tail with stabilizers. Tail 2 is similar to Tail 1 except it has been flattened, whereas Tail 1 was curved laterally as evidenced in Figure 14 and Figure 15.

Figure 14. Rear Profile of Tail 1

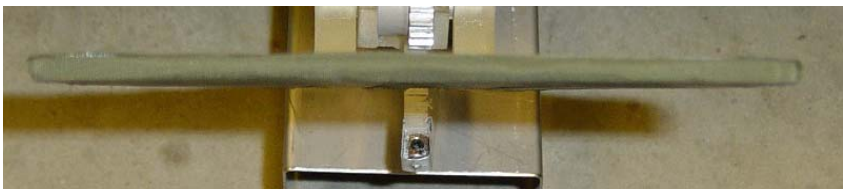

Figure 15. Rear Profile of Tail 3

Tail 3 was designed using Tail 1 as a guide. Their internal structures are similar. Besides being flat, Tail 3 differs from Tail 1 in that its attachment points are offset from

the plane of the tail, Figure 16. This offset allows Tail 3 to be fully folded, as it offsets the tail.

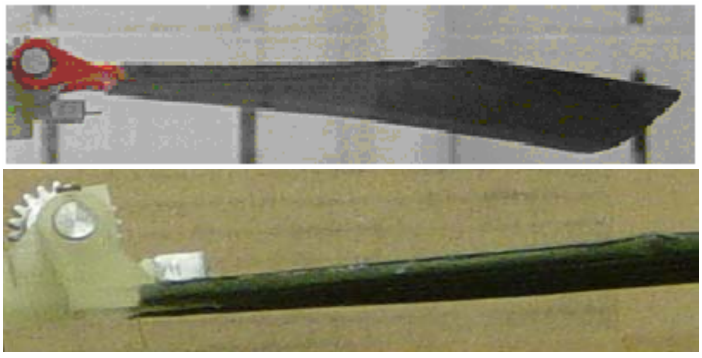

Figure 16. Attachment of Tail 1 (top) and Tail 3 (bottom)

Due to the offset in attachment, Tail 3 is now closer to the vertical position of the CG. This means less vertical variation in CG position as the tail is deflected. Also, when rotated, the tail now rotates around the x body axis; before, Tail 1 was positioned higher on the model resulting in a slight lateral CG shift when it was rotated.

Wind Tunnel Description

The AFIT low speed wind tunnel is located in building 644, room L154. It was constructed by New York Blower Company, who also manufactured the fan. The tunnel is an open circuit design that draws and ejects air from within the room. The test section is closed and measures approximately 3' x 3'. This tunnel has a design test speed of 150 mph and has been tested to a speed of 148 mph. The low speed wind tunnel can be broken down into 6 components: the inlet, converging section, test section, diverging section, exhaust, and fan. Figure 17 depicts each of these sections.

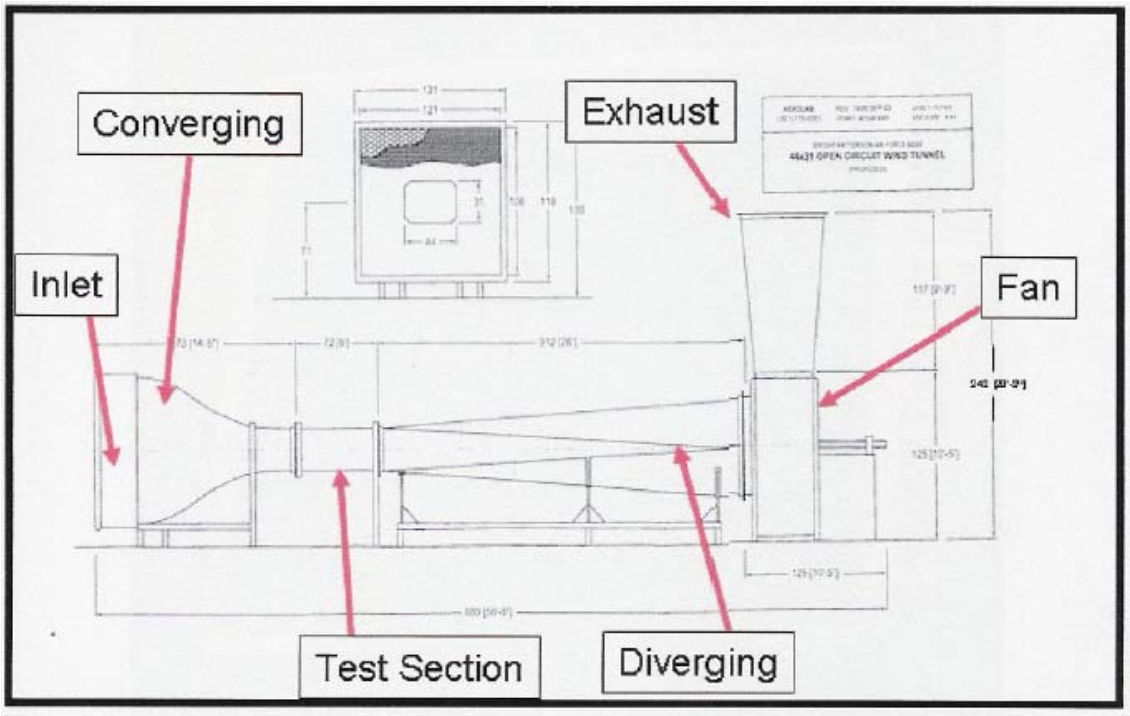

Figure 17. Wind Tunnel Sketch (Parga, 2004: 62)

The inlet is sized to dimensions of 111" high x 122" wide x 70" deep. In the front of the inlet, where room air is first introduced into the tunnel, a quarter inch aluminum honeycomb structure acts as a flow straightener. This is followed by four anti-turbulence screens. The idea of the large inlet section is to reduce velocity gradients of the air entering the tunnel. The average turbulence intensity of the tunnel has been measured to be 2.25% (DeLuca, 2004: 85).

After the inlet section the air is channeled and sped up in the converging section. Here the tunnel converges from a height of 11" to a height of 31.5"; giving the section a contraction ratio of 9.5:1. The converging section leads into the test section.

The test section measures 31" high x 44" wide x 72" in length. The top and sides are constructed of Plexiglas. The sides function as moveable doors for accessing the test section. The top consist of a removable Plexiglas panel with openings for a traversing

hot-wire anemometry system. Within the test section is the sting, used for mounting the balance. In turn the sting is mounted on a support system attached to a turn table.

The sting support system is able to move 20 degrees up or down from its neutral zero angle of attack position. The turn table is able to rotate from sideslip angles of +15 degrees to -15 degrees. These movements are controlled from the control room, located in room L154 using Lab View Virtual Instrument® software. The user interface of this software is presented in Figure 18.

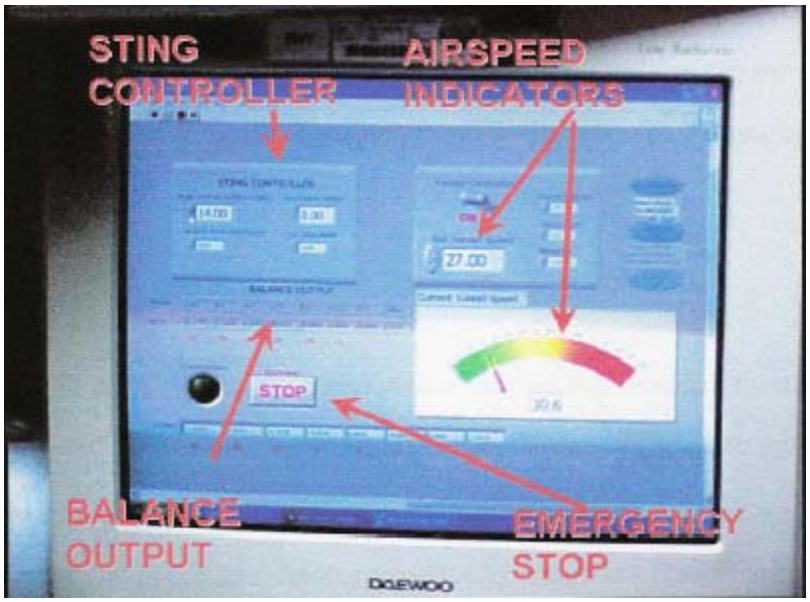

Figure 18. Wind Tunnel Control Interface (Parga, 2004: 75)

The wing span to tunnel width ratio is: $\frac{b}{w} = \frac{24''}{44''} = .0545 \approx 0.55$ (DeLuca, 2004: 25). The general rule is that wing span to tunnel width should be $\frac{b}{w} \leq 0.8$ (Barlow et al., 1999:28). Having a ratio less than 0.8 will reduce large interferences between the sides of the model and shed vortices from the wing (Barlow et al, 1999: 381).

After moving through the test section, air flows to the diverging section. In this section air is diffused to reduce its speed without flow separation occurring (Barlow et al, 1999: 80), The length of the diffuser section in the AFIT low speed wind tunnel is 312". The diffuser connects to the fan.

The fan is an ACFL/PLR Class IV type fan manufactured by New York Blower Company. It is powered by a Premium Efficiency electrical motor manufactured by Toshiba. This in turn is controlled by an adjustable frequency controller manufactured by Siemens. Table 4 shows motor characteristics. Upon exiting the fan, air is exhausted upward into room L154.

Table 4. Wind Tunnel Motor Properties (Parga, 2004: 68)

Type	EQP III, 3face induction
Power	200 BHP
Poles	4
Max. operating speed	1785 RPM
Voltage	230/460 Volts
Frequency	60 Hz Max
Amperage	444/222amp.

Balance Description

AFIT-1, a six-component internal balance was used in tests conducted for this thesis. This balance was manufactured by Modern Machine & Tool Company, Inc.

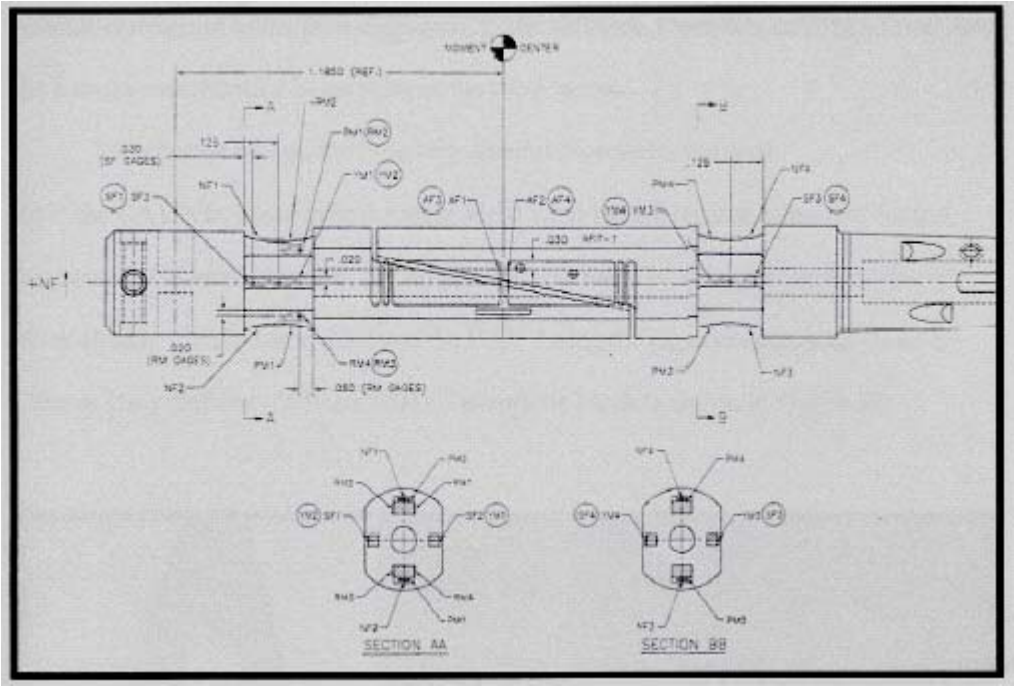

Figure 19. Position of Strain Gages in AFIT-1 Balance (Modern Machine & Tool Co., 2004)

For the tests conducted, the balance was placed inside a mounting block and attached to the model. The mounting block is geometrically similar to a camera pod that would be used on the MAV, and the intrusive effects are not considered here.

The balance is composed of strain gauges. Each strain gauge is composed of a thin wire filament wound in a serpentine pattern. The gauges are placed in a Wheatstone bridge, and a voltage is supplied across the bridge continuously (Parga, 2004:71).

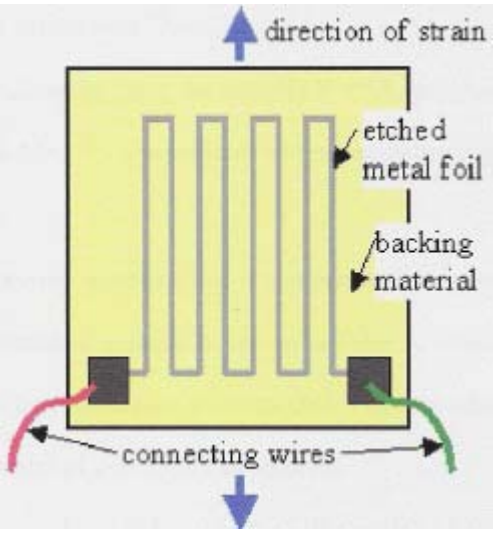

Figure 20. Typical Strain Gage (Penn State, 2004)

As a load is applied the wire filaments, denoted as etched foil in Figure 20, the filaments elongate or shrink, resulting in a change of resistance in the wires. The resulting difference in applied voltage to output voltage can be used to calculate the strain in the wire.

Resistance Calculation (DeLuca, 2004: 149-152)

$$R = \rho * (L / A)$$

Where: ρ = Resistivety of the wire

L = Length of the wire

A = Cross sectional area of the wire

Calculation of strain (Parga, 2004: 71)

$$E = 4 * (Vo / Vs) * (1 / SF)$$

Where: Vo = Output voltage of the bridge

Vs = Voltage applied to the bridge

SF = Strain gage factor

Applying Hooke's Law allows the stress applied to be calculated:

$$\Sigma = E * \varepsilon$$

Where: E = Modulus of elasticity of the material

Forces and moments can then be calculated using:

$$Force = \sigma * \varepsilon$$

$$Moment = F * L$$

When taking data the balance will output six voltages that are then interpreted as forces by the software. The forces these voltages represent are presented in Table 5. The maximum load the balance can handle in each direction is also given. An understanding of these maximums is important for calibration which will be discussed in further paragraphs.

Table 5. Load Limits for AFIT-1 Balance

Component	Maximum Load
N1 - Normal Force	10 lbs.
N2 - Pitch Moment	10 in. lbs.
A1 - Axial Force	5 lbs.
S1 - Side Force	5 lbs.
S2 - Yaw Moment	5 in. lbs.
L1 - Roll Moment	4 in lbs.

Experimental Procedure

Before starting the experiments for this study the AFIT-1 balance was calibrated and installed into the tunnel. Calibration and installation was done by Mr. Dwight Gehring, the wind tunnel technician. Steps used in the balance calibration are in Appendix B.

Before starting the experiments for this study, the AFIT-1 balance was calibrated and installed into the tunnel. Calibration and installation was done by Mr. Dwight

Gehring, the wind tunnel technician. Steps used in the balance calibration are in Appendix B.

Once calibrated the balance and holder were passed up through the bottom of the tunnel and attached to the fixed part of the sting. The model was then attached to the sting with a mounting block. The mounting block is described in greater detail on page 74 of the Parga thesis. The only difference is that the mounting block used for this test, Figure 22, allowed the balance to come into the block at a 5^{o} angle relative to the MAV. This was done to facilitate larger positive elevator deflections of the tail. Figure 21 depicts the original mounting block used for previous studies in which the balance attached to the block at an angle of 0^{o}.

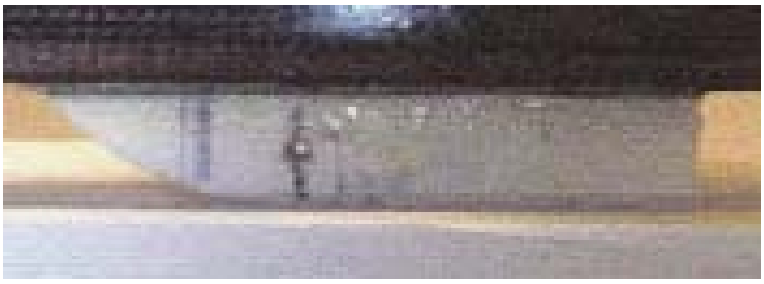

Figure 21. Mounting Block, Previous Studies

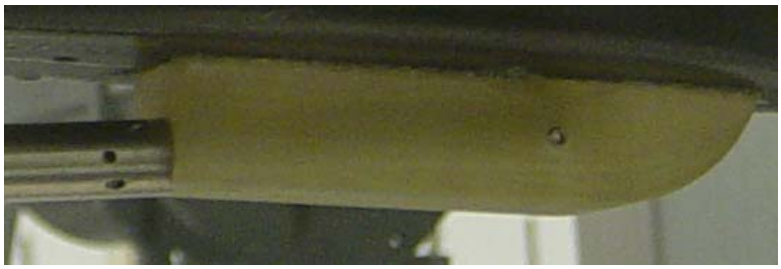

Figure 22. Mounting Block, Current Study, 5^{o} offset

Tunnel tests were conducted at 20 and 30 miles per hour. The 20 mph runs were done only for spoiler characterization to ensure that the balance load limits were not exceeded. Thirty mile-per-hour runs were chosen because that is the speed that was chosen in Parga's thesis, thus allowing a more direct comparison of results.

To acquire data a tare file was first created by running the model through a sweep of attack angles with the tunnel motor off. This gave a baseline for how model weight would interact with the various forces being measured by the balance. Once this file was saved a new file was created ready to accept data from the run with the wind on. With the fan on and tunnel up to speed, the wind produces the forces and moments on the model that are sensed by the balance. These voltage signals are then sent through a 16 bit electronic data acquisition card, and then the analog signal is transformed to a digital signal. Signals are then amplified and conditioned by a low pass filter before being stored on a Pentium computer (Parga, 2004: 76).

Data for each flight condition during the run was taken in 30 second intervals, providing enough data to account for any variations due to vibrations when conditions were changed. For the spoiler characterization runs, data was taken with the tail at 0^o rotation angle and with the tail deflected in various elevator positions of -20^o to -85^o with the model at -4^o, 0^o, and $+4^o$ angles attack. The data collection runs labeled as matrix runs combined rotation angle and deflection which were taken at +4 degrees angle of attack and elevator deflection ranging from $+18^o$ to -30^o. Rotation angle was varied from as much as -30^o to $+30^o$. Beta, negative yaw angle, runs comprised the last of the runs for this thesis. Here beta was swept from -8^o to $+8^o$. The tail was rotated at 0^o and as far as 67^o, with angle of attack being held at $+4^o$.

Data from all the runs was stored in a text file by the LabView software. These files were then "cleaned" by erasing header and superfluous data that occurred while the tunnel was brought up to speed. The clean tab-delimited file was then called by a MATLAB® program. The program used was initially developed by Capt. Deluca and Lt. Gebbie (Gebbie, 2005, 113). The code was then adapted by Parga for use with his thesis (Parga, 2004: 188). ENS Leveron then readapted it to include further revisions to the original program by Lt. Gebbie, and to account for the balance being at a 5 degree angle to the MAV.

The MATLAB® program takes each test condition within the file, for most cases 3 different α's, and averages the [$U\infty$, α, β, N_1, N_2, S_1, S_2, A_1, ℓ] data for that condition. This data is then used to calculate the aerodynamic properties. Results are then written by the MATLAB® program to a file that is easily readable by Microsoft Excel®. The specific equations and processes used by the MATLAB® program may be seen in Appendix D, and pages 36-45 of DeLuca, as well as pages 77-88 of Parga.

IV. Results and Analysis

Introduction

This chapter presents the data and results of the tests conducted in the wind tunnel on the two tails discussed in Chapter III. For data presented from this point, tail deflection as an elevator is denoted as δ_e, and rotation deflection is denoted as δ_{rn}. Both δ_e and δ_{rn} were measured before each run with a hand-held inclinometer. Various trim positions on the controller were noted for corresponding angle deflections of the tail. This allowed multiple δ_{rn} angles to be tested for a specific δ_e without having to stop the tunnel and re-measure the angle for each data point. The sign convention used is the same as that used in Parga's thesis. Figure 23 and Figure 24, illustrate the sign convention.

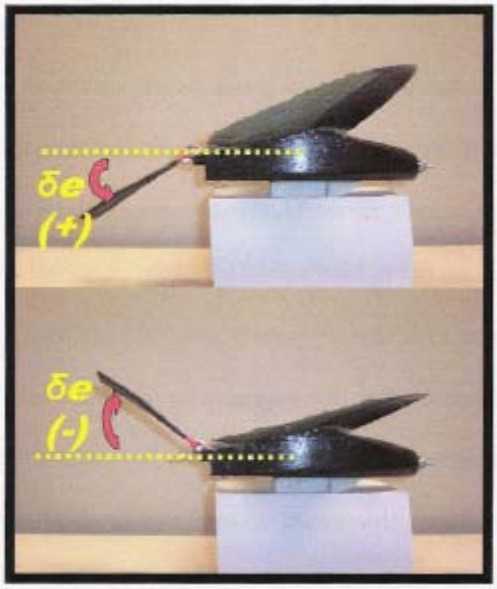

Figure 23. Elevator Deflection Convention (Parga, 2004: 59)

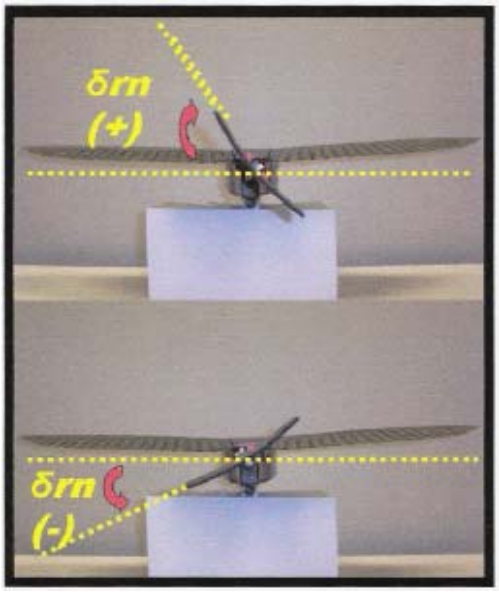

Figure 24. Rudder Deflection Condition (Parga, 2004: 59)

For all runs the horizontal distance from the balance center of gravity to the model center of gravity, Xcm, was 0.71 inches. While this study did not consider the movement of the center of gravity of the model and its affects on stability, Lt. Parga did conduct such a study. His results will be brought into this study later. A pictorial representation of the definition of Xcm in this thesis is displayed in Figure 25.

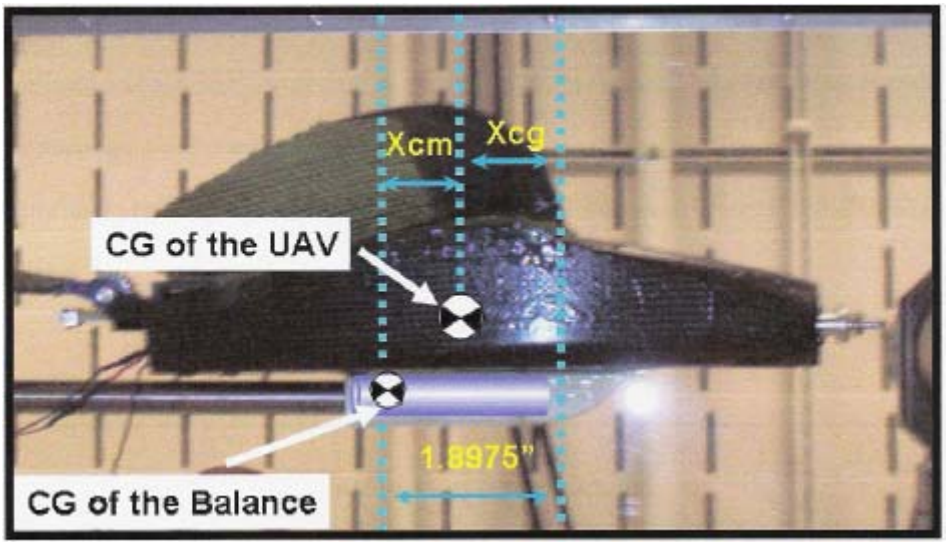

Figure 25. CG Notation (Parga, 2004: 90)

The tests run at 20 and 30 miles per hour had the following average aerodynamic properties:

Table 6. Summary of Flight Conditions

U_∞ (mph)	Mach #	q_c (lb_f / ft^2)	Re_c
20	0.027	1.09	9.3×10^4
30	0.039	2.2	1.33×10^5

Additionally roll angle, φ, was set to zero for all test and therefore $\beta = -\psi$. The data is presented by breaking it into three main parts:

a. Characterization of tails as a spoiler.

b. Characterization of tails as an elevator and rudder.

c. Determination of directional stability of tail and stabilizer configurations.

Spoiler Characterization

The goal of these experiments was to determine how effectively the tail could be used to rapidly descend in altitude and act as an air brake during or immediately prior to touch down of the MAV. The goal of a spoiler is to reduce lift and increase drag. Though reducing lift will reduce induced drag, the spoiler should be capable of overcoming this loss with additional form drag.

During testing the elevator deflection angle, δ_e, was noted to have some variance in it once the tunnel was brought up to speed. This was due to tolerances in the mechanism being too great and in the lack of torque of the servo actuators. By visual estimation, the elevator deflection angle did not appear to become more positive by any more than 5^o - 8^o. Once the tunnel was in the process of slowing to a stop, the tail could again visually be seen moving back to its pre-tunnel run-up position. The result of this action may be evident in the data as different elevator deflections may have similar coefficients or overlap. Figures presented with respect to elevator deflection (δ_e) are based upon commanded deflection, and do not take into account loss of deflection angle due to the previously described factors.

Lt. Parga summarized the characterization of lift with respect to elevator deflection angle on page 126 of his thesis. Those observations are:

1. Lift is a function of δ_e.
2. To increase lift a positive δ_e should be used, similar to increasing the angle of attack of a wing. To decrease lift a negative δ_e should be used.
3. Tail rotation, δ_{rn}, within the range of $\pm 20^o$ will not greatly affect lift coefficient. Outside of this range affects start to be seen in the form of decreasing lift coefficient.

Tail 1 was first run in the wind tunnel. The internal linkage allowed this tail to have a maximum deflection of -64^o. The tunnel was first run at 20 mph to avoid overloading the balance.

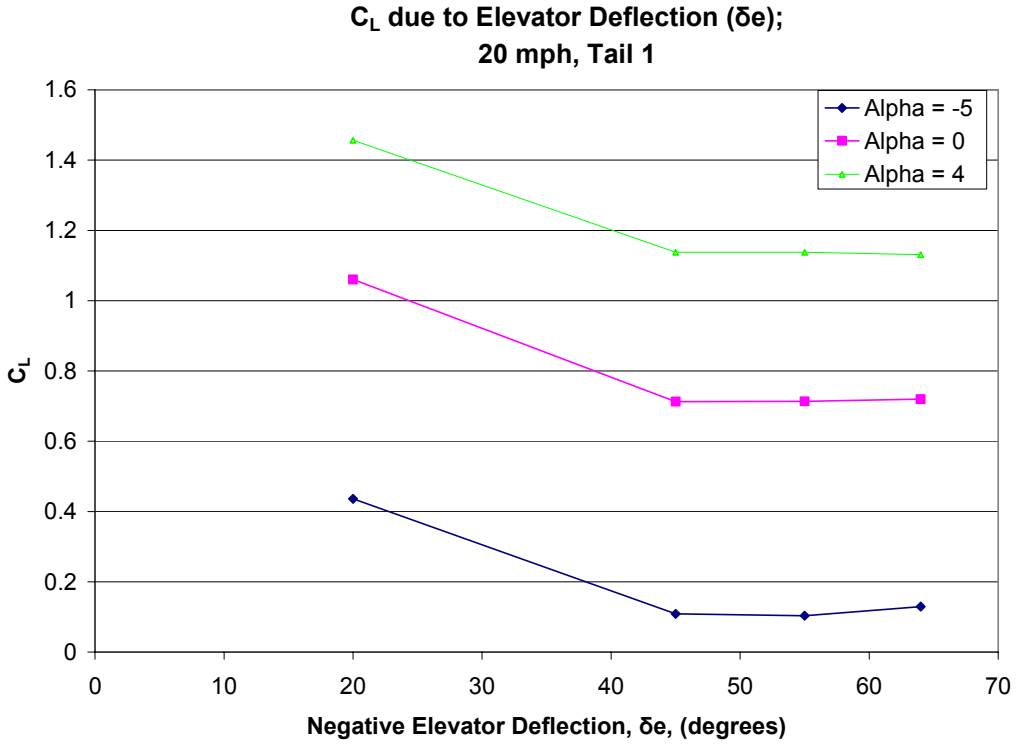

Figure 26. C_L of Tail 1 in Spoiler Configuration

The maximum lift coefficient displayed in Figure 26, which is for Tail 1 at 20 miles per hour without stabilizers, is 1.45. Over all the tests conducted the maximum lift

coefficient developed was 1.54. The figure above starts below this maximum and continues with the downward trend in lift that was summarized in the Parga thesis.

Drag increased as expected with a spoiler. The data did show the lift coefficient leveled out at an elevator deflection above 45° while the drag coefficient decreased. One possible explanation for this decrease is that at the higher deflection angle the tail was more aeroelastically deformed more by the wind force on it than it was at other deflection angles. Higher tunnel speeds typically produced a higher deflection value.

Above deflection of 45° the C_D takes on roughly a sine curve shape, seen in Figure 27. This is similar to what is seen on a flat plate at incidence. After approximately 45° angle of attack the drag normal becomes dependent upon sine of the deflection angle. A similar anomaly is found in the Tail 3 at 30 mph case. Coefficient of normal force on a flat plate is further described to accompany those figures.

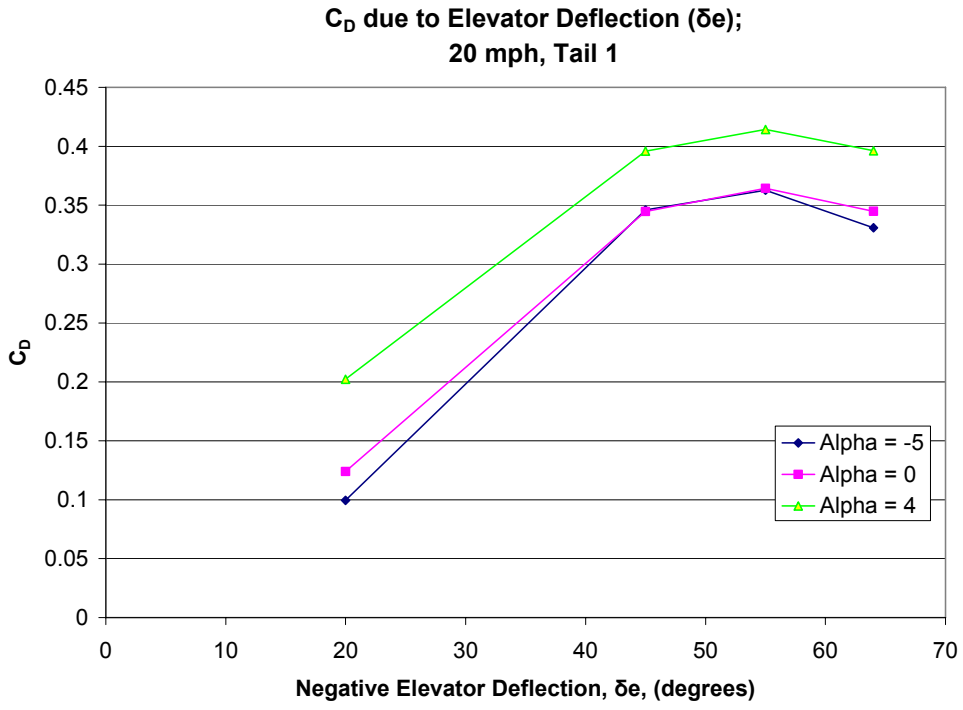

Figure 27. C_D of Tail 1 in Spoiler Configuration, 20 mph

The 30 mph run for Tail 1 did not show same trend in the decrease of drag coefficient, Figure 28. This would seem contrary to the previous statement of higher speeds leading to larger tail deflections. The tail may have deflected roughly equally for the 30 mph runs such that a loss in coefficients would not be witnessed. Lift coefficient, presented in Figure 29, for the 30 mph case did not level off as it did in the 20 mph case.

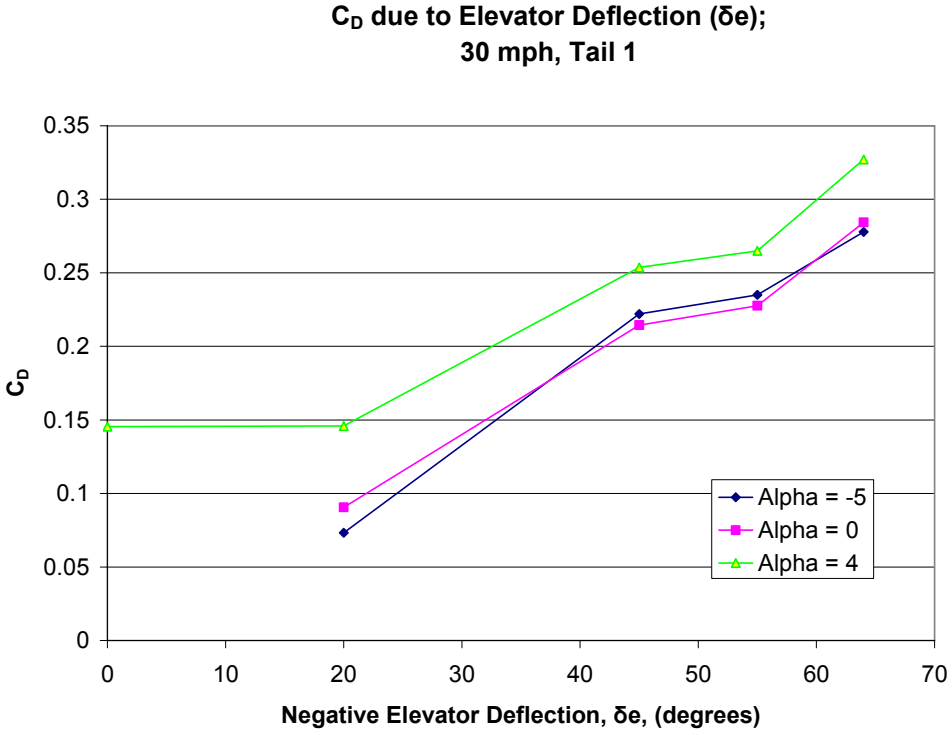

Figure 28. C_D of Tail 1 in Spoiler Configuration, 30 mph

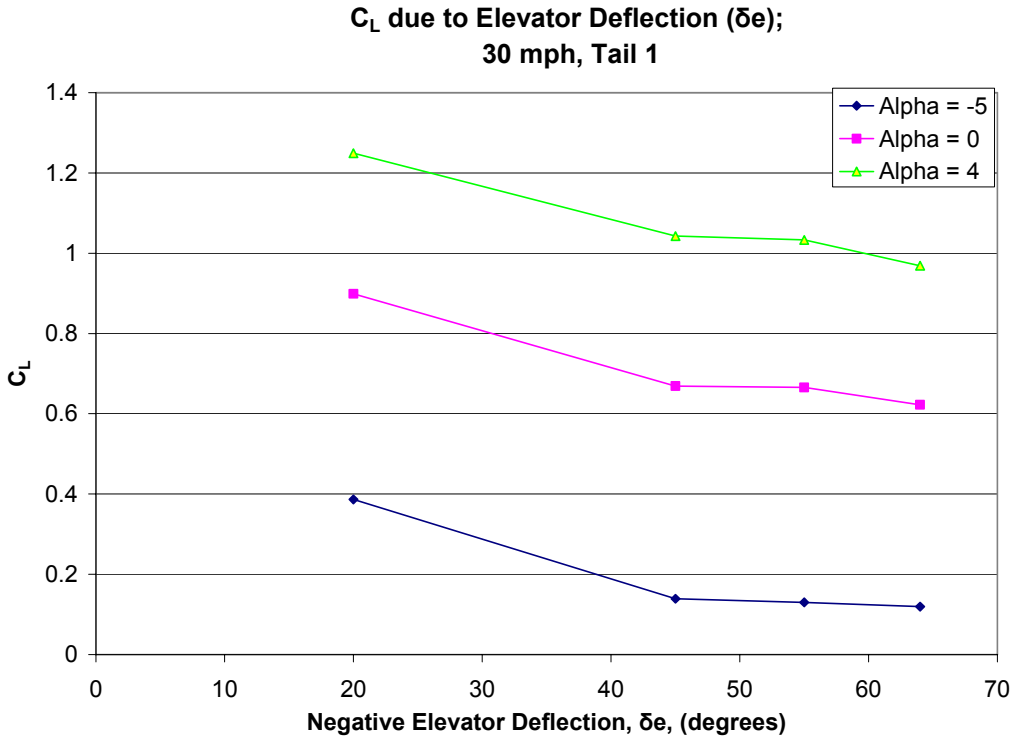

Figure 29. C_L of Tail 1 in Spoiler Configuration, 30 mph

Tail 3, with its different attachment orientation, is capable of reaching a maximum δ_e of -85°. Thus trends in the aerodynamic forces and moments may be further characterized beyond what they were for Tail 1. These trends continued as would be expected with the tail projecting more of its area perpendicular to the free stream flow. However, with Tail 3 being centered vertically a loss of area projected into the free stream flow occurs. The MAV fuselage blocks a portion of this area where with Tail 1, being attached at the trailing edge of the wing, does not experience this blockage when deflected in the negative elevator deflection. This affect of this blockage is seen when comparing Tail 1 and Tail 3 figures and noting that Tail 3 curves are shallower.

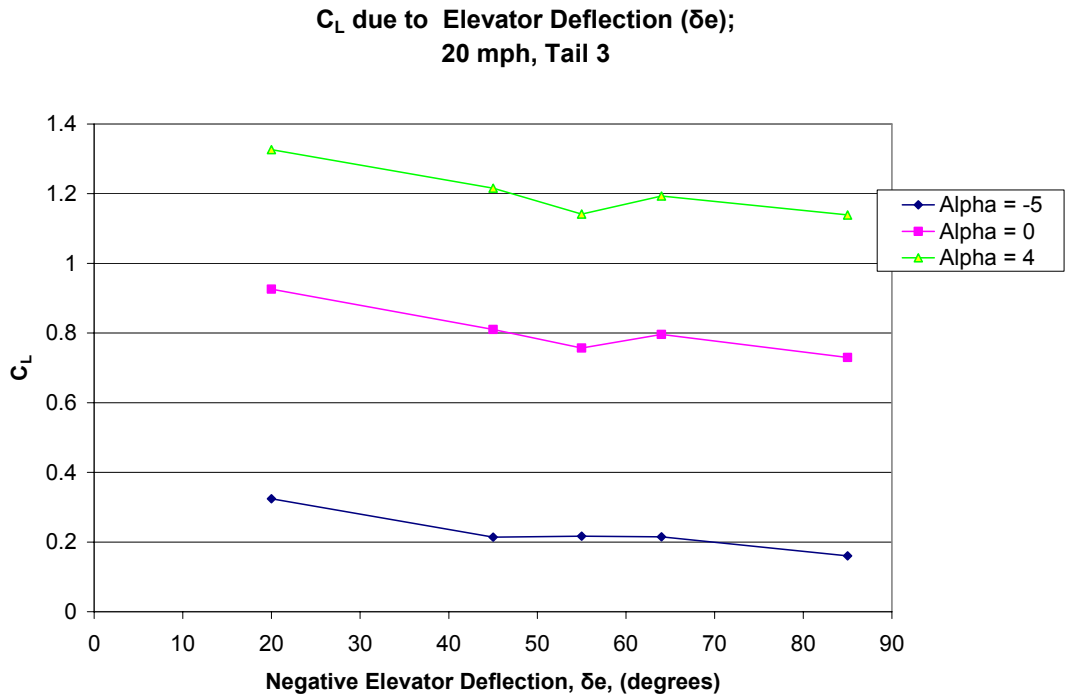

Figure 30. CL of Tail 3 in Spoiler Configuration, 20 mph

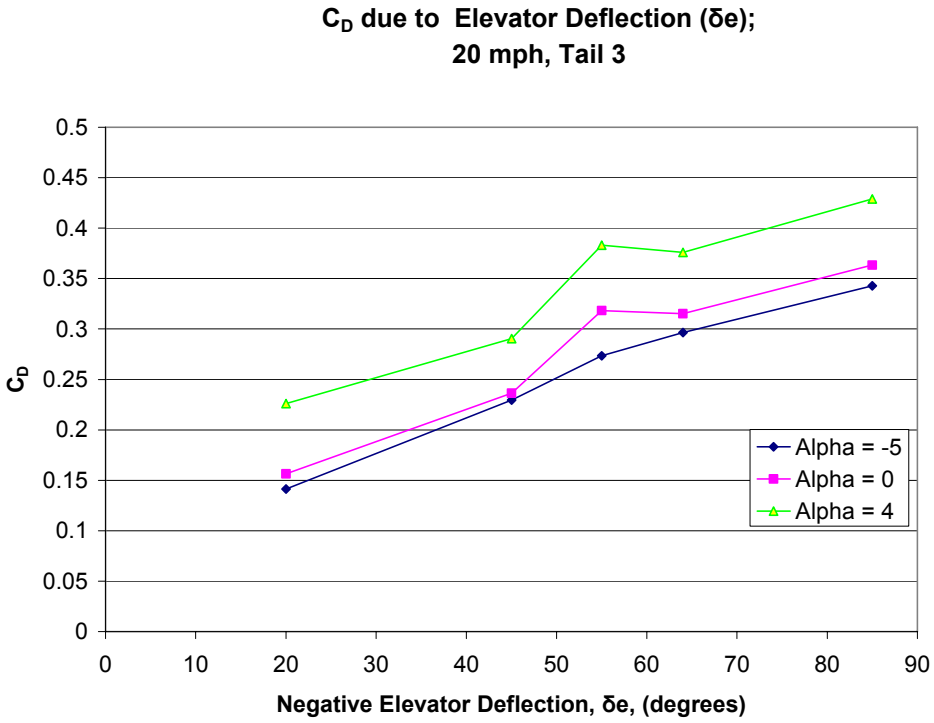

Figure 31. CD of Tail 3 in Spoiler Configuration, 20 mph

In Figure 30 and Figure 31, above, a divergence from the linear trend can be seen at δ_e, of 55°, for angles of attack of 0° and 4°. Even though the highest lift coefficient does not occur at 55° the largest pitch moment coefficient does. While the lift coefficient plots show a higher lift for larger alphas the same is not true for the pitch moment. Blockage by the model on the airflow reaching the tail is one explanation for this result. CG effects should not be present when comparing different alphas since a tare file was taken to factor out these interactions.

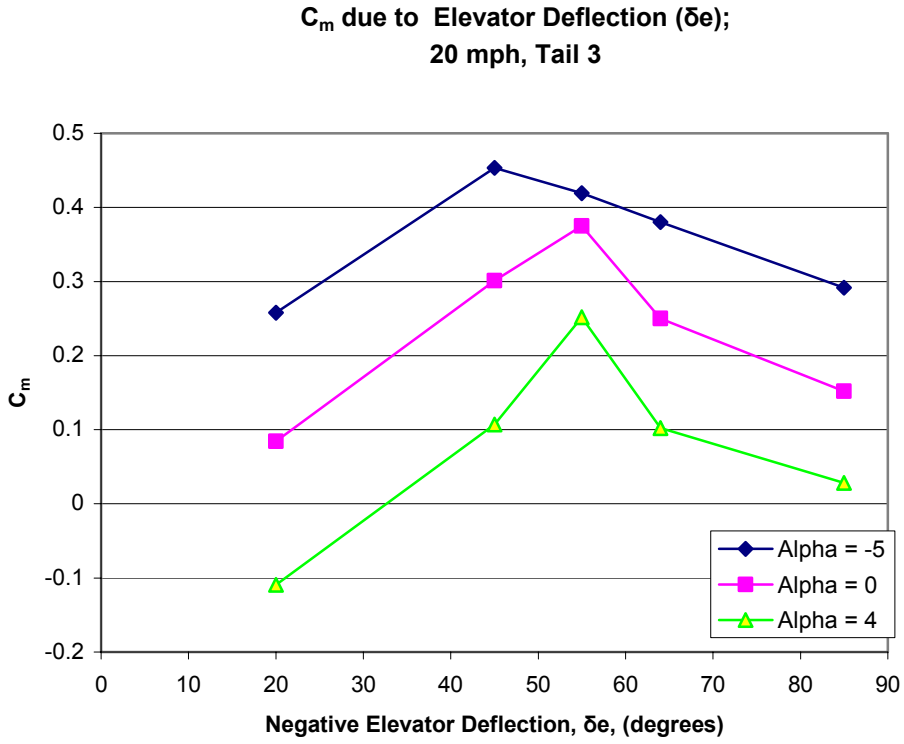

Figure 32. C_m for Tail 3 as a Spoiler, 20 mph

The anomaly at δ_e of 55° is somewhat similar to that of Tail 1 in the 20 mph case. First the deflection of 55° may be closer to 45° when taking into account the deformation due to previously described factors. Flat plate tests conducted by Sighard Hoerner found

the coefficient of normal force was found to increase linearly until approximately 45°. After this angle a sharp drop of the normal force coefficient to a constant value is noticed. Above 45°, C_{normal} becomes constant with C_L normal becoming a function of cosine α and C_D normal a function of sine α.

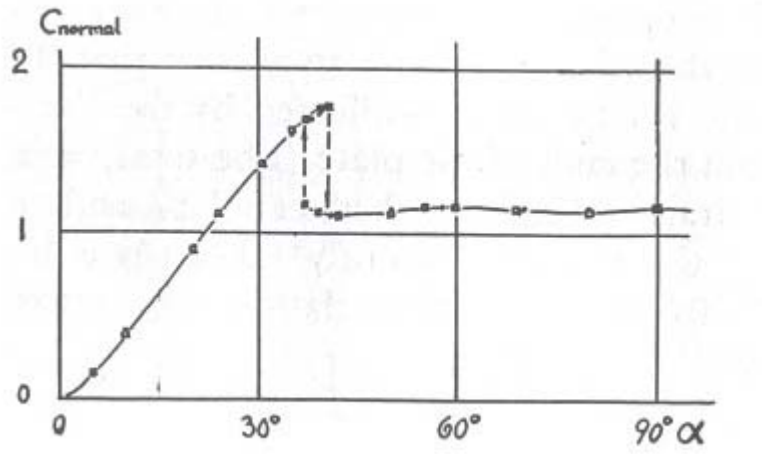

Figure 33. Normal Force Coefficient on a Square Plate (Hoerner, 1965: 3-16)

This reference does prove beneficial in determining the anomalies found in Figure 30, Figure 31, and Figure 32. The equations for C_L normal and C_D normal show that beyond 45° C_L would continue to decrease to 0 at 90° while C_D would increase, reaching its maximum value at 90°. The fact that C_{normal} reaches a maximum then drops fits the shape of the Cm plot, Figure 32. The largest moment would be expected to correspond with the largest forces on the tail. Additionally the pitch moment arm changes with respect to the elevator deflection angle. For a constant normal force applied to the tail the resulting moment about the CG would decrease as deflection increases through 45°. This would give a similar shape to the pitch moment curves as depicted in Figure 32.

Another interesting result is that the similar anomalies were not found at 30 mph. In this case, peak value of C_m was found at 65^o. C_L showed the greatest change from the previous deflection value while C_D showed a similar trend. However where C_L leveled off, C_D continued to rise; again this holds fairly consistent with the equations of each as a trigonometric function of alpha.

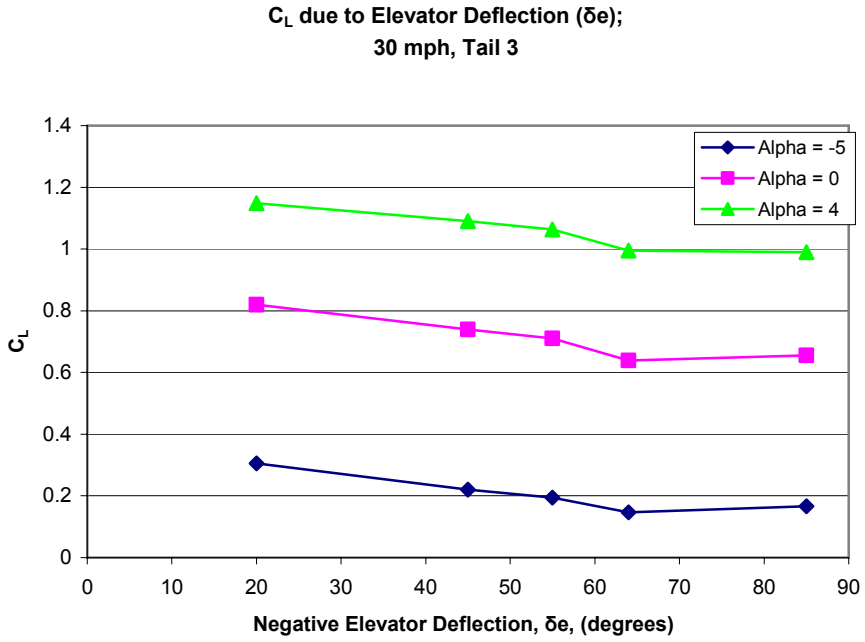

Figure 34. C_L for Tail 3 as a Spoiler, 30 mph

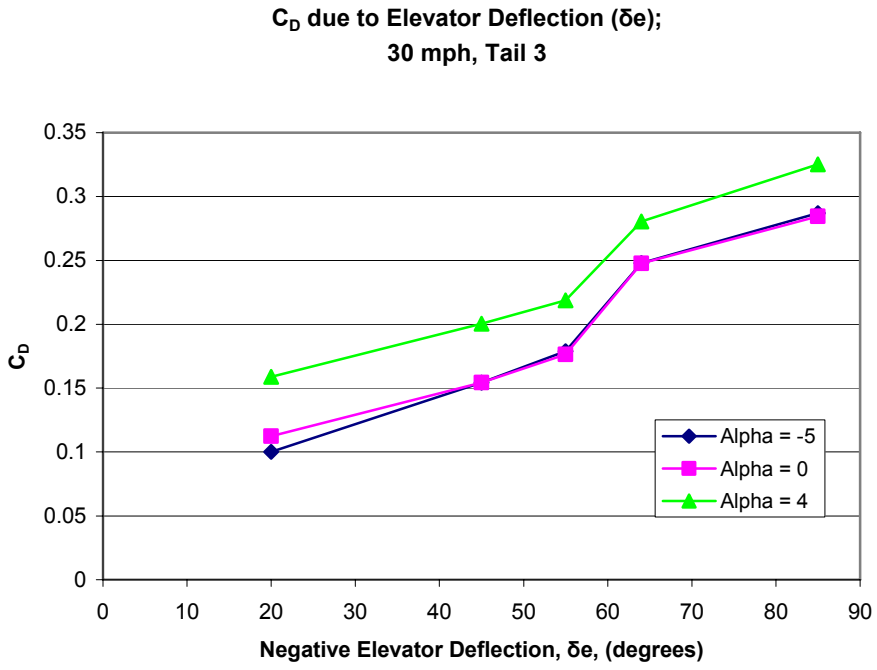

Figure 35. C_D of Tail 3 as a Spoiler, 30 mph

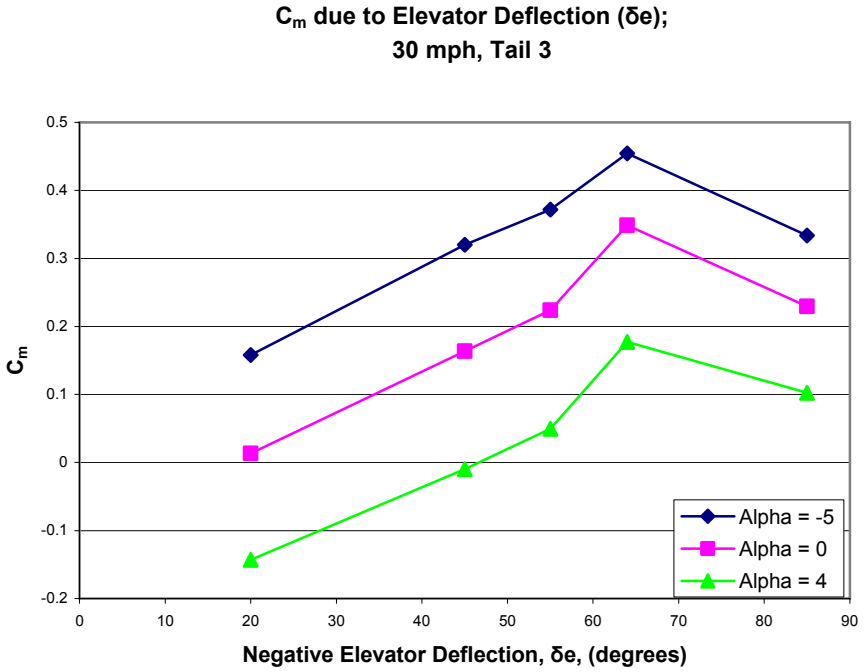

Figure 36. C_m of Tail 3 as a Spoiler, 30 mph

Overall the two tails gave similar results for the spoiler tests. The added increase in deflection was needed to lower the lift coefficient to the value that Tail 1 achieved at a less negative angle. The general shapes of the coefficient plots varied while their values stayed roughly similar. C_L and C_D of the two tails generally did not differ by any more than 0.1, while C_m varied by 0.2 or slightly more.

The attachment of the two tails no doubt had an effect on the pitching moment. Referring to the attachment differences in the tails described in Chapter III, Tail 3 experienced more blockage of its area from the fuselage than Tail 1. As discussed, the attachment also reduced the length of the tail, thus possibly accounting for some of the loss of moment that is evident in Figure 37. Both tails did function as spoilers and would be suitable to act as an air brake upon landing. Tail 3 gave the highest drag for a large negative deflection angle.

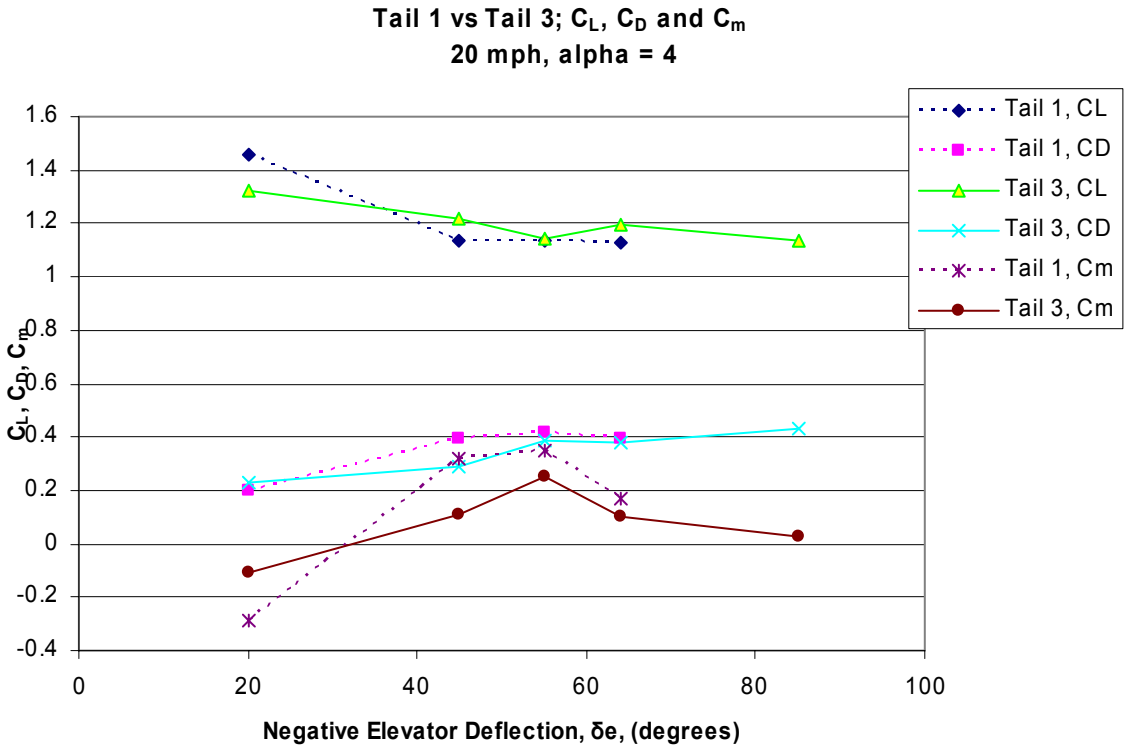

Figure 37. Comparison of Tail 1 and 3 Selected Properties

Rudder and Elevator Characterization

All wind tunnel tests presented in the current section were conducted at an angle of attack of 4^o, $\beta = 0^o$, and at 30 mph. Similar test were conducted by Lt. Parga. However, tests here sought to extend the δ_{rn} range. His test were conducted at and between $\delta_{rn} = +/- 20^o$, while rotation angles in this study were up to $+/- 30^o$.

Data was collected in a matrix form similar to Table 7 and Table 8. Again rotation and deflection angles were measured with a hand-held inclinometer prior to the test and angles were matched with specific trim positions on the hand-held controller. Differences in the rotation angles used were a result of the tail being used. Each tail was

capable of different rotation angles based upon its attachment and constant tweaking of the internal control linkages while changing configurations between tests.

Table 7. Test Matrix for Tail 3

δ_e \ δ_{rn}	-30	-15	-8	0	10	20	30
-30							
-20							
-10							
0							
18							

Table 8. Test Matrix for Tail 1

δ_e \ δ_{rn}	-20	-12	0	7	14	25
-30						
-20						
-10						
0						
18						

Additionally, these tests were performed to determine whether the rotatable tail is a worthy substitute for a rudder and is capable of supplying similar forces and moments as a conventional rudder. The range of rotation angles, for Tail 3, fall within the range of most conventional rudders as they are often limited to +/- 30^o because beyond this range effectiveness falls off abruptly (Perkins, 1958: 329).

Tail effects on Lift coefficient

Results are similar to those in the spoiler characterization section and to those in the thesis of Parga, page 126. Figure 38 and Figure 39 show lift coefficient to be a

function of elevator deflection. It is not affected greatly by rotation angles inside of - 20^o $\leq \delta_{rn} \leq +20^o$. Above the absolute value of 20^o, a slight drop off in lift starts to be noticeable. As the tail rotates the projected horizontal area is becoming a vertical projected area. With area that once was producing lift now producing a side force, loss of lift is expected.

Negative elevator deflection gives a decrease in lift coefficient from the neutral position C_L, while positive deflection gives an increase in lift coefficient. This is consistent with a wing or flat plat producing higher lift when at a positive angle of attack and less lift when at a negative angle of attack.

All contour plots are for $\alpha = 4^o$; which was chosen, not because of maximum L/D, but, because the work of Deluca and Parga was performed at this angle of attack. This allowed a comparison to be easily drawn between values obtained from one study to the next.

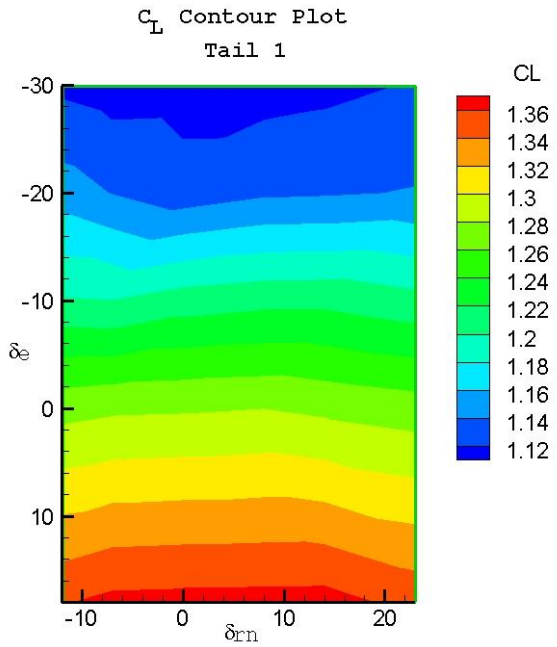

Figure 38. C_L Contour Plot, Tail 1

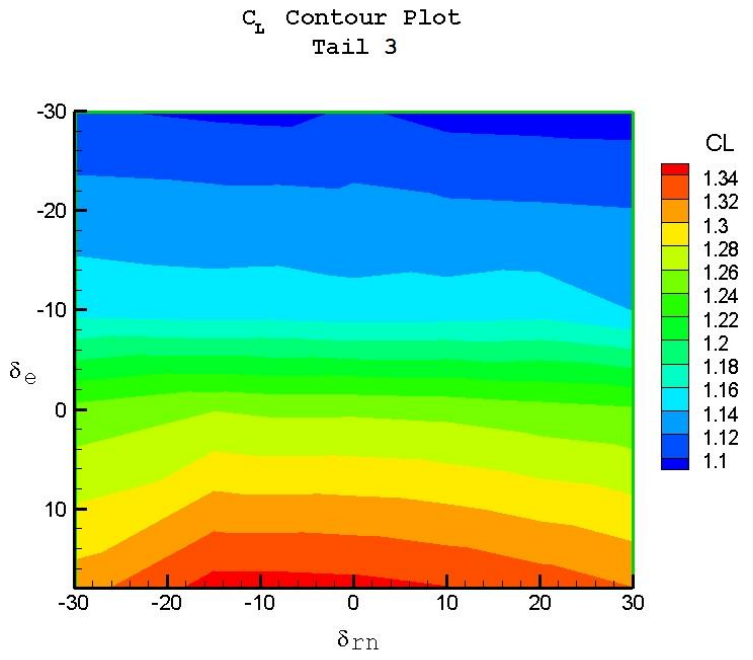

Figure 39. CL Contour Plot, Tail 3

Tail Effects on Drag Coefficient

As would be expected and presented in the spoiler section, drag coefficient is a function of elevator deflection angle. The Tail 1 plot, Figure 40, shows no dependence of drag on δ_{rn}. Plots of both tails show a "drag bucket" where, as elevator deflection is increased from either side of zero, the increase in parasitic drag overcomes the loss of induced drag for a net incase causes an total drag.

A negative δ_e results in loss of lift, as witnessed in Figure 38 and Figure 39. This loss of lift also results in loss of induced drag, however; drag is seen to increase as δ_e increases. The tail acting as a spoiler and increasing form drag is attributed. For a positive δ_e lift is seen to increase once δ_e drops below $\approx 10^o$. The corresponding increase

in induced drag is attributed to the increase seen in Figure 40 and Figure 41, for increasing positive δ_e.

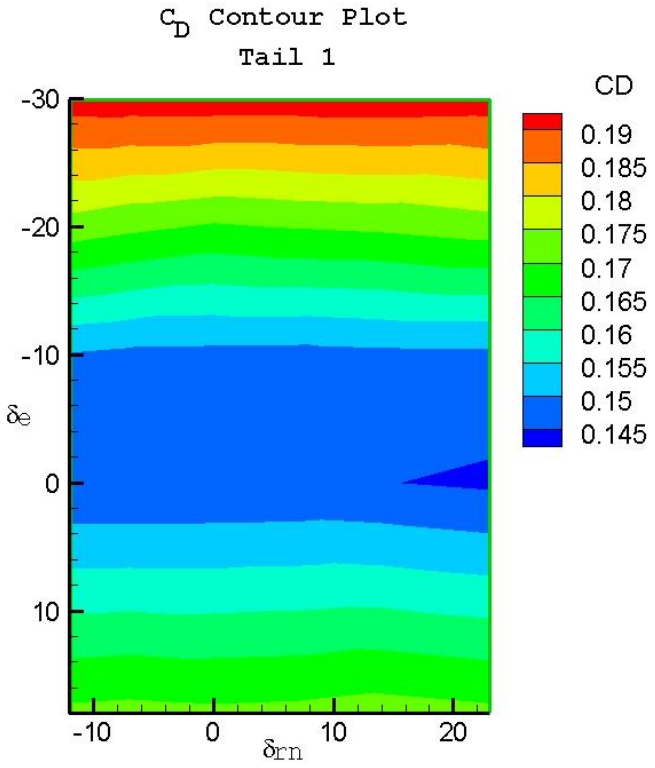

Figure 40. CD Contour Plot, Tail 1

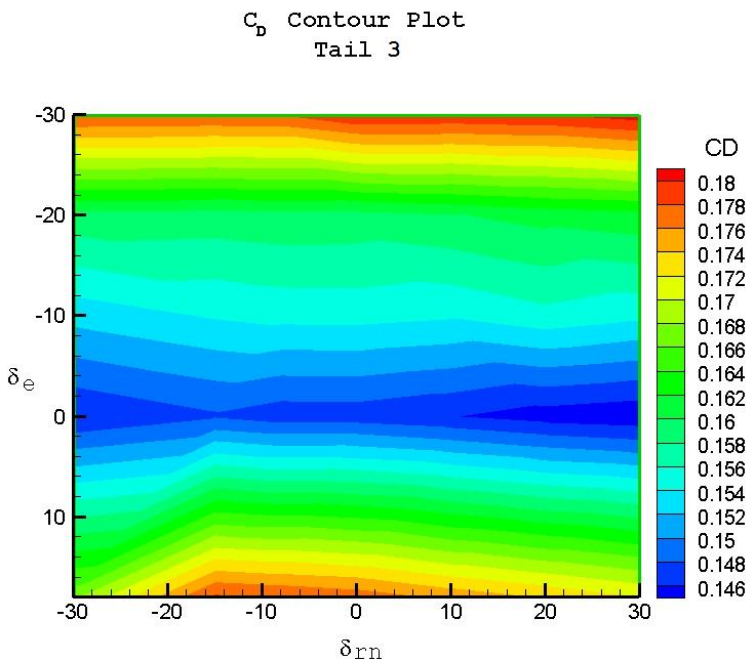

Figure 41. C_D Contour Plot, Tail 3

Tail Effects on Pitch Moment Coefficient

Similar to the characterization in Parga's thesis on page 132, pitch moment was again found to be dependent upon elevator deflection with little influence due to δ_{rn}. Positive elevator deflection gave a negative increase in moment coefficient. Similarly, a negative elevator deflection gives a positive increase in pitch moment coefficient. Values for the moment coefficient are different from those of Lt. Parga. Figure 99 of Parga's thesis, page 133, shows C_m values in the range of 0.0175 to -0.2636 while the current study values in the range of -0.05 to -0.5 were attained with larger deflection angles. This is attributed to a different location of the CG of the MAV but also position of the tail with respect to vertical position of the downwash from the wing must be brought into consideration. Additionally, the new balance block introduced some affects on location of balance CG to MAV CG that were ignored. The wing was also

removed and reattached. Even though it was placed in its original position any difference in incidence angle or location would have an effect of differing values calculated from this and the previous study by changing downwash from the wing. However, values obtained may be changed by varying the CG location. The range of values obtained is the main area of interest.

The data presented does state that the MAV will have a problem trimming because the elevator will have to be deflected to a considerable negative angle which would be detrimental to efficient flight. Based upon the dependence of C_m to CG location, changing the CG would be the best course of action to achieve desirable moment coefficients.

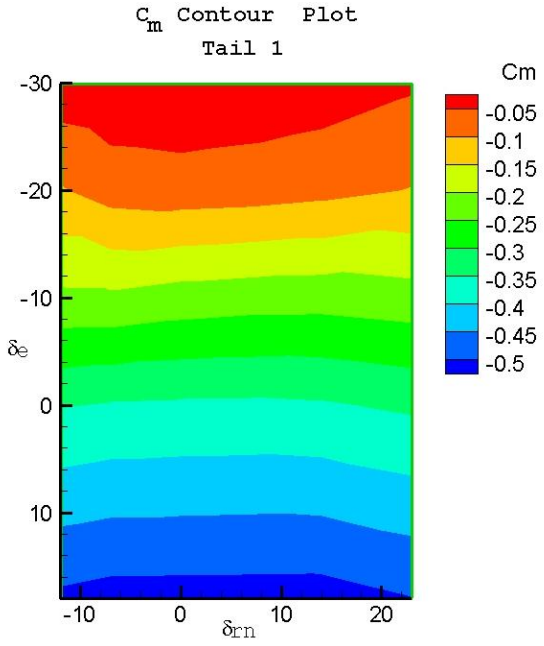

Figure 42. C_m Contour Plot, Tail 1

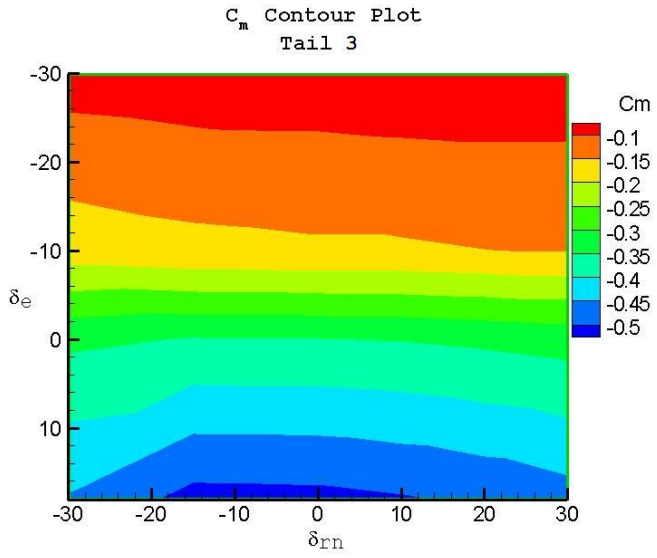

Figure 43. C_m Contour Plot, Tail 3

Tail Effects on Yaw Moment Coefficient

As mentioned earlier in this chapter, the previous study on this subject did not show the rotatable tail measuring up to traditional rudders in yaw moment coefficient. Lt. Parga showed a C_n range of -0.013 to +0.013 for tail 1. A typical rudder has a C_n range of -0.02 to + 0.02 (Barlow et. al., 1999: 527).

Behavior exhibited by the tail on C_n, is again similar to previous observations. (Parga; 2004). Tests conduced pointed to the following behavior of C_n with respect to tail movements.

1. C_n is a combination of δ_e and δ_{rn}.
2. Positive δ_e and δ_{rn} is seen to produce more favorable C_n values for a turn. This is similar to some observations of birds using a depressed and twisted tail to execute a level turn.

3. Control reversal is possible. For a given δ_e and δ_{rn} a value of C_n is achieved. Changing δ_e only will result in a change in the sign of the C_n value. Thus leading to a different yaw than was originally commanded.

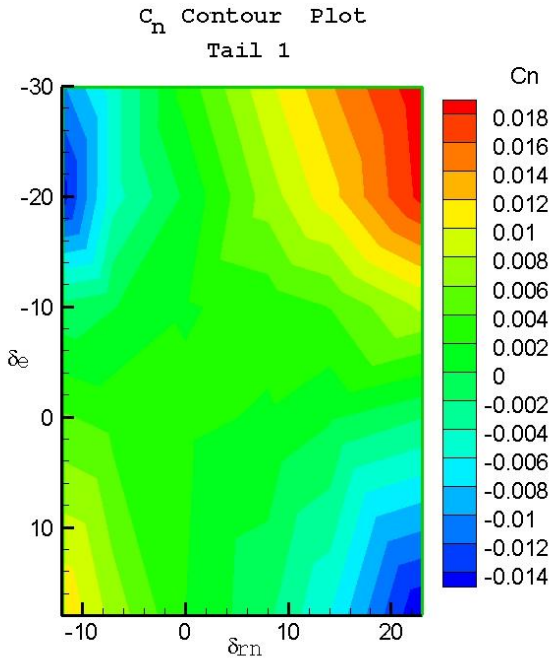

Figure 44. C_n Contour Plot, Tail 1

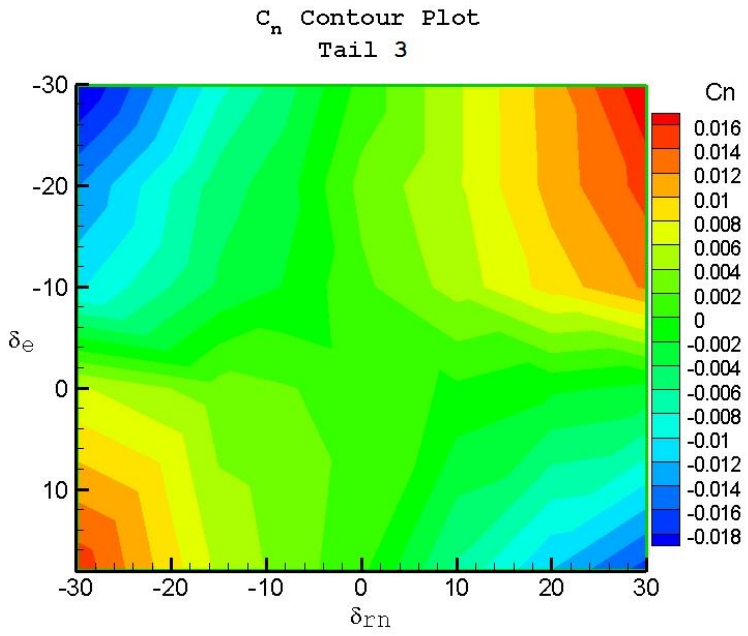

Figure 45. C_n Contour Plot, Tail 3

The greatest change in C_n range is seen in Figure 45 for Tail 3, as it had the highest rotation angles, -30^o to $+30^o$. Tail 3 was capable or reaching a C_n value of -0.02 however it reached a slightly less positive value 0.016. This showed that the rotatable tail is capable of delivering essentially the same values as a typical rudder. Extending the range of C_n is possible, and will be discussed in a future section on improving stability.

Figure 46 represents a rudder power curve for a traditional rudder. The data from this figure is plotted in Figure 47 and Figure 48 against values obtained for Tail 1 and Tail 3. The severity of the elevator deflection greatly affects the rudder power the tail generates. An equivalent range and slope to that seen Figure 46 is achieved by the rotatable tail at the large negative elevator deflection.

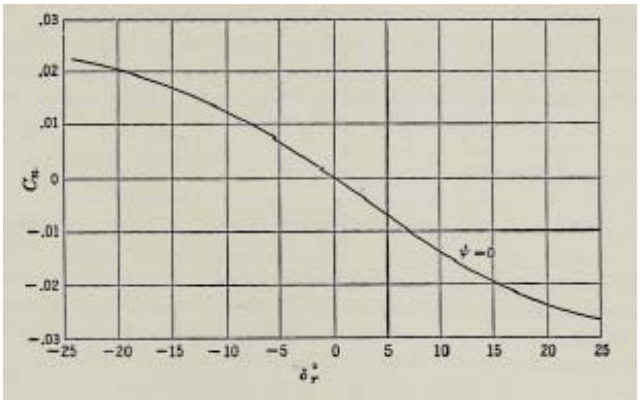

Figure 46. Rudder Power Curve (Perkins, 1958: 330)

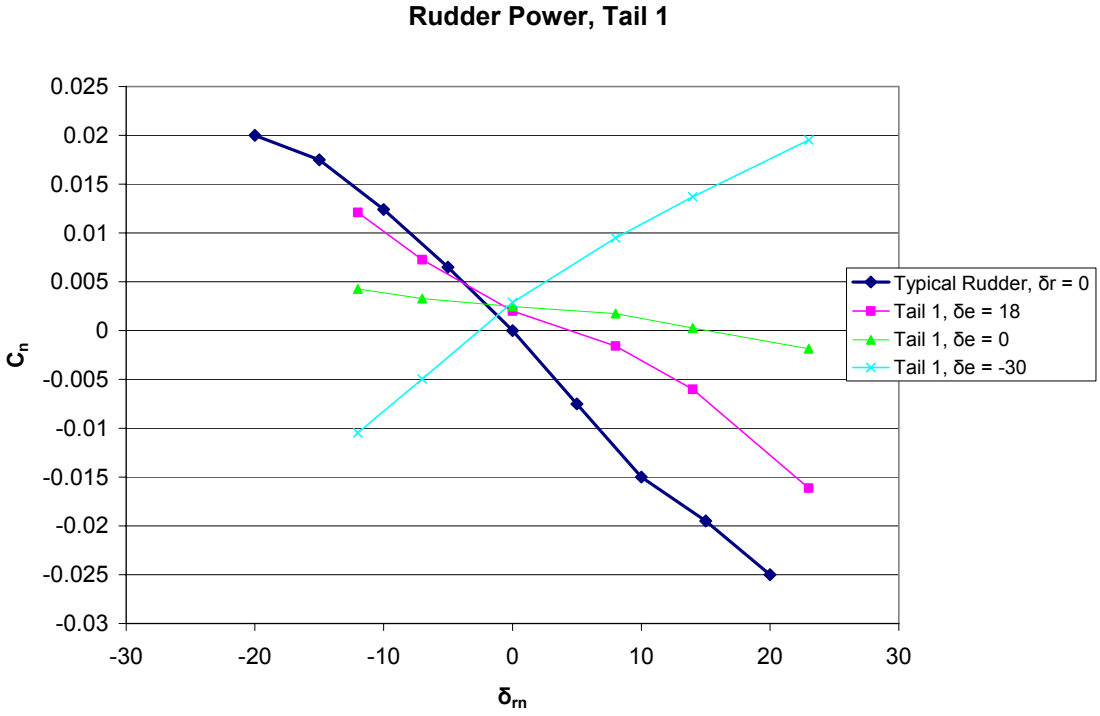

Figure 47. Rudder Power Curve for Tail 1

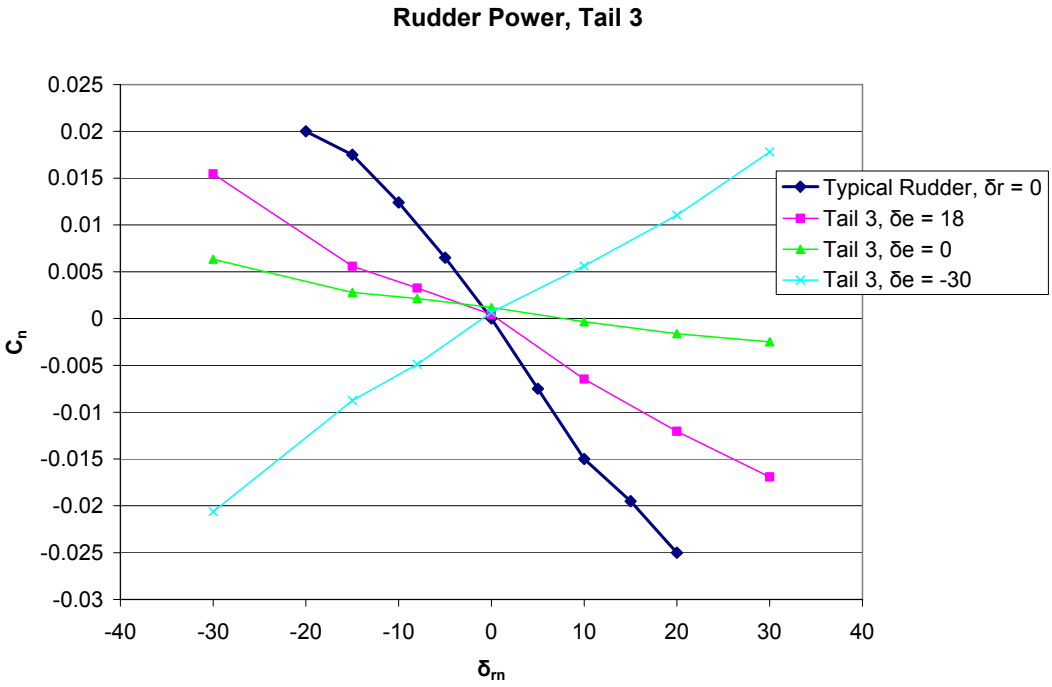

Figure 48. Rudder Power Curve for Tail 3

Tail Effects on Roll Moment Coefficient

Similar characteristics were found between prior results and data taken for this test (Parga; 2004). The rotatable tail did not display the amount of roll control that is present in aileron control surfaces. Tail 3 does not display any noteworthy differences over Tail 1 as far as roll moment coefficient is concerned. The effects of both rotatable tails are characterized by roll moment being a function of both δ_e and δ_{rn} with the largest achieved values being at the extremes of each commanded angle, as evidenced in Figure 49 and Figure 50.

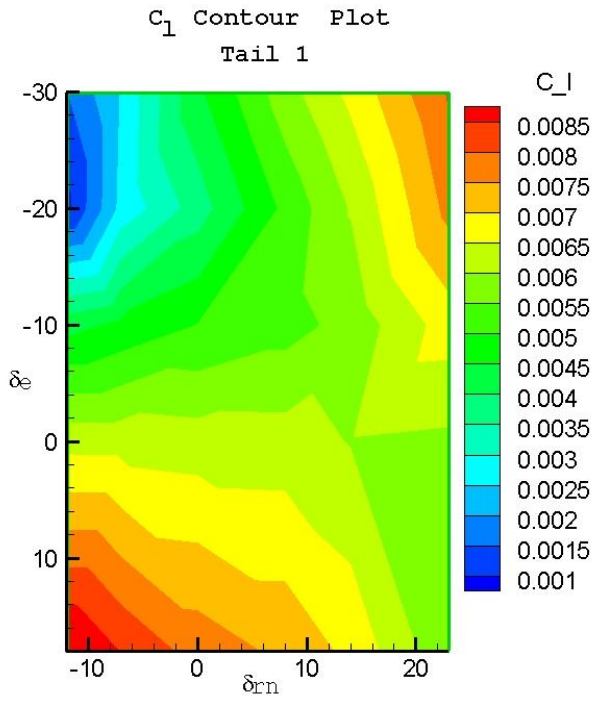

Figure 49. C_l Contour Plot, Tail 1

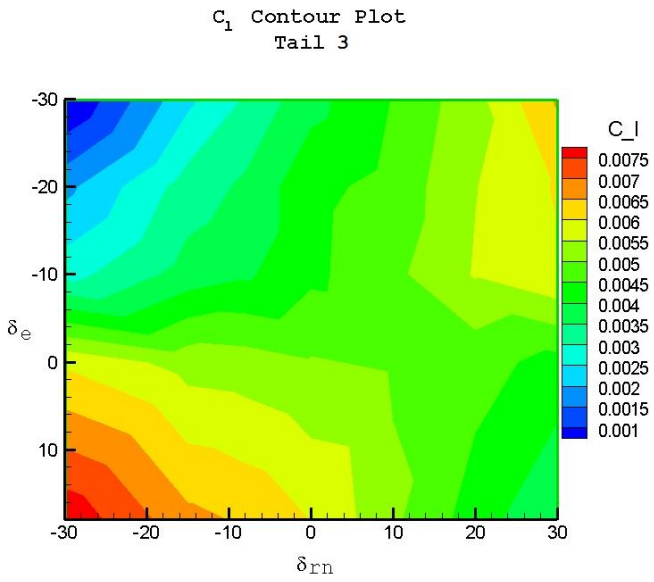

Figure 50. C_l Contour Plot, Tail 3

Directional Stability Investigation

As presented earlier, the aircraft configured with the rotatable tail exhibits problems with directional stability. An attempt to alleviate this problem was carried out in research done by Parga by attaching vertical stabilizers to a rotatable tail. This was found to improve stability some but not enough to be considered stable. Reviewing the stabilizer used in this study it consisted of an area of 7.13 in^2 attached at the lower aft end of the fuselage. The vertical tail coefficient for the stabilizer is 0.04 for the tail with δ_e and $\delta_{rn} = 0^o$, and the horizontal tail coefficient is 0.34. The tail coefficient values would change with a change in δ_{rn}. If δ_{rn} was deflected to 90^o, horizontal tail coefficient would be 0 while vertical tail coefficient would be greater than .34, due to the contribution of tail area being projected vertically. Chapter 3 describes the stabilizer more completely and Table 2 gives stabilizer properties.

Data was taken by varying β angles. β had the range of -8^o to $+8^o$ for this test. Angle of attack was held constant at 4^o and the tunnel speed was 30 mph. Data was taken for both Tail 1 and Tail 3, each with and without the stabilizer attached. Some of the following plots are duplicates of those presented earlier; this is done for ease of comparison. The stabilizer had little effect on the tail C_L, C_m, and C_D. The stabilizer no doubt added drag, but did not affect the tail contribution of drag other than causing minor flow interference at the positive angles of elevator deflection.

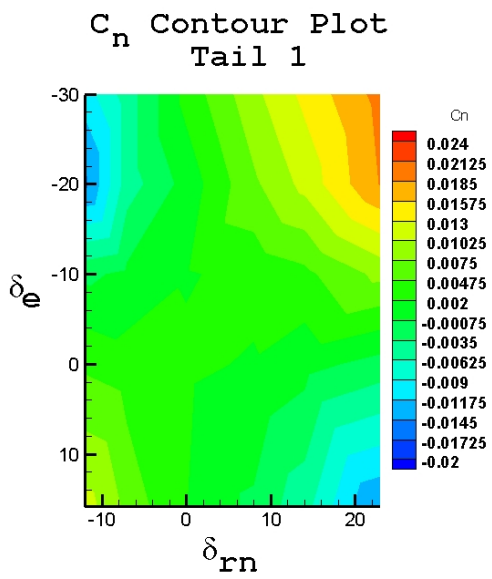

Figure 51. C_n Contour Plot, Tail 1

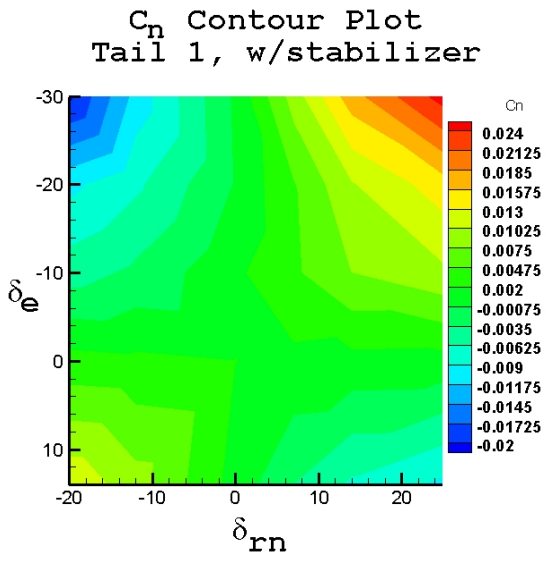

Figure 52. C_n Contour Plot, Tail 1 w/stabilizers

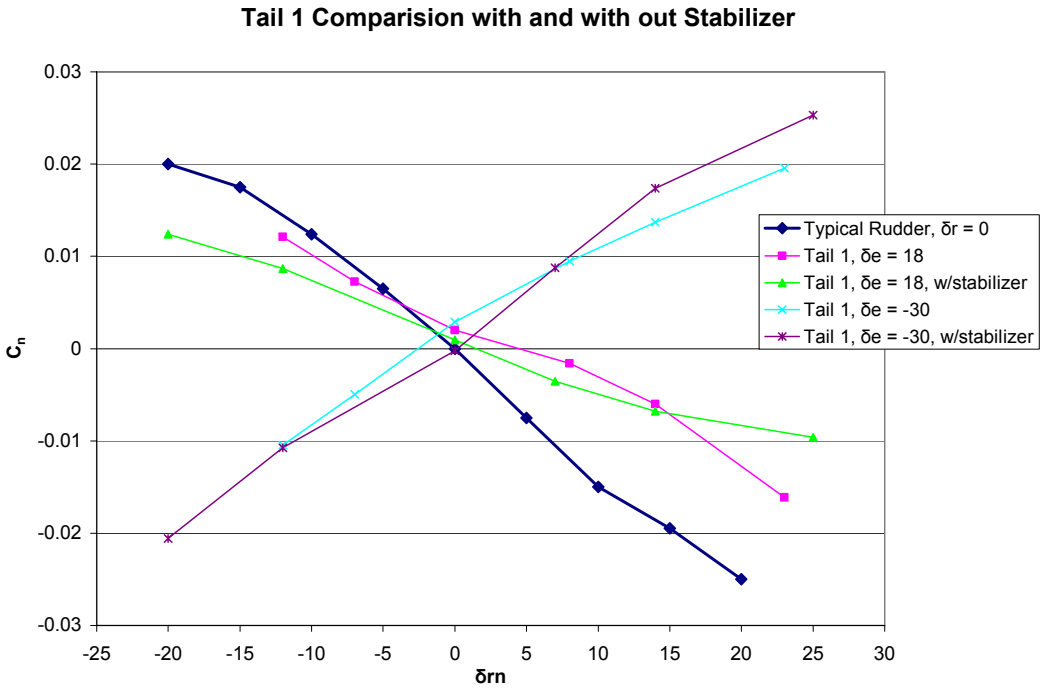

Figure 53. Tail 1 Stabilizer Comparison

The stabilizer did have the effect of increasing the range of C_n. The properties of the tail with respect to C_n were kept the same as without a stabilizer. The stabilizer's affect on Tail 3 again served to increase the C_n range. It did however slightly decrease the positive range from 0.016 to 0.01. C_n properties remained the same as discussed in the elevator/rudder section. The stabilizers did have the affect of allowing a larger value of yaw coefficient to be reached for each incremental increase in δ_e and δ_{rn}. Both plots, Figure 54 and Figure 55, show how elevator and rotation deflection must be used together to achieve an effective yaw moment.

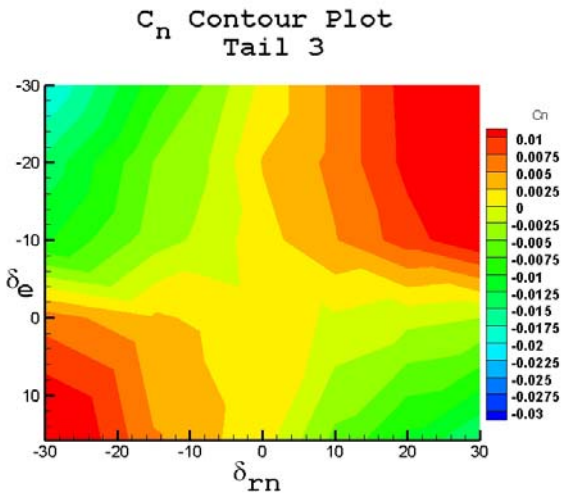

Figure 54. C_n Contour Plot, Tail 3

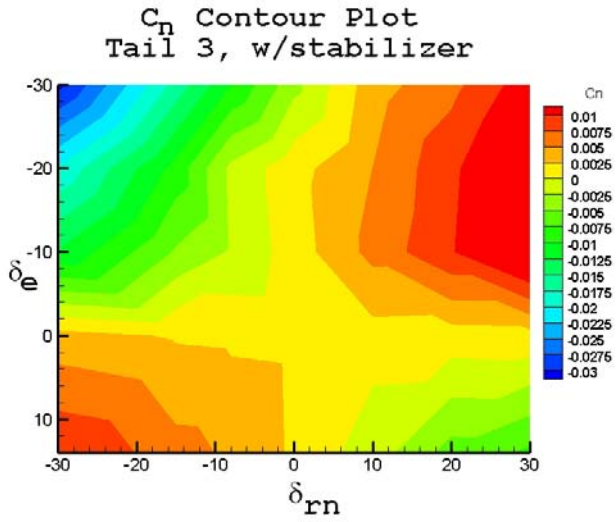

Figure 55. C_n Contour Plot, Tail 3 w/stabilizers

Comparison charts show that it is possible for both tails to give the same yaw moment coefficient values as a traditional rudder despite the relative small tail volume coefficients. A typical rudder will provide a C_n of ± 0.02. The configurations and deflections used in this study produced maximum absolute values of 0.018 and 0.03. Figure 56 allows a comparison between a typical rudder and the tails tested to be drawn.

The range and attainable values are shown to be similar. While the slope of C_n for the tested tails is not as great as that of a typical rudder, the attainable values are of more interest. Even though an additional 10^o of rotation is needed the desirable value of 0.02 is reached.

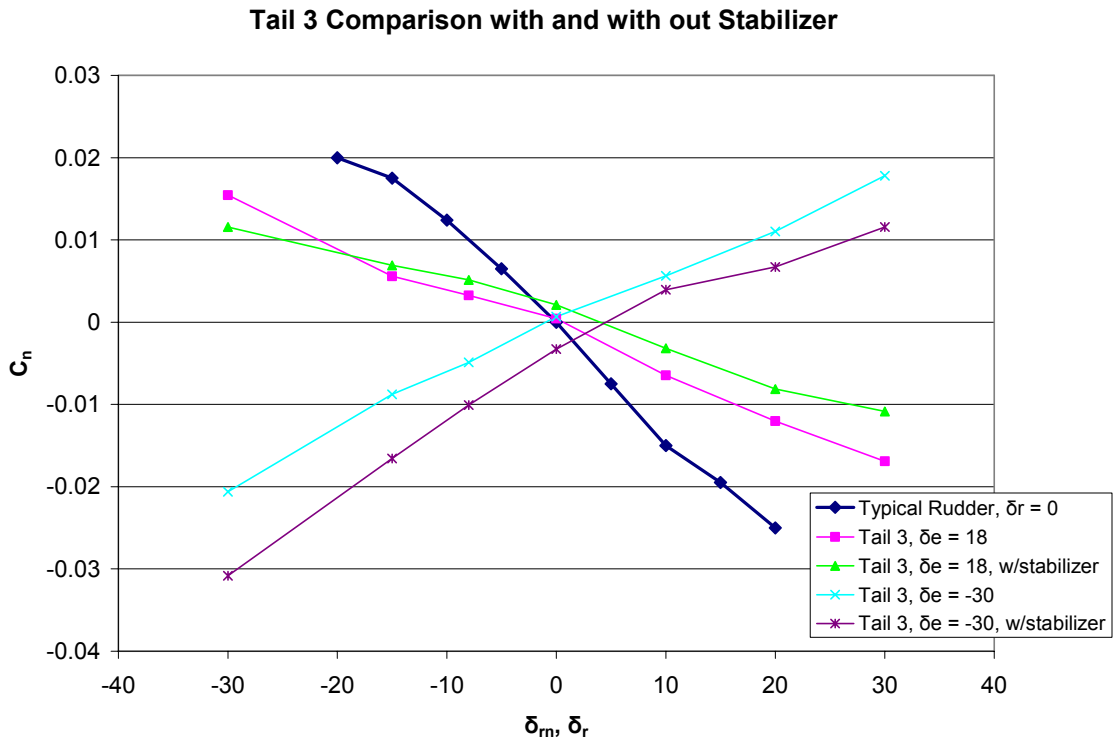

Figure 56. Tail 3 Stabilizer comparison

The stabilizer had a mixed effect with regards to directional stability at a cruise condition, $\delta_e = 0^o$. The stabilizer did have the affect of improving stability for both Tail 1 and Tail 3 when no rotation deflection is present. When a δ_{rn} is present the stabilizers had the affect reducing the C_n maximum values. However, the slope of the C_n curve was increased. The stabilizers generally shifted the C_n curve down to what a typical curve would look like with 0^o yaw producing a zero C_n value. The data presented in Figure 57 and Figure 58 show that with and without stabilizer, the MAV would be more

directionally stable in a turn, i.e. with a δ_{rn} of a value other than zero. A typical data set for both directional and roll stability is shown in Figure 59.

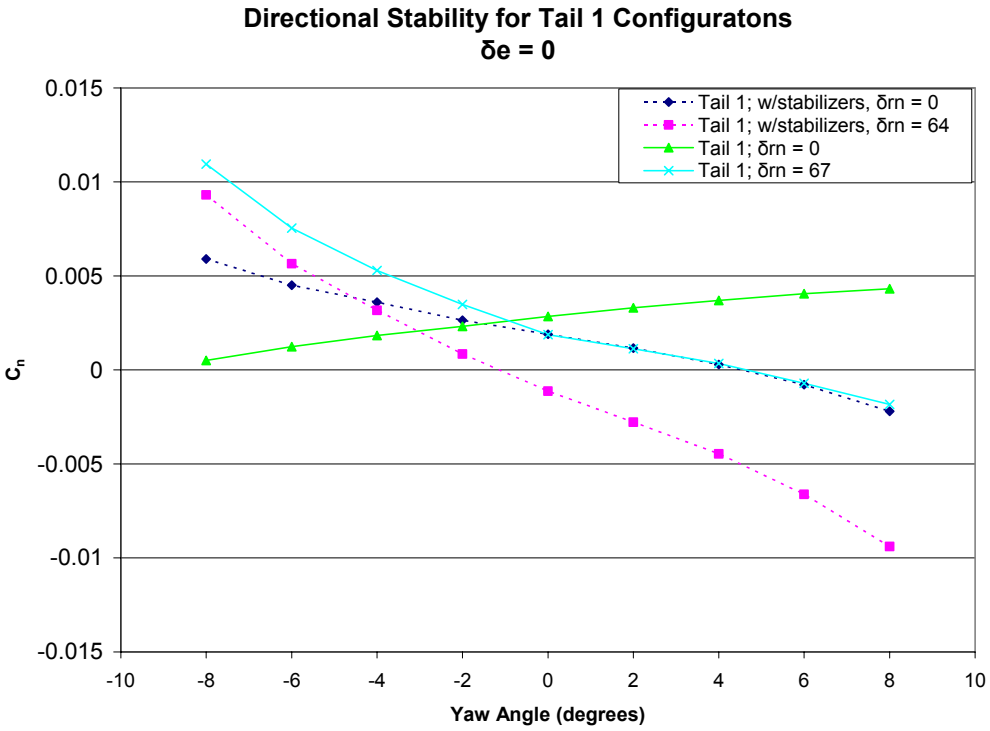

Figure 57. Directional Stability Tail 1 Configurations

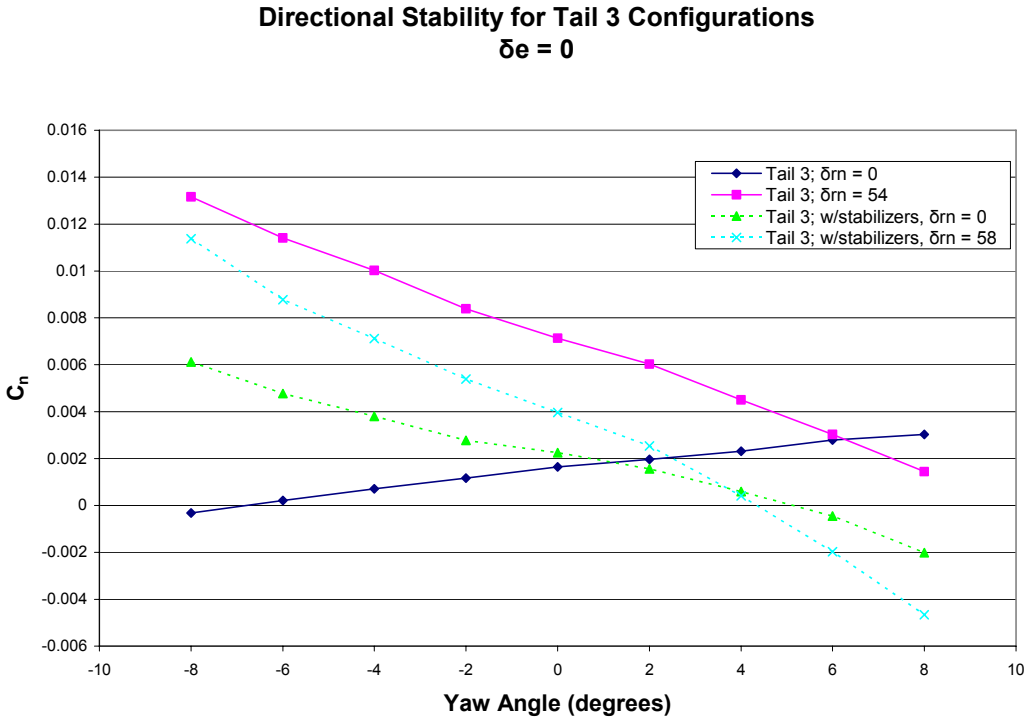

Figure 58. Directional Stability Tail 3 Configurations

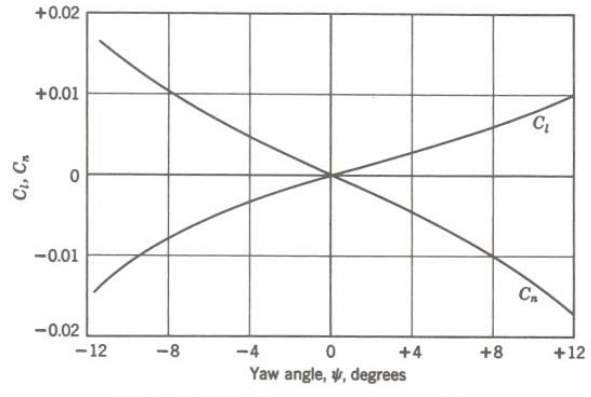

Figure 59. Typical Yaw Characteristics (Barlow et al, 1999: 531)

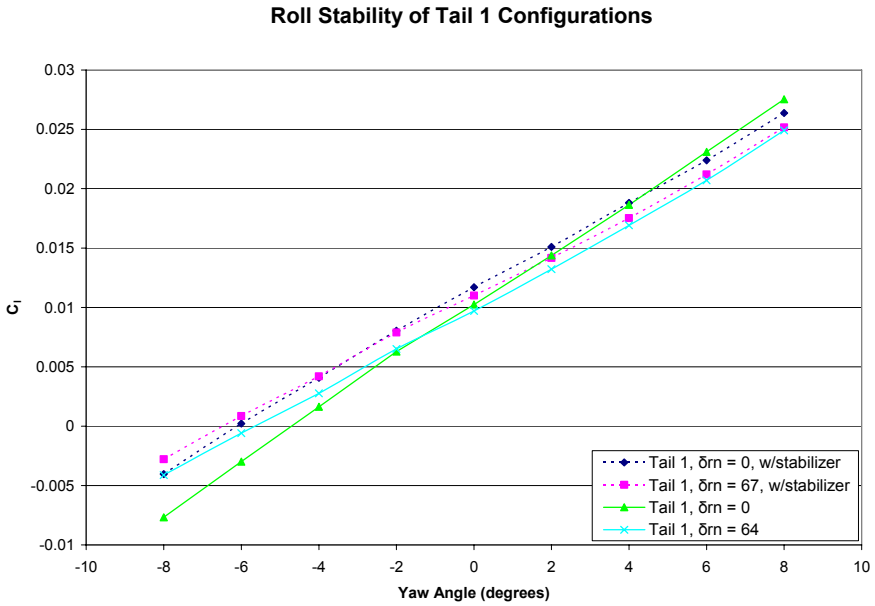

Figure 60. Roll Stability, Tail 1

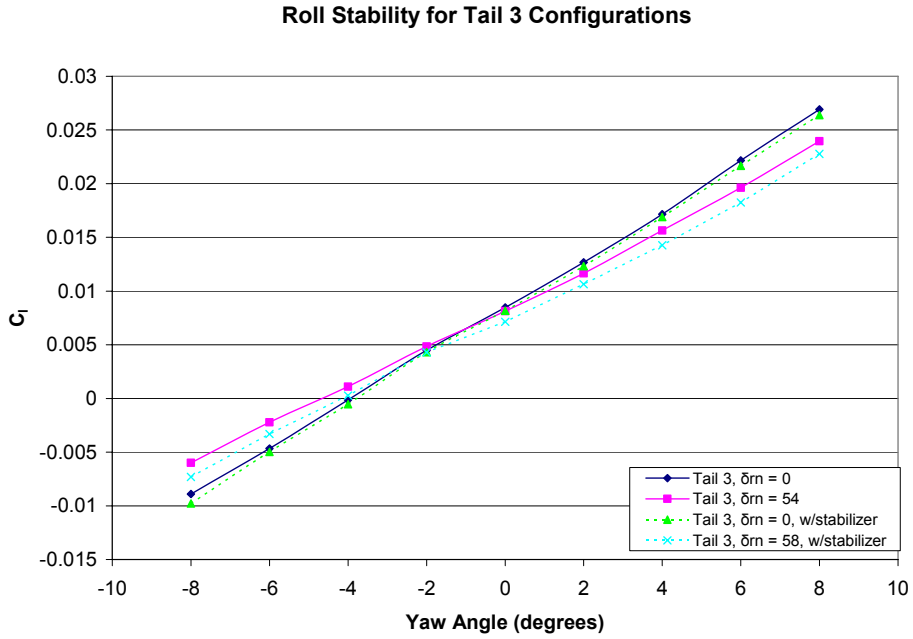

Figure 61. Roll Stability, Tail 3

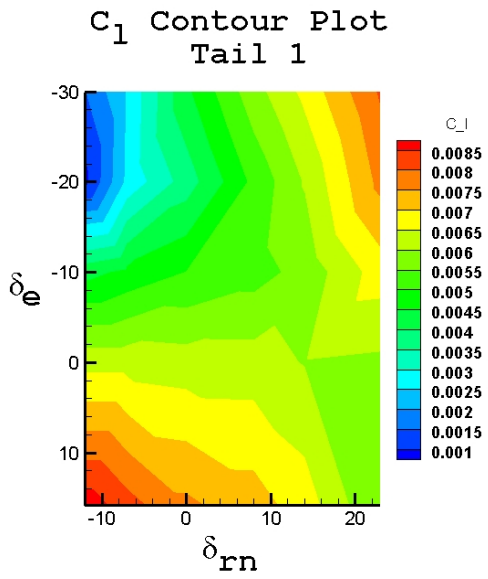

Figure 62. C_l Contour Plot, Tail 1

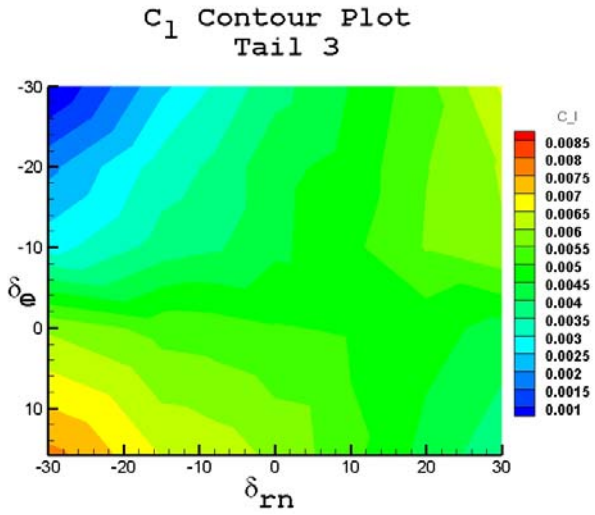

Figure 64. C_l Contour Plot, Tail 3

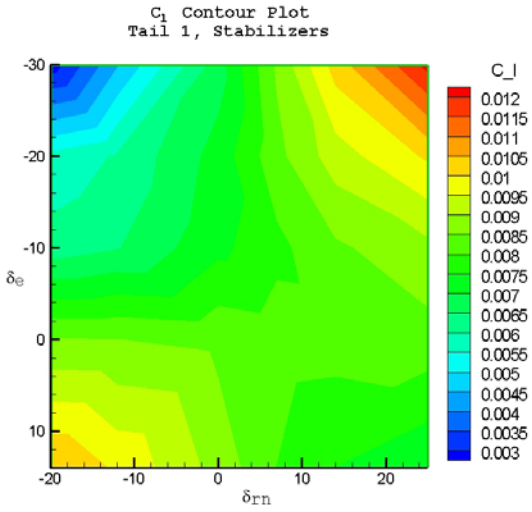

Figure 63. C_l Contour Plot, Tail 1 w/stabilizers

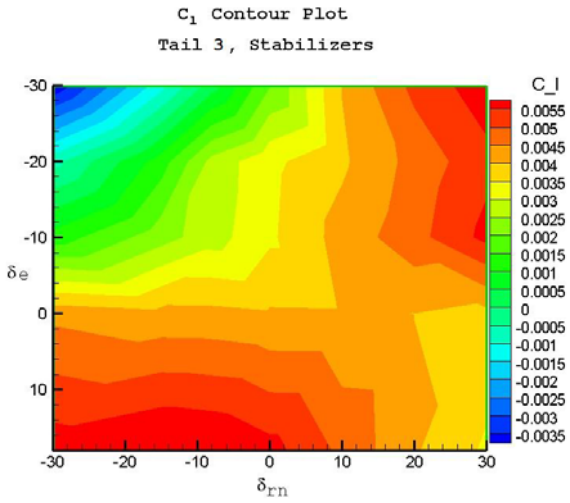

Figure 65. C_l Contour Plot, Tail 3 w/stabilizers

The roll moment coefficient is only slightly affected by the rotation of the tail.

Common values are within the range of -0.02 to + 0.02, when an aileron is used (Barlow

et al, 1999: 500). The range of values obtained with the rotatable tail was about ten times smaller, as shown in Figures 60-65.

Stabilizers had little effect on roll moment coefficient properties and more on the range of C_l value. Clearly, from comparing the four figures directly above, the effect on Tail 1 is extending the attainable values. The small offset from $C_l = 0$ has also been noted by DeLuca and Parga. One possible reason may be that a slight offset in the wing attachment exists.

The directional stability of the MAV is probably the area of greatest improvement and offers the most improvement for future development. As stated before the original MAV with the rotatable tail had directional stability problems. The work of Parga added stabilizers to the tails to address this problem, but this complicated the results. Adding stationary vertical stabilizers in the manner of this study again improved stability but not enough to be considered a satisfactory stable model. The lack of stability would require automatic controls if it were to be flown by a human pilot. Improving stability to an acceptable level would allow a human to pilot the model with simply a remote control transmitter.

Static stability derivatives calculated by Lt. Parga are displayed in Table 9.

Table 9. Static Stability Derivatives by Lt. Parga

Derivative	Tail 1	Tail 2	Original UAV	Generic Value
$\partial C_m / \partial \alpha$ *	-0.0166	-0.01	-0.0466	-0.0119
$\partial C_n / \partial \beta$	-0.0003	0.0007	0.00078	0.00123
$\partial C_l / \partial \beta$	-0.0018	-0.0017	-0.00076	-0.00129

* CG dependent

Figure 66 represents the correlation of C_n and C_l stability derivatives with respect to yaw and their affect on stable flight.

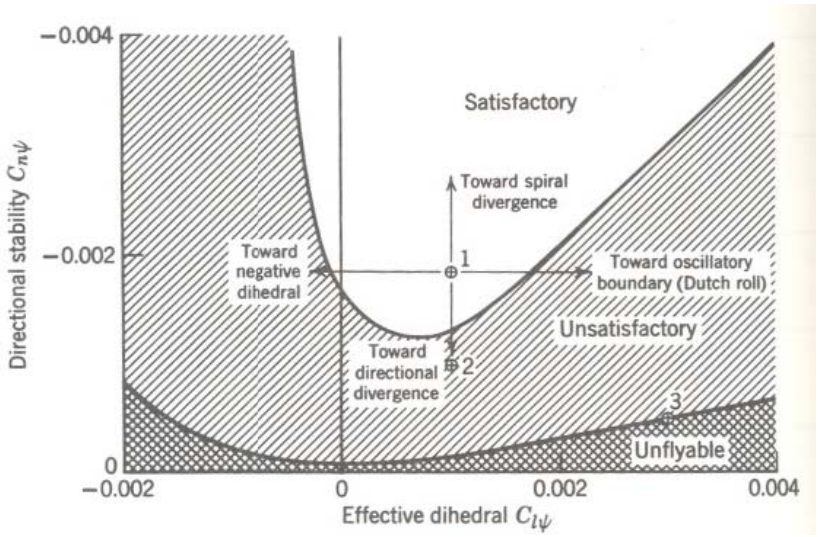

Figure 66. Stability Combinations of $C_{n\psi}$ and $C_{l\psi}$ (Barlow et al, 1999: 530)

Changing the derivatives in Table 9 so they are with respect to yaw angle, will allow a more direct comparison with the data presented in this study, in which derivatives are given with respect to yaw angle. Similar stability derivates found in this test for both the stabilizer on and off conditions are presented in the following table, Table 10, for which elevator and rotation deflection were zero.

Table 10. Static Stability Derivatives

Derivative	Tail 1	Tail 3	Tail 1 w/stabilizer	Tail 3 w/stabilizer
$\partial C_n / \partial \psi$	0.0002	0.0002	-0.0005	-0.0005
$\partial C_l / \partial \psi$	0.0022	0.0019	0.0022	0.0022

Recalculating the derivatives with a rotation angle present allows the fact that the MAV is more stable in a turn than when in straight level flight to be witnessed. Table 11, below, is one condition for Tail 3 with stabilizers and rotation deflection of 54^o.

Table 11. Static Stability Derivatives for $\delta_{rn} = 54^o$

Derivative	Tail 3
$\partial C_n / \partial \psi$	-0.0009
$\partial C_l / \partial \psi$	0.0018

Plotting values from each of the above tables onto Figure 71 gives an idea of how the MAV performs with respect to directional stability.

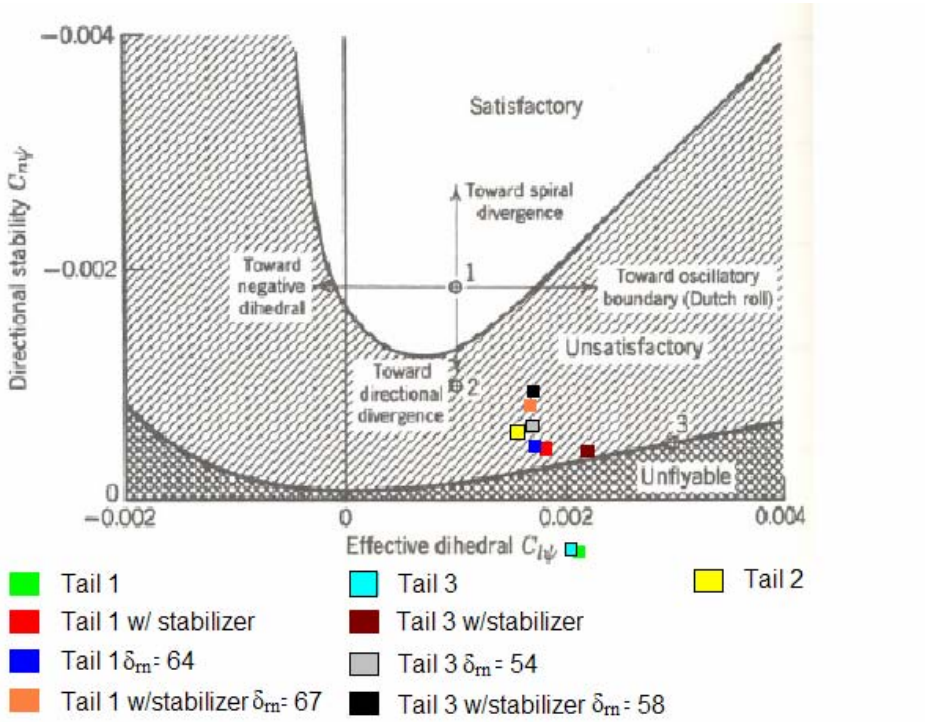

Figure 67. Plotted Stability Derivatives (Barlow et al, 1999: 530)

Taking the above figure and the relative "weakness" of the stability derivatives leads to one conclusion about the stability of the MAV. The CG of the MAV is too far aft or rather too much of the model is forward of the CG. Parga mentioned this in his thesis and conducted a study on how CG affects the MAV stability.

Limitations of Experimental Effort

No matter how meticulous one is in set up and data acquisition, errors will always be present. Numerous sources of error in this study are easily identifiable. The first error source was discussed in previous chapters with the drift in tail δ_e due to dynamic pressure and its actuation and structural limits. Additionally, deflection and rotation angle drifts were present when using the remote controller to adjust the tail position. Ideally moving controller settings from one position to another and then back again should have produced the original commanded deflection or rotation. However this was not the case due to errors within the hand held controller, servo actuation system, and tail attachment all compounding upon one another. Lt. Parga suggests variations of -2^o to $+2^o$ in controller settings. This test found that similar variations were present.

Balance accuracy is another source of error. The AFIT-1 balance limited resolution. Reviewing Appendix B and the balance calibration plots, shows that the accuracy of the balance is consistent throughout the range of loadings. Table 12 describes the resolution of the balance for the varying forces and moments it measures.

Table 12. Balance Error

Measurement	Resolution (lbf)	Accuracy (%)
Normal Force	0.012	0.12%
Axial Force	0.002	0.04%
Side Force	0.0035	0.07%
Pitch Moment	0.005	0.05%
Roll Moment	0.0044	0.11%
Yaw Moment	0.0035	0.07%

The tail attachment, discussed in Chapter III, is not perfectly symmetric. This accounts as a partial explanation for some of the forces and moments not being zero or centered about δ_e and δ_{rn} of zero degrees. Figure 68 taken from Lt. Parga displays the asymmetric attachment of the tails.

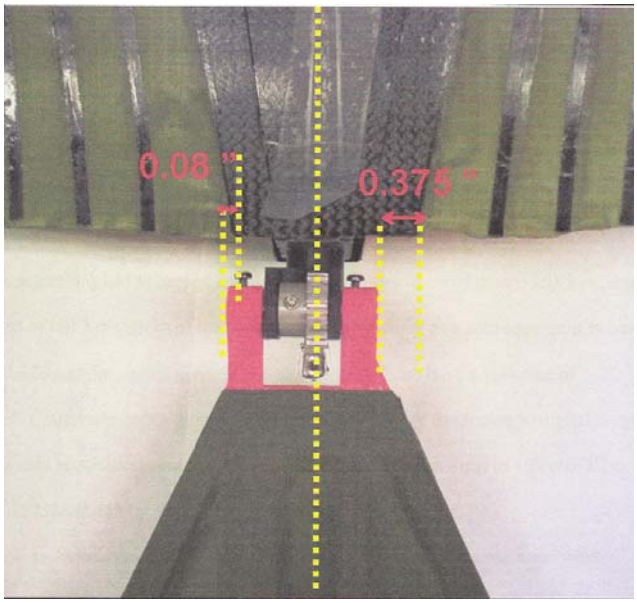

Figure 68. Asymmetric Attachment of Tails

Minute mathematical errors were introduced by MATLAB which used a 4^{th} degree polynomial to calculate tare values (Parga, 2004: 159). The MATLAB software had a floating point precision 2.22×10^{-16}. Using a 4^{th} order polynomial vice a 5^{th} order introduced an errors starting at the 1×10^{-5} decimal place. Errors introduced into the test signal by the quantization of the analog to digital converter 16 bit acquisition card had an accuracy of ±1.53 micro volts (DeLuca, 2004: 131). These error sources, though present, are insignificant.

V. Conclusion

This study sought to determine whether the rotatable tail can: be used to aid a survivable recovery; provide a yaw moment equal to that of a traditional tail configuration; and be utilized on a directionally stable aircraft. Extending the range of deflections added to data and plots that were produced in that theses and provided a more complete picture of the characteristics of the rotatable tail. It was noted that the physical values obtained were slightly different from those reported earlier (Parga; 2004). A difference in the CG reference position has been noted as a probable cause. Additionally, changes in wing position and incidence angle to the fuselage may attribute to these differences. The range of obtained values remains the most important factor in tests conducted. Extending the deflection angles resulted in an increase of the range of achievable yaw moment coefficient values.

The research completed by Parga concluded that the rotatable tail was capable of providing roughly 65% of the yaw control force of a typical rudder. This study proved that the rotatable tail configuration was capable of providing yaw control equivalent to a normal rudder. Roll control was less than the typical desired value, but was comparable to that achieved with the original MAV with the V-Tail (DeLuca; 2004).

The rotatable tail with large negative δ_e, less than negative 40^o, changes from a streamlined lifting surface to a bluff body producing drag to slow the velocity of the MAV. Research conduced showed that the general trend from increasing negative δ_e was a reduction in C_L and an increase in C_D.

By extending the range of elevator and rotation deflection (δ_e and δ_{rn}), the rotatable tail is capable of delivering a yaw similar to that of a traditional redder, despite a small tail volume coefficient. However, the coupled controls mandate a more complex flight control system.

The large area of the model forward of the CG counteracts the stabilizing affects the tail and stabilizer produces. A longer moment arm is needed between the tail and the CG to improve directional stability, and is recommended. The large elevator deflection needed to trim the MAV for level flight also confirms this conclusion. To achieve a more forward CG, the wing should also shift forward.

This solution would allow for the increase in moment arm desired while negating pitch and trim problems of having the CG far forward of the wing.

Suggestions for future work include:

1. Developing a mixing algorithm to account for or use the control reversal to an advantage in a remote control device.
2. Moving the wing forward to allow for more tail effectiveness.
3. Consider, increasing the size of the tail, thereby slightly increasing length of the moment arm and area that is capable of providing control.
4. Consider, increasing stabilizer size to improve stability.

Appendix A: Data Tables

*Tail 3 is referred to as Tail 2 in data tables.

Table 13. Spoiler Run Data, Tail 1 w/stabilizer

Beta	Delta e	Delta rn	Tail	stabalizers	M#	Re#	q_c	Uoo	alpha_c	C_L	C_D_c	Cl_cg_w	Cm_cg_c	Cn_cg_w	C_Y\r
0	64	0	1	1	0.02635	89826.4	1.0004	20.4124	-4.9335	0.15045	0.34857	0.00247	0.48379	-0.006	0.00263
0	64	0	1	1	0.02632	89730	0.99825	20.3905	0.48235	0.79735	0.36569	0.00652	0.33931	-0.0054	-0.015
0	64	0	1	1	0.02622	89383.7	0.99056	20.3118	4.7732	1.25864	0.42961	0.00884	0.17556	-0.0052	-0.0282
0	20	0	1	1	0.02637	89905.8	1.00217	20.4305	-4.8147	0.41941	0.12595	0.0033	0.17964	0.00166	-0.0209
0	20	0	1	1	0.02633	89760.6	0.99893	20.3975	0.61074	1.08789	0.14669	0.00767	-0.0143	0.00207	-0.037
0	20	0	1	1	0.02622	89380.4	0.99049	20.3111	4.89874	1.54273	0.23084	0.01092	-0.2412	0.0018	-0.0492
0	45	0	1	1	0.02645	90186.3	1.00843	20.4942	-4.9135	0.19583	0.27119	0.00257	0.56789	-0.0036	-0.0048
0	45	0	1	1	0.0264	89996.3	1.00419	20.451	0.50869	0.85696	0.2718	0.00663	0.38763	-0.0026	-0.0219
0	45	0	1	1	0.02636	89872.5	1.00142	20.4229	4.8011	1.32179	0.33285	0.0095	0.16564	-0.0022	-0.0358
0	55	0	1	1	0.02614	89127.9	0.9849	20.2537	-4.9271	0.16486	0.33959	0.00209	0.49831	-0.0063	0.00434
0	55	0	1	1	0.02617	89211.7	0.98675	20.2727	0.49449	0.82483	0.35275	0.00595	0.34424	-0.0054	-0.0144
0	55	0	1	1	0.02612	89057.2	0.98334	20.2376	4.78139	1.27718	0.42204	0.00872	0.18388	-0.0054	-0.0276
0	20	0	1	1	0.0384	130904	2.12457	29.747	-4.8462	0.34815	0.09439	0.00111	0.11842	0.00113	-0.0162
0	20	0	1	1	0.03834	130729	2.1189	29.7073	0.52885	0.90256	0.10757	0.00419	-0.0441	0.00211	-0.0334
0	20	0	1	1	0.03823	130354	2.10674	29.622	4.77578	1.26447	0.16172	0.00702	-0.2175	0.00244	-0.0444
0	45	0	1	1	0.03803	129653	2.08416	29.4628	-4.9517	0.10937	0.28329	0.00073	0.56501	-0.0037	-0.0026
0	45	0	1	1	0.03831	130617	2.11525	29.6817	0.41758	0.65078	0.26884	0.00292	0.4101	-0.0024	-0.0194
0	45	0	1	1	0.03831	130608	2.11496	29.6797	4.67485	1.03609	0.30687	0.00557	0.23163	-0.0018	-0.0308
0	55	0	1	1	0.03818	130182	2.10119	29.5829	-4.9498	0.11364	0.27908	0.00052	0.55959	-0.0032	-0.0044
0	55	0	1	1	0.03818	130164	2.10061	29.5788	0.42186	0.66047	0.26938	0.00308	0.41162	-0.002	-0.021
0	55	0	1	1	0.0382	130234	2.10286	29.5947	4.67889	1.04522	0.30743	0.00551	0.23173	-0.0013	-0.0326
0	64	0	1	1	0.03823	130331	2.10602	29.6169	-4.9344	0.14835	0.26656	0.00063	0.41896	-0.0038	-0.0018
0	64	0	1	1	0.0382	130243	2.10317	29.5969	0.40469	0.62161	0.31941	0.00264	0.45756	-0.0037	-0.0169
0	64	0	1	1	0.03827	130471	2.11054	29.6486	4.65972	1.00186	0.35135	0.00504	0.28786	-0.0032	-0.028

Table 14. Spoiler Run Data, Tail 1

Beta	Delta e	Delta rn	Tail	stabalizers	M#	Re#	q_c	Uoo	alpha_c	C_L	C_D_c	Cl_cg_w	Cm_cg_c	Cn_cg_w	C_Y\r
0	20	0	1	0	0.0274	93407.5	1.08175	21.2262	-4.8075	0.43562	0.09941	0.00311	0.09665	-0.0011	-0.0066
0	20	0	1	0	0.02733	93177.7	1.07644	21.174	0.59845	1.06007	0.12399	0.00683	-0.0838	-0.0003	-0.0196
0	20	0	1	0	0.02729	93042.4	1.07331	21.1432	4.8605	1.4562	0.20221	0.00896	-0.2852	-0.0003	-0.0293
0	45	0	1	0	0.02732	93140.5	1.07558	21.1655	-4.9521	0.10841	0.34595	0.00163	0.65719	-0.0077	0.00794
0	45	0	1	0	0.02735	93236.9	1.07781	21.1874	0.4449	0.7126	0.34456	0.00428	0.50961	-0.0067	-0.0049
0	45	0	1	0	0.02732	93139	1.07554	21.1652	4.71971	1.13761	0.39579	0.00653	0.32137	-0.0067	-0.0131
0	55	0	1	0	0.02732	93152.3	1.07585	21.1682	-4.9544	0.10311	0.36266	0.00195	0.66951	-0.0077	0.00753
0	55	0	1	0	0.02723	92849.5	1.06887	21.0994	0.44513	0.71313	0.36437	0.00482	0.52986	-0.0068	-0.0058
0	55	0	1	0	0.0272	92733	1.06619	21.0729	4.71978	1.13777	0.41417	0.0066	0.34544	-0.0068	-0.0148
0	64	0	1	0	0.02757	93999.7	1.09551	21.3608	-4.9428	0.12946	0.33088	0.00126	0.45466	-0.0053	0.00272
0	64	0	1	0	0.0276	94115.4	1.09821	21.3871	0.4479	0.71938	0.34477	0.00491	0.32181	-0.0045	-0.012
0	64	0	1	0	0.02762	94162.9	1.09932	21.3979	4.71668	1.13074	0.39617	0.00696	0.17191	-0.0042	-0.022
0	20	0	1	0	0.03922	133711	2.21668	30.385	-4.8292	0.38653	0.07321	0.00146	0.02688	-0.0005	-0.0067
0	20	0	1	0	0.03916	133529	2.21062	30.3435	0.52715	0.89873	0.09053	0.00385	-0.121	0.00061	-0.0206
0	20	0	1	0	0.03911	133338	2.20431	30.3001	4.76912	1.24942	0.14578	0.00631	-0.282	0.00133	-0.0312
0	45	0	1	0	0.03912	133381	2.20575	30.31	-4.9384	0.13934	0.22196	0.00076	0.48293	-0.0021	-0.0031
0	45	0	1	0	0.03917	133543	2.21111	30.3468	0.42561	0.66895	0.21441	0.00274	0.33179	-0.0008	-0.0165
0	45	0	1	0	0.03917	133535	2.21082	30.3448	4.67779	1.04275	0.25373	0.00507	0.14895	0.00017	-0.0272
0	55	0	1	0	0.03911	133334	2.20418	30.2992	-4.9425	0.13003	0.23508	0.00071	0.50275	-0.0081	0.0123
0	55	0	1	0	0.03904	133108	2.19672	30.2479	0.4241	0.66553	0.22761	0.00184	0.35253	-0.0061	-0.0043
0	55	0	1	0	0.03913	133412	2.20676	30.317	4.67343	1.03288	0.26491	0.00393	0.17234	-0.0049	-0.0152
0	64	0	1	0	0.03927	133889	2.22258	30.4254	-4.9471	0.11966	0.2779	0.00022	0.38828	-0.0057	0.00448
0	64	0	1	0	0.03933	134100	2.22957	30.4733	0.40495	0.62219	0.28433	0.00224	0.27262	-0.0049	-0.008
0	64	0	1	0	0.03938	134268	2.23518	30.5115	4.6451	0.96877	0.32711	0.00323	0.14774	-0.0042	-0.0187

Table 15. Spoiler Run Data, Tail 3

Beta	Delta e	Delta rn	Tail	stabalizers	M#	Re#	q_c	Uoo	alpha_c	C_L	C_D_c	Cl_cg_w	Cm_cg_c	Cn_cg_w	C_Y\r
0	20	0	2	0	0.02755	93930.4	1.0939	21.345	-4.8566	0.3246	0.14138	0.0012	0.25781	-0.0016	-0.0085
0	20	0	2	0	0.0276	94107.7	1.09803	21.3853	0.53907	0.9257	0.15638	0.00416	0.08451	-0.0007	-0.0226
0	20	0	2	0	0.02748	93694.5	1.08841	21.2914	4.80306	1.32622	0.22598	0.007	-0.1094	-0.0002	-0.033
0	45	0	2	0	0.02741	93459.3	1.08295	21.238	-4.9055	0.21385	0.22944	8.6E-06	0.45349	-0.0034	-0.0061
0	45	0	2	0	0.02742	93488.4	1.08363	21.2446	0.48784	0.80978	0.23637	0.0036	0.30115	-0.0027	-0.0185
0	45	0	2	0	0.02749	93710.5	1.08878	21.2951	4.75413	1.21549	0.29054	0.0061	0.10705	-0.0022	-0.0288
0	55	0	2	0	0.02748	93674.7	1.08795	21.2869	-4.9042	0.21684	0.27346	0.00036	0.41907	-0.0042	-0.005
0	55	0	2	0	0.02737	93312.4	1.07955	21.2046	0.46452	0.75701	0.31824	0.00295	0.37491	-0.0037	-0.0188
0	55	0	2	0	0.02734	93226.7	1.07757	21.1851	4.72143	1.1415	0.38326	0.00531	0.25196	-0.0033	-0.029
0	64	0	2	0	0.02747	93665.6	1.08774	21.2848	-4.9049	0.21519	0.29663	0.001	0.38034	-0.0075	0.00316
0	64	0	2	0	0.02745	93582.4	1.08581	21.2659	0.48165	0.79577	0.31512	0.0035	0.25003	-0.007	-0.0104
0	64	0	2	0	0.02742	93479.6	1.08342	21.2426	4.7443	1.19325	0.37584	0.00477	0.1021	-0.0063	-0.0218
0	85	0	2	0	0.02774	94583.2	1.10916	21.4934	-4.9291	0.16035	0.34274	0.00164	0.2916	-0.0037	0.0008
0	85	0	2	0	0.02769	94393.2	1.1047	21.4502	0.45257	0.72995	0.36341	0.00436	0.15176	-0.003	-0.0137
0	85	0	2	0	0.0275	93743	1.08954	21.3024	4.72016	1.13862	0.42906	0.0068	0.02835	-0.0025	-0.0244
0	20	0	2	0	0.03931	134039	2.22754	30.4593	-4.8649	0.30565	0.10005	-0.0001	0.15786	-0.0008	-0.0092
0	20	0	2	0	0.03926	133868	2.22188	30.4206	0.49227	0.81979	0.11243	0.00186	0.01321	0.00039	-0.024
0	20	0	2	0	0.03922	133716	2.21682	30.386	4.72443	1.14828	0.15881	0.00409	-0.1432	0.00124	-0.035
0	45	0	2	0	0.03918	133567	2.2119	30.3522	-4.9027	0.22009	0.15428	-0.0008	0.32021	-0.002	-0.0071
0	45	0	2	0	0.03926	133854	2.22139	30.4173	0.45692	0.73979	0.15425	0.00097	0.16354	-0.0006	-0.022
0	45	0	2	0	0.03924	133801	2.21964	30.4053	4.69899	1.09071	0.20039	0.00368	-0.0099	0.00019	-0.0321
0	55	0	2	0	0.03914	133443	2.20778	30.324	-4.914	0.19458	0.1789	-0.0013	0.37209	-0.0021	-0.0075
0	55	0	2	0	0.03919	133613	2.21341	30.3626	0.44394	0.71043	0.17639	0.00073	0.22391	-0.0007	-0.0225
0	55	0	2	0	0.03921	133672	2.21536	30.376	4.68698	1.06354	0.21877	0.00331	0.0498	2.1E-05	-0.0323
0	64	0	2	0	0.03907	133201	2.1998	30.2691	-4.9352	0.14664	0.24792	-0.0021	0.45432	-0.0066	0.00083
0	64	0	2	0	0.03913	133410	2.20669	30.3165	0.4121	0.63839	0.24756	-0.0007	0.34897	-0.0053	-0.0137
0	64	0	2	0	0.03914	133451	2.20804	30.3257	4.6566	0.99479	0.28044	0.00149	0.17736	-0.0041	-0.0243
0	85	0	2	0	0.03921	133672	2.21535	30.3759	-4.9267	0.16598	0.28698	-0.0008	0.33369	-0.0047	-0.0013
0	85	0	2	0	0.03922	133706	2.21651	30.3839	0.41959	0.65533	0.28462	0.00078	0.22956	-0.0036	-0.0151
0	85	0	2	0	0.03924	133775	2.21878	30.3994	4.65433	0.98965	0.32526	0.0019	0.10227	-0.0026	-0.0261

Table 16. Spoiler Run Data, Tail 3 w/stabilizer

Beta	Delta e	Delta rn	Tail	stabalizers	M#	Re#	q_c	Uoo	alpha_c	C_L	C_D_c	Cl_cg_w	Cm_cg_c	Cn_cg_w	C_Y\r
0	20	0	2	1	0.0276	94086.3	1.09753	21.3804	-4.8402	0.36162	0.12395	0.00152	0.19285	0.00073	-0.0152
0	20	0	2	1	0.02755	93918.3	1.09362	21.3423	0.55189	0.95471	0.1458	0.00485	0.02396	0.00115	-0.0257
0	20	0	2	1	0.02786	94981.1	1.11851	21.5838	4.79602	1.31028	0.21129	0.00697	-0.1632	0.00139	-0.0327
0	45	0	2	1	0.02738	93365.7	1.08078	21.2167	-4.9263	0.16673	0.28592	-0.0006	0.52448	-0.002	-0.0142
0	45	0	2	1	0.02741	93464.4	1.08307	21.2391	0.4578	0.74178	0.2936	0.00248	0.38749	-0.0013	-0.0244
0	45	0	2	1	0.02739	93372.4	1.08094	21.2182	4.72941	1.15955	0.3404	0.00513	0.19102	-0.0009	-0.0323
0	55	0	2	1	0.02744	93547.1	1.08499	21.2579	-4.9212	0.17838	0.26979	-0.0005	0.50804	-0.0002	-0.0176
0	55	0	2	1	0.02738	93352	1.08047	21.2136	0.46649	0.76146	0.27898	0.00271	0.36594	0.00043	-0.0282
0	55	0	2	1	0.02742	93470.6	1.08321	21.2405	4.73624	1.17502	0.32624	0.0057	0.16428	0.00071	-0.0347
0	64	0	2	1	0.02737	93307.3	1.07943	21.2034	-4.9062	0.21226	0.28334	0.0005	0.43128	-0.0015	-0.0134
0	64	0	2	1	0.02736	93292.5	1.07909	21.2001	0.46586	0.76004	0.31598	0.00309	0.3471	-0.0007	-0.025
0	64	0	2	1	0.02733	93168.1	1.07622	21.1718	4.7261	1.15205	0.3794	0.0054	0.20832	5.6E-05	-0.0352
0	85	0	2	1	0.02748	93683.6	1.08816	21.2889	-4.9259	0.16771	0.35138	0.00204	0.31324	-0.0036	-0.001
0	85	0	2	1	0.02736	93268	1.07852	21.1945	0.45667	0.73924	0.37449	0.00458	0.17759	-0.0029	-0.0151
0	85	0	2	1	0.02728	93001.1	1.07236	21.1338	4.7241	1.14754	0.43663	0.00672	0.04639	-0.0025	-0.0243
0	20	0	2	1	0.03928	133934	2.22406	30.4356	-4.8729	0.28771	0.10948	-0.0003	0.18881	0.00054	-0.0137
0	20	0	2	1	0.03925	133816	2.22014	30.4087	0.48197	0.79648	0.12117	0.00124	0.04229	0.00161	-0.0266
0	20	0	2	1	0.03915	133488	2.20927	30.3342	4.72322	1.14554	0.17249	0.00354	-0.134	0.00218	-0.0339
0	45	0	2	1	0.0391	133293	2.20281	30.2898	-4.9329	0.15192	0.23148	-0.0019	0.4415	-0.0014	-0.0135
0	45	0	2	1	0.03911	133349	2.20469	30.3027	0.41715	0.64981	0.22811	-0.0004	0.30994	-0.0002	-0.0254
0	45	0	2	1	0.03913	133396	2.20625	30.3134	4.65838	0.99882	0.2645	0.00188	0.14122	0.00046	-0.0319
0	55	0	2	1	0.03921	133674	2.21544	30.3765	-4.9017	0.22244	0.15397	-0.0011	0.31712	0.00065	-0.0162
0	55	0	2	1	0.03922	133706	2.21649	30.3837	0.4556	0.73681	0.15507	0.00069	0.1579	0.0016	-0.0276
0	55	0	2	1	0.03923	133745	2.21779	30.3926	4.69467	1.08095	0.20112	0.00317	-0.0127	0.00171	-0.0327
0	64	0	2	1	0.0391	133322	2.20377	30.2964	-4.9244	0.17114	0.20641	-0.0017	0.41054	0.0003	-0.0168
0	64	0	2	1	0.03912	133372	2.20543	30.3078	0.42873	0.676	0.20377	-0.0001	0.27145	0.00152	-0.0292
0	64	0	2	1	0.03916	133528	2.2106	30.3433	4.67045	1.02612	0.24269	0.00253	0.09582	0.00208	-0.0351
0	85	0	2	1	0.03903	133066	2.19531	30.2382	-4.9289	0.16082	0.29953	-0.0004	0.34457	-0.0019	-0.0081
0	85	0	2	1	0.03899	132947	2.19142	30.2114	0.41363	0.64183	0.30343	0.0012	0.23867	-0.0009	-0.0201
0	85	0	2	1	0.03902	133050	2.1948	30.2347	4.64966	0.97909	0.34333	0.00226	0.10933	-0.0002	-0.0289

Table 17. Matrix Run Data, Tail 1

Beta	δ_e	δ_m	Tail	stabalizers	M#	Re#	q_c	Uoo	alpha_c	C_L	C_D	$C_{\_l}$	C_m	C_n	C_Y\r
0	0	23	1	0	0.03925	133798	2.21963	30.4058	4.77815	1.26986	0.14408	0.0059	-0.3418	-0.0019	-0.0236
0	0	14	1	0	0.03927	133896	2.22287	30.4279	4.8677	1.27562	0.14519	0.00598	-0.3553	0.00025	-0.0291
0	0	8	1	0	0.03924	133785	2.21918	30.4027	4.86959	1.27989	0.14571	0.00623	-0.3588	0.00174	-0.0334
0	0	0	1	0	0.03922	133699	2.21635	30.3833	4.86869	1.27785	0.14549	0.00625	-0.3571	0.00248	-0.0355
0	0	-7	1	0	0.03925	133808	2.21996	30.408	4.86809	1.2765	0.1453	0.00632	-0.3538	0.00328	-0.0376
0	0	-12	1	0	0.03922	133699	2.21633	30.3831	4.86662	1.27318	0.14538	0.00633	-0.3474	0.00426	-0.04
0	-10	23	1	0	0.03918	133560	2.21173	30.3516	4.75029	1.2068	0.14905	0.00675	-0.2211	0.00835	-0.0516
0	-10	14	1	0	0.03915	133475	2.20893	30.3324	4.8408	1.21474	0.14884	0.00568	-0.2307	0.00404	-0.0394
0	-10	8	1	0	0.03915	133471	2.20878	30.3314	4.84062	1.21434	0.14835	0.00529	-0.2289	0.00278	-0.036
0	-10	0	1	0	0.03916	133523	2.21052	30.3433	4.83857	1.2097	0.14847	0.00501	-0.2217	0.00178	-0.0332
0	-10	-7	1	0	0.0392	133646	2.21458	30.3711	4.83444	1.20036	0.14884	0.00462	-0.2093	-0.0001	-0.0277
0	-10	-12	1	0	0.03917	133526	2.2106	30.3439	4.83515	1.20195	0.14967	0.00431	-0.21	-0.0014	-0.0242
0	-20	23	1	0	0.03927	133896	2.22286	30.4279	4.72128	1.14115	0.17264	0.00766	-0.1021	0.01869	-0.0781
0	-20	14	1	0	0.03925	133816	2.22023	30.4099	4.80686	1.13793	0.17103	0.00604	-0.0853	0.01115	-0.0578
0	-20	8	1	0	0.03924	133768	2.21862	30.3988	4.80626	1.13659	0.17052	0.00513	-0.0784	0.00698	-0.0467
0	-20	0	1	0	0.03934	134137	2.23089	30.4828	4.80263	1.12836	0.16945	0.00374	-0.0727	0.00032	-0.0287
0	-20	-7	1	0	0.03918	133587	2.21261	30.3577	4.80753	1.13947	0.17122	0.00263	-0.0784	-0.0049	-0.0149
0	-20	-12	1	0	0.03919	133605	2.21322	30.3618	4.81195	1.14946	0.17288	0.00084	-0.1044	-0.0152	0.01357
0	-30	23	1	0	0.03921	133688	2.21598	30.3808	4.71256	1.12142	0.19293	0.00806	-0.0429	0.01954	-0.0794
0	-30	14	1	0	0.03927	133889	2.22263	30.4263	4.79658	1.11467	0.19348	0.00664	-0.0229	0.0137	-0.0638
0	-30	8	1	0	0.03924	133774	2.21884	30.4004	4.79539	1.11198	0.19333	0.0058	-0.0139	0.0095	-0.0528
0	-30	0	1	0	0.03924	133777	2.21892	30.4009	4.79518	1.1115	0.19326	0.00439	-0.0071	0.00289	-0.0355
0	-30	-7	1	0	0.03926	133838	2.22094	30.4147	4.7949	1.11087	0.19303	0.00254	-0.0097	-0.0049	-0.0149
0	-30	-12	1	0	0.03926	133845	2.22117	30.4163	4.79702	1.11568	0.19275	0.00147	-0.0187	-0.0105	-0.0003
0	18	23	1	0	0.03925	133828	2.22061	30.4125	4.81533	1.35398	0.17115	0.00559	-0.5019	-0.0161	0.01468
0	18	14	1	0	0.03924	133784	2.21917	30.4026	4.90835	1.36761	0.17238	0.00688	-0.5209	-0.006	-0.0134
0	18	8	1	0	0.03925	133820	2.22035	30.4107	4.90807	1.36697	0.1715	0.00738	-0.5204	-0.0016	-0.0259
0	18	0	1	0	0.03926	133856	2.22156	30.419	4.90787	1.36652	0.17109	0.0078	-0.5196	0.00201	-0.0361
0	18	-7	1	0	0.03925	133798	2.21962	30.4057	4.90738	1.36541	0.17166	0.00848	-0.5187	0.00726	-0.0507
0	18	-12	1	0	0.03926	133859	2.22166	30.4196	4.90432	1.35848	0.17111	0.00911	-0.5106	0.0121	-0.0641

Table 18. Matrix Run Data, Tail 1 w/stabilizer

Yaw	δ_e	δ_m	Tail	stabalizers	M#	Re#	q_c	Uoo	alpha_c	C_L	C_D	$C_{\_l}$	C_m	C_n	C_Y\r
0	0	-20	1	1	0.03839	130876	2.12373	29.7416	4.81178	1.34594	0.15763	0.00853	-0.3593	0.00299	-0.0471
0	0	-12	1	1	0.03839	130897	2.12442	29.7465	4.89991	1.3485	0.15803	0.00851	-0.3605	0.00261	-0.0462
0	0	0	1	1	0.03841	130941	2.12584	29.7564	4.90119	1.3514	0.15734	0.00837	-0.3649	0.00203	-0.0453
0	0	7	1	1	0.0384	130920	2.12517	29.7517	4.89991	1.34851	0.15684	0.00826	-0.3596	0.0014	-0.0438
0	0	14	1	1	0.0384	130928	2.12543	29.7536	4.89868	1.34573	0.15649	0.00821	-0.3546	0.00115	-0.0435
0	0	25	1	1	0.03838	130855	2.12306	29.737	4.89758	1.34323	0.15642	0.0083	-0.3489	0.001	-0.0434
0	-10	-20	1	1	0.03834	130721	2.11872	29.7066	4.78136	1.27712	0.16489	0.00621	-0.2273	-0.0048	-0.025
0	-10	-12	1	1	0.03837	130822	2.12197	29.7293	4.8678	1.27584	0.16517	0.00647	-0.2243	-0.0029	-0.0302
0	-10	0	1	1	0.03834	130705	2.11818	29.7028	4.86759	1.27537	0.16418	0.00737	-0.2198	0.00148	-0.0431
0	-10	7	1	1	0.03835	130743	2.11942	29.7114	4.8673	1.27472	0.16443	0.00786	-0.221	0.0043	-0.0512
0	-10	14	1	1	0.03836	130775	2.12046	29.7188	4.86692	1.27385	0.16511	0.00841	-0.2215	0.00751	-0.0601
0	-10	25	1	1	0.03835	130747	2.11955	29.7123	4.86684	1.27366	0.16623	0.00887	-0.2192	0.00971	-0.0663
0	-20	-20	1	1	0.03843	131014	2.12823	29.7731	4.76611	1.24259	0.17807	0.00563	-0.1585	-0.0097	-0.0112
0	-20	-12	1	1	0.0384	130912	2.1249	29.7499	4.85204	1.24019	0.17868	0.00606	-0.1496	-0.0068	-0.0194
0	-20	0	1	1	0.03837	130819	2.12188	29.7287	4.85031	1.23626	0.17794	0.0072	-0.1396	-0.0006	-0.0374
0	-20	7	1	1	0.03838	130850	2.1229	29.7359	4.85044	1.23656	0.17782	0.00835	-0.1411	0.00457	-0.0513
0	-20	14	1	1	0.03841	130939	2.12579	29.7561	4.85026	1.23616	0.17787	0.00927	-0.1483	0.01005	-0.0662
0	-20	25	1	1	0.03849	131231	2.13528	29.8224	4.84988	1.2353	0.17863	0.01008	-0.1562	0.0145	-0.0785
0	-30	-20	1	1	0.03848	131174	2.13342	29.8094	4.7498	1.2057	0.21286	0.00269	-0.0671	-0.0206	0.01789
0	-30	-12	1	1	0.03847	131140	2.13232	29.8017	4.83001	1.19034	0.21414	0.00445	-0.0342	-0.0108	-0.009
0	-30	0	1	1	0.03848	131182	2.13368	29.8113	4.8276	1.18488	0.21376	0.00675	-0.0207	-0.0002	-0.0376
0	-30	7	1	1	0.03846	131136	2.13219	29.8009	4.82815	1.18613	0.21374	0.00859	-0.0283	0.00875	-0.0616
0	-30	14	1	1	0.03844	131068	2.12997	29.7853	4.83239	1.19572	0.21345	0.01023	-0.0545	0.01737	-0.0846
0	-30	25	1	1	0.03843	131033	2.12884	29.7774	4.83563	1.20305	0.2143	0.01219	-0.0814	0.0253	-0.1057
0	14	-20	1	1	0.03849	131219	2.13489	29.8197	4.84565	1.4226	0.17478	0.01054	-0.4975	0.01242	-0.0761
0	14	-12	1	1	0.03855	131414	2.14123	29.864	4.9319	1.42089	0.17347	0.00991	-0.4969	0.0087	-0.0659
0	14	0	1	1	0.03852	131331	2.13851	29.845	4.93476	1.42736	0.1724	0.00882	-0.5031	0.00093	-0.0447
0	14	7	1	1	0.03847	131143	2.1324	29.8023	4.93432	1.42638	0.17154	0.00799	-0.4987	-0.0035	-0.0322
0	14	14	1	1	0.03842	130997	2.12766	29.7692	4.93298	1.42333	0.17013	0.00749	-0.4902	-0.0068	-0.0233
0	14	25	1	1	0.03845	131079	2.13031	29.7877	4.92834	1.41284	0.16789	0.00705	-0.4742	-0.0096	-0.0157

Table 19. Matrix Run Data, Tail 3

Yaw	δ_e	δ_m	Tail	stabalizers	M#	Re#	q_c	Uoo	alpha_c	C_L	C_D	$C_{\_l}$	C_m	C_n	C_Y\r
0	0	-30	2	0	0.03939	134835	2.23741	30.4136	4.76786	1.24656	0.14607	0.00591	-0.34	0.00634	-0.0517
0	0	-15	2	0	0.03931	134561	2.22832	30.3517	4.86051	1.25935	0.14773	0.0053	-0.3532	0.0028	-0.0408
0	0	-8	2	0	0.03936	134731	2.23396	30.3901	4.85877	1.25541	0.14685	0.00523	-0.3516	0.00216	-0.0388
0	0	0	2	0	0.03933	134624	2.23041	30.3659	4.85917	1.25631	0.14693	0.00504	-0.3517	0.00117	-0.0359
0	0	10	2	0	0.03935	134702	2.233	30.3836	4.85801	1.25369	0.14611	0.00494	-0.3476	-0.0003	-0.0311
0	0	20	2	0	0.03937	134772	2.23531	30.3993	4.85533	1.24762	0.145	0.00469	-0.3402	-0.0016	-0.027
0	0	30	2	0	0.03936	134734	2.23405	30.3907	4.85317	1.24273	0.14435	0.00433	-0.3309	-0.0025	-0.0243
0	-10	-30	2	0	0.03935	134703	2.23303	30.3838	4.72593	1.15167	0.15275	0.00278	-0.1715	-0.0104	-0.0027
0	-10	-15	2	0	0.03931	134571	2.22865	30.3539	4.8114	1.14821	0.15427	0.00371	-0.1606	-0.0037	-0.0217
0	-10	-8	2	0	0.03928	134453	2.22474	30.3273	4.81172	1.14894	0.15466	0.00392	-0.1588	-0.0018	-0.0269
0	-10	0	2	0	0.03928	134448	2.22456	30.3261	4.81042	1.14601	0.15478	0.00439	-0.1558	0.00153	-0.0364
0	-10	10	2	0	0.03924	134326	2.22054	30.2987	4.81128	1.14794	0.15428	0.00488	-0.1558	0.00483	-0.0455
0	-10	20	2	0	0.03917	134077	2.2123	30.2424	4.81257	1.15086	0.15541	0.00554	-0.1505	0.00885	-0.0568
0	-10	30	2	0	0.03932	134582	2.229	30.3564	4.80758	1.13957	0.15448	0.00595	-0.1478	0.01236	-0.0662
0	-20	-30	2	0	0.03938	134815	2.23675	30.4091	4.71647	1.13027	0.15933	0.00185	-0.134	-0.0143	0.00739
0	-20	-15	2	0	0.03934	134680	2.23226	30.3785	4.80265	1.1284	0.15911	0.00323	-0.1263	-0.0049	-0.0188
0	-20	-8	2	0	0.03929	134512	2.2267	30.3407	4.80284	1.12885	0.15937	0.00359	-0.1251	-0.0028	-0.0247
0	-20	0	2	0	0.03932	134593	2.22937	30.3588	4.80206	1.12708	0.15927	0.00436	-0.1242	0.00267	-0.0401
0	-20	10	2	0	0.03932	134593	2.22936	30.3588	4.80069	1.12398	0.15987	0.00467	-0.1184	0.00569	-0.0483
0	-20	20	2	0	0.0393	134542	2.22767	30.3473	4.80006	1.12256	0.16072	0.00548	-0.1138	0.01076	-0.0623
0	-20	30	2	0	0.03934	134654	2.23139	30.3726	4.79917	1.12055	0.16137	0.00605	-0.1135	0.01482	-0.0736
0	-30	-30	2	0	0.0394	134887	2.23911	30.4251	4.70374	1.10146	0.17841	0.00041	-0.0732	-0.0206	0.0244
0	-30	-15	2	0	0.03941	134897	2.23947	30.4275	4.78857	1.09656	0.17805	0.00237	-0.0593	-0.0088	-0.0082
0	-30	-8	2	0	0.03935	134713	2.23335	30.386	4.78785	1.09493	0.17825	0.00305	-0.0549	-0.0049	-0.0189
0	-30	0	2	0	0.03921	134221	2.21706	30.2749	4.79093	1.10189	0.18009	0.00382	-0.0528	0.00068	-0.0346
0	-30	10	2	0	0.03934	134650	2.23127	30.3718	4.78717	1.09338	0.17974	0.00452	-0.0504	0.00563	-0.0479
0	-30	20	2	0	0.03936	134747	2.23447	30.3936	4.78667	1.09225	0.18004	0.00533	-0.052	0.01104	-0.0625
0	-30	30	2	0	0.03939	134826	2.2371	30.4115	4.78634	1.09151	0.18122	0.00657	-0.0557	0.0178	-0.0809
0	18	-30	2	0	0.03947	135100	2.24619	30.4731	4.79596	1.31016	0.16739	0.0079	-0.4552	0.01545	-0.0797
0	18	-15	2	0	0.03948	135159	2.24816	30.4865	4.89991	1.34851	0.17848	0.00665	-0.5164	0.00559	-0.0505
0	18	-8	2	0	0.03949	135166	2.24841	30.4882	4.89999	1.34869	0.17799	0.00643	-0.516	0.00327	-0.0437
0	18	0	2	0	0.03948	135152	2.24794	30.485	4.89919	1.34687	0.17724	0.00599	-0.5141	0.00044	-0.0354
0	18	10	2	0	0.03946	135084	2.24568	30.4697	4.89666	1.34115	0.1754	0.0051	-0.5048	-0.0065	-0.015
0	18	20	2	0	0.03949	135181	2.24891	30.4916	4.89241	1.33153	0.17377	0.00427	-0.4902	-0.012	0.00175
0	18	30	2	0	0.03946	135063	2.24496	30.4648	4.88755	1.32054	0.17211	0.00347	-0.4707	-0.0169	0.01618

Table 20. Matrix Run Data, Tail 3 w/stabilizer

Yaw	δ_e	δ_m	Tail	stabalizers	M#	Re#	q_c	Uoo	alpha_c	C_L	C_D	$C_{\_l}$	C_m	C_n	C_Y\r
0	0	-30	2	1	0.03932	134598	2.22954	30.36	4.75971	1.22811	0.14823	0.00437	-0.3133	0.0035	-0.0397
0	0	-15	2	1	0.03925	134372	2.22207	30.3091	4.84839	1.23193	0.14886	0.00416	-0.3127	0.00225	-0.0354
0	0	-8	2	1	0.03929	134486	2.22584	30.3348	4.84705	1.22889	0.14825	0.00415	-0.3109	0.00208	-0.0348
0	0	0	2	1	0.03925	134354	2.22146	30.3049	4.84683	1.22839	0.14804	0.00405	-0.3092	0.00191	-0.0344
0	0	10	2	1	0.03926	134404	2.22313	30.3163	4.84571	1.22585	0.14746	0.00404	-0.3065	0.0016	-0.0332
0	0	20	2	1	0.03932	134583	2.22905	30.3567	4.84391	1.22179	0.14727	0.004	-0.3039	0.00142	-0.0324
0	0	30	2	1	0.03929	134482	2.2257	30.3339	4.84301	1.21976	0.14723	0.00388	-0.301	0.00161	-0.033
0	-10	-30	2	1	0.03936	134738	2.23417	30.3916	4.72261	1.14416	0.16011	0.0012	-0.1681	-0.0123	0.00653
0	-10	-15	2	1	0.03941	134899	2.23954	30.428	4.80551	1.13488	0.16049	0.0023	-0.1547	-0.0047	-0.015
0	-10	-8	2	1	0.03935	134696	2.2328	30.3822	4.80786	1.14021	0.15886	0.00277	-0.163	-0.0022	-0.0222
0	-10	0	2	1	0.03922	134255	2.21819	30.2826	4.81065	1.14651	0.15942	0.00341	-0.1641	0.0012	-0.0321
0	-10	10	2	1	0.03926	134387	2.22257	30.3125	4.80885	1.14244	0.1597	0.00419	-0.1588	0.00577	-0.0451
0	-10	20	2	1	0.03926	134391	2.22268	30.3133	4.80765	1.13973	0.16021	0.00482	-0.1529	0.00978	-0.0566
0	-10	30	2	1	0.0394	134888	2.23917	30.4255	4.80397	1.13141	0.15966	0.00565	-0.1507	0.01507	-0.0716
0	-20	-30	2	1	0.03936	134752	2.23464	30.3947	4.70937	1.1142	0.18133	-0.0007	-0.1042	-0.0197	0.02608
0	-20	-15	2	1	0.03936	134733	2.234	30.3904	4.79331	1.10728	0.18115	0.00125	-0.0891	-0.009	-0.0034
0	-20	-8	2	1	0.03933	134616	2.23014	30.3641	4.80769	1.13981	0.1632	0.00267	-0.1551	-0.0018	-0.0239
0	-20	0	2	1	0.03924	134333	2.22076	30.3002	4.81366	1.15334	0.15748	0.00337	-0.1777	0.00158	-0.0335
0	-20	10	2	1	0.03925	134349	2.2213	30.3039	4.81254	1.1508	0.15758	0.00391	-0.1735	0.00503	-0.0435
0	-20	20	2	1	0.03928	134457	2.22488	30.3283	4.81049	1.14616	0.1575	0.00467	-0.1678	0.00937	-0.0558
0	-20	30	2	1	0.03932	134600	2.2296	30.3604	4.80973	1.14444	0.15792	0.00535	-0.1652	0.0147	-0.0716
0	-30	-30	2	1	0.03945	135047	2.24443	30.4612	4.67596	1.0386	0.22725	-0.0039	0.00312	-0.0308	0.05331
0	-30	-15	2	1	0.03941	134891	2.23925	30.426	4.75924	1.03019	0.22642	-0.0012	0.04042	-0.0166	0.01404
0	-30	-8	2	1	0.03944	135001	2.24289	30.4508	4.75633	1.02359	0.22593	0.00024	0.05492	-0.0101	-0.0035
0	-30	0	2	1	0.03938	134820	2.2369	30.4101	4.7566	1.02421	0.22573	0.00196	0.06412	-0.0033	-0.0219
0	-30	10	2	1	0.03954	135359	2.25483	30.5317	4.77631	1.0688	0.19461	0.00402	-0.0423	0.00395	-0.0406
0	-30	20	2	1	0.03925	134370	2.22198	30.3085	4.8194	1.16631	0.15243	0.00514	-0.2024	0.00672	-0.0488
0	-30	30	2	1	0.03927	134411	2.22333	30.3177	4.81744	1.16189	0.15231	0.00579	-0.1955	0.01158	-0.0635
0	18	-30	2	1	0.03927	134411	2.22333	30.3177	4.81744	1.16189	0.15231	0.00579	-0.1955	0.01158	-0.0635
0	18	-15	2	1	0.03937	134778	2.23551	30.4007	4.88744	1.32028	0.16827	0.00612	-0.462	0.00691	-0.0505
0	18	-8	2	1	0.03936	134733	2.23401	30.3905	4.88858	1.32286	0.16856	0.00604	-0.4652	0.00514	-0.0454
0	18	0	2	1	0.0394	134856	2.23811	30.4183	4.88614	1.31734	0.16803	0.00569	-0.4623	0.00209	-0.0368
0	18	10	2	1	0.03933	134622	2.23035	30.3655	4.88538	1.31562	0.16764	0.00489	-0.4575	-0.0032	-0.021
0	18	20	2	1	0.0393	134522	2.22702	30.3429	4.88171	1.30733	0.16615	0.00406	-0.4417	-0.0081	-0.0058
0	18	30	2	1	0.03928	134475	2.22546	30.3322	4.87811	1.29918	0.16492	0.00342	-0.4285	-0.0108	0.00249

Table 21. Beta Run Data, All Tail and All Configurations

Yaw	Delta rn	Tail	stabalizers	M#	Re#	q_c	Uoo	alpha_c	C_L	C_D_c	Cl_cg_w	Cm_cg_c	Cn_cg_w	C_Y\r
-8	0	1	1	0.03858	132082	2.14695	29.7924	4.78967	1.29591	0.1748	-0.004	-0.3569	0.00591	-0.1057
-6	0	1	1	0.03863	132226	2.15165	29.825	4.7932	1.30391	0.1701	0.00022	-0.3653	0.00451	-0.0881
-4	0	1	1	0.03858	132072	2.14665	29.7903	4.80139	1.32243	0.16483	0.00408	-0.3677	0.0036	-0.0745
-2	0	1	1	0.03858	132066	2.14644	29.7889	4.80458	1.32966	0.1589	0.00803	-0.3643	0.00264	-0.0598
0	0	1	1	0.03856	132001	2.14432	29.7742	4.80611	1.33312	0.15347	0.01171	-0.3549	0.0019	-0.0463
2	0	1	1	0.03856	132012	2.14469	29.7767	4.80265	1.32529	0.15588	0.01509	-0.3603	0.00116	-0.0328
4	0	1	1	0.03851	131809	2.13808	29.7308	4.798	1.31477	0.16016	0.01881	-0.362	0.00029	-0.0177
6	0	1	1	0.03848	131715	2.13506	29.7098	4.79106	1.29906	0.16321	0.02238	-0.3591	-0.0008	-0.0013
8	0	1	1	0.03842	131513	2.12851	29.6642	4.78344	1.28182	0.16749	0.02637	-0.3551	-0.0022	0.01649
-8	64	1	1	0.03875	132641	2.16517	29.9186	4.77126	1.25426	0.1743	-0.0028	-0.3023	0.00931	-0.116
-6	64	1	1	0.03884	132946	2.17514	29.9874	4.77777	1.26898	0.16887	0.00085	-0.318	0.00565	-0.0932
-4	64	1	1	0.03889	133139	2.18147	30.0309	4.78424	1.28363	0.16268	0.0042	-0.326	0.00317	-0.0748
-2	64	1	1	0.03881	132863	2.17243	29.9687	4.79132	1.29964	0.15742	0.00788	-0.3329	0.00085	-0.0564
0	64	1	1	0.03887	133063	2.17897	30.0137	4.79195	1.30108	0.15134	0.011	-0.3306	-0.0011	-0.0397
2	64	1	1	0.03881	132851	2.17203	29.9659	4.79223	1.30171	0.15471	0.01416	-0.3393	-0.0028	-0.0241
4	64	1	1	0.0388	132812	2.17076	29.9572	4.78562	1.28676	0.15812	0.01752	-0.3408	-0.0045	-0.0071
6	64	1	1	0.03872	132560	2.16254	29.9004	4.78007	1.27419	0.16177	0.02121	-0.342	-0.0066	0.01228
8	64	1	1	0.03872	132530	2.16155	29.8936	4.77085	1.25334	0.16601	0.02516	-0.3394	-0.0094	0.03368
-8	0	1	0	0.0394	134876	2.23877	30.4228	4.76754	1.24584	0.16335	-0.0077	-0.3775	0.00051	-0.0634
-6	0	1	0	0.03939	134825	2.23705	30.4111	4.77374	1.25988	0.16008	-0.003	-0.387	0.00124	-0.0576
-4	0	1	0	0.03939	134830	2.23723	30.4123	4.77862	1.27091	0.15544	0.00164	-0.3903	0.00183	-0.0516
-2	0	1	0	0.03937	134771	2.23526	30.399	4.78255	1.2798	0.15058	0.00628	-0.3888	0.00232	-0.0447
0	0	1	0	0.0394	134886	2.23909	30.425	4.78193	1.2784	0.14507	0.01025	-0.3805	0.00284	-0.0385
2	0	1	0	0.03931	134571	2.22863	30.3538	4.77957	1.27306	0.14817	0.01437	-0.3822	0.00331	-0.0313
4	0	1	0	0.03931	134559	2.22823	30.3511	4.77438	1.26132	0.15123	0.01864	-0.3798	0.00369	-0.0236
6	0	1	0	0.03927	134443	2.22441	30.3251	4.76877	1.24863	0.15379	0.02311	-0.3741	0.00405	-0.015
8	0	1	0	0.03928	134465	2.22515	30.3301	4.75825	1.22481	0.15647	0.02753	-0.3654	0.00432	-0.0068
-8	67	1	0	0.03932	134589	2.22924	30.358	4.73765	1.1782	0.16253	-0.0041	-0.2495	0.01096	-0.0939
-6	67	1	0	0.03936	134731	2.23395	30.3901	4.7456	1.1962	0.15677	-0.0006	-0.2664	0.00755	-0.0764
-4	67	1	0	0.03937	134774	2.23538	30.3998	4.75303	1.21301	0.15113	0.00276	-0.2768	0.00529	-0.0629
-2	67	1	0	0.03936	134724	2.23372	30.3885	4.75898	1.22647	0.14624	0.00651	-0.2863	0.00348	-0.0498
0	67	1	0	0.03934	134659	2.23157	30.3738	4.76162	1.23243	0.14075	0.0097	-0.2881	0.00187	-0.0378
2	67	1	0	0.03929	134500	2.22629	30.3379	4.76158	1.23235	0.14376	0.01323	-0.2972	0.00113	-0.0272
4	67	1	0	0.03931	134569	2.22859	30.3535	4.7548	1.21701	0.14688	0.01691	-0.3023	0.00035	-0.0165
6	67	1	0	0.03924	134330	2.22065	30.2995	4.75116	1.20878	0.14914	0.0207	-0.3049	-0.0007	-0.0045
8	67	1	0	0.03922	134239	2.21766	30.2791	4.74552	1.19601	0.15263	0.02492	-0.3073	-0.0018	0.00748
-8	0	2	0	0.03939	134849	2.23787	30.4167	4.75058	1.20746	0.16014	-0.0089	-0.322	-0.0003	-0.0651
-6	0	2	0	0.0394	134876	2.23874	30.4226	4.7596	1.22786	0.15787	-0.0047	-0.3436	0.00021	-0.0589
-4	0	2	0	0.03941	134920	2.24021	30.4326	4.76688	1.24434	0.15462	-0.0001	-0.3566	0.00071	-0.0523
-2	0	2	0	0.0394	134869	2.23851	30.4211	4.77055	1.25266	0.15054	0.0045	-0.3614	0.00117	-0.0451
0	0	2	0	0.03938	134788	2.23582	30.4028	4.77077	1.25314	0.14582	0.00847	-0.3561	0.00164	-0.0386
2	0	2	0	0.03929	134508	2.22655	30.3397	4.77022	1.25191	0.14813	0.01268	-0.3582	0.00197	-0.0312
4	0	2	0	0.0393	134519	2.22694	30.3423	4.76556	1.24135	0.15073	0.01716	-0.3563	0.00231	-0.0229
6	0	2	0	0.0393	134535	2.22747	30.3459	4.76273	1.23495	0.15343	0.02217	-0.3609	0.00279	-0.0149
8	0	2	0	0.03926	134399	2.22294	30.3151	4.75538	1.21832	0.15591	0.02692	-0.3534	0.00302	-0.0064
-8	54	2	0	0.03946	135077	2.24544	30.4681	4.71849	1.13485	0.16132	-0.006	-0.2198	0.01316	-0.1017
-6	54	2	0	0.03948	135144	2.24767	30.4832	4.72546	1.15061	0.15571	-0.0022	-0.2348	0.01141	-0.0889
-4	54	2	0	0.03945	135058	2.24481	30.4638	4.73456	1.17121	0.1504	0.0011	-0.2471	0.01002	-0.0771
-2	54	2	0	0.03944	135022	2.24359	30.4556	4.74136	1.18661	0.14476	0.00484	-0.2571	0.00839	-0.0638
0	54	2	0	0.0394	134859	2.23819	30.4189	4.74484	1.19448	0.13893	0.00814	-0.2587	0.00714	-0.0523
2	54	2	0	0.03936	134749	2.23456	30.3942	4.74482	1.19441	0.14019	0.01164	-0.2678	0.00603	-0.0405
4	54	2	0	0.03937	134755	2.23474	30.3954	4.74067	1.18502	0.14246	0.01565	-0.276	0.0045	-0.0268
6	54	2	0	0.03935	134716	2.23344	30.3866	4.73664	1.17591	0.14467	0.01963	-0.2818	0.00303	-0.0134
8	54	2	0	0.03933	134645	2.23109	30.3706	4.73208	1.1656	0.1478	0.02396	-0.2866	0.00144	0.0004
-8	0	2	1	0.03937	134776	2.23543	30.4001	4.76012	1.22904	0.17168	-0.0098	-0.3648	0.00612	-0.0951
-6	0	2	1	0.03944	134999	2.24283	30.4504	4.76344	1.23656	0.16701	-0.005	-0.3747	0.00477	-0.0785
-4	0	2	1	0.03937	134777	2.23547	30.4004	4.76939	1.25003	0.16229	-0.0005	-0.3811	0.0038	-0.0642
-2	0	2	1	0.03938	134793	2.23601	30.404	4.77423	1.26097	0.15679	0.00432	-0.3819	0.00277	-0.0498
0	0	2	1	0.03936	134747	2.23447	30.3936	4.77575	1.26441	0.15362	0.00817	-0.3797	0.00225	-0.0381
2	0	2	1	0.03935	134686	2.23244	30.3798	4.77413	1.26076	0.15538	0.01232	-0.384	0.00156	-0.0248
4	0	2	1	0.03935	134712	2.23333	30.3858	4.76859	1.24823	0.15826	0.01691	-0.3835	0.00059	-0.0096
6	0	2	1	0.03927	134441	2.22433	30.3245	4.76351	1.23671	0.1615	0.02167	-0.381	-0.0005	0.00631
8	0	2	1	0.03926	134400	2.223	30.3154	4.75503	1.21753	0.16506	0.02638	-0.3745	-0.002	0.02425
-8	58	2	1	0.03984	136368	2.28855	30.7592	4.71478	1.12644	0.16128	-0.0073	-0.2467	0.01137	-0.1075
-6	58	2	1	0.03977	136154	2.28139	30.711	4.72235	1.14358	0.15698	-0.0033	-0.2619	0.00878	-0.0876
-4	58	2	1	0.03968	135834	2.27067	30.6388	4.73202	1.16546	0.15237	0.00027	-0.2726	0.00712	-0.0714

Appendix B: Balance Calibration Plots

The following method was used by Mr. Gehring to calibrate and install the balance. For the starting point of this process it is assumed that the balance is not attached to anything and the sting (balance holder) is removed from the tunnel. These steps are not meant to replace proper training as important information may have gone unobserved.

Excitation voltage is first changed within the tunnel controller program. Excitation voltages are specific for the balance in question, with the AFIT-1 balance using 5V. By first changing the voltage, problems with forgetting to change the voltage later are nullified.

Wires attached to the balance must first be threaded through the balance holder. These wires are very fine and to not have enough stiffness on their own to push through the holder. To overcome this problem, shrink tubing, roughly 6 inches long, was placed over the ends of the wire. Care had to be taken before this step to assure the wire marker tags were slid to different positions so they would not bunch and form a blockage. After using the shrink-tubed wire to push the initial length of wire through the sting, the shrink tubing was removed using a fine-pointed pair of tweezers. Tweezers were slid into the opening of the shrink tubing and pulled upward to cut it. The fine point would miss any wires so they would not be cut. Upon pulling the rest of the balance wire through the holder the balance is ready to be attached to the sting.

Within the balance are a number of screws that attach the balance to the sting. These screws can be grouped into three groups: “push in”, “vertical”, and “push out”.

The names refer to the way the screws and their holes are canted and how they appear to affect the balance.

While inserting the balance into the sting, the screw holes must be aligned properly. The alignment of these holes can be seen in the right edge of Figure 19. When this is accomplished, the "push in" screws are finger tightened first. Following are the vertical screws and then the "push out" screws. This entire assembly is then slid into the calibration holder, located adjacent to the wind tunnel in room L154. After the balance assembly is securely fastened into the calibration fixture, the balance wires can then be attached to the power terminals. Upon applying power it is advisable to allow 24 hours for the internal components of the balance to warm up.

After the 24 hour period, the tunnel controller program is run to zero out the balance. This is accomplished by changing preset voltages in the block diagram portion of the program. The controller/data acquisition program is started and a null of the balance is taken. The maximum load for a particular direction is applied. Voltage gains, located on the front panel of the controller/acquisition program are changed so the read-out displays the proper load. The load is then removed and the program is again checked to ensure the read-out returns to zero. This is repeated for each of the other force and moment directions taken by the balance.

Calibration of the balance is a lengthy process. Pitch itself has 4 configurations to be tested. The first is orienting the balance with normal positive facing up. When the pitch calibration fixture is applied two pitch moments are calibrated, positive and negative. The balance is then inverted so positive normal force is down. The pitch moment is then calibrated again. Yaw moment also has 4 configurations, very similar to

pitch. The normal force, side force, and roll all have 2 configurations. Normal direction is with the positive markings on the balance up and down. Side force is with the either side of the balance up and down. Roll is calibrated clockwise and counter clockwise. Axial force is tested by attaching a pulley mechanism to the balance calibration fixture. A string is then attached to the balance and then over the pulley. Weights are then added to the end of the string resulting in an axial force applied to the balance. Graphs were taken of the calibration before the MAV tests. The graphs in Figures 69-79 demonstrate the varying directions the balance is calibrated.

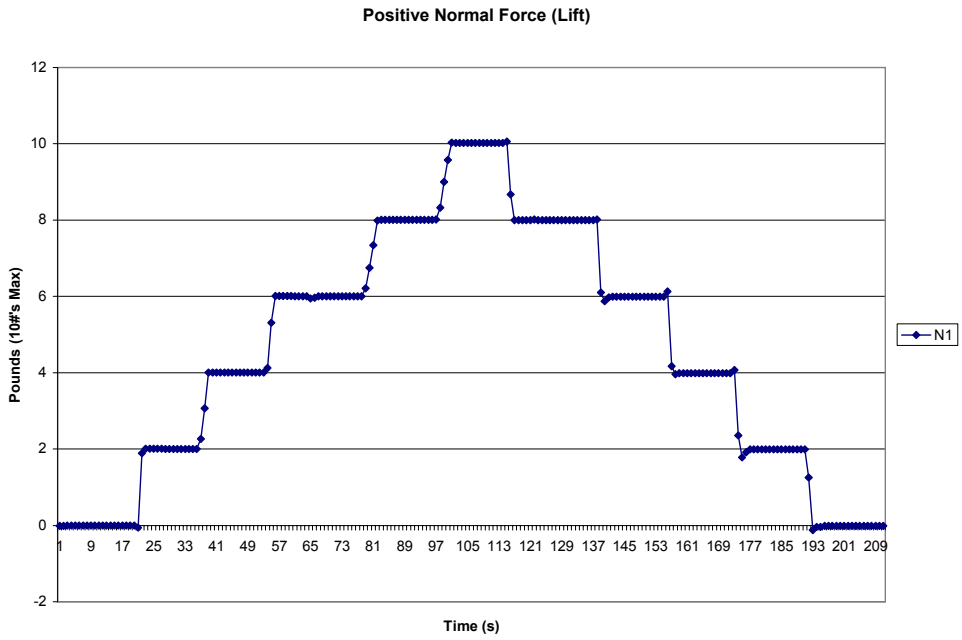

Figure 69. Normal Force Calibration Curve (positive)

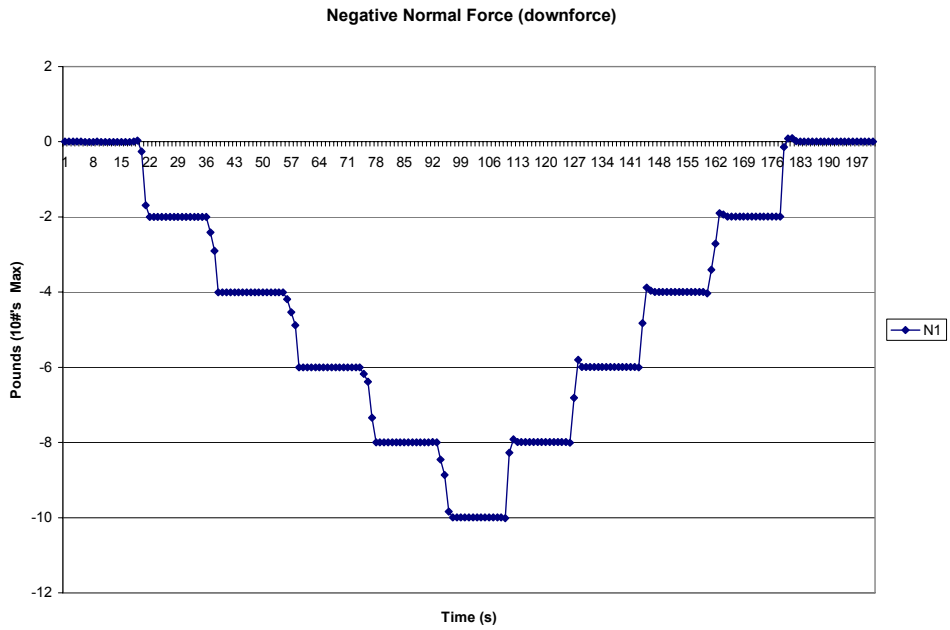

Figure 70. Normal Force Calibration Curve (negative)

Figure 69 and Figure 70 were produced in the manner described previously. The positive normal force sensor on the balance was positioned facing up and weights hung from it. To gather the negative data, the positive was placed down and weights hung from the sensor. The remaining graphs from this calibration are included below.

These plots show that the balance and software gains have been adjusted properly to give an indication of the actual load applied to the balance. In cases where a spike is present in the data, as in Figure 74 and Figure 75, this is from a number of smaller weights being removed and one larger weight being added. Smaller spikes at the beginning of each step in weights are expected as the weight is placed on the weight tray and then transient responses from the weight addition diminish.

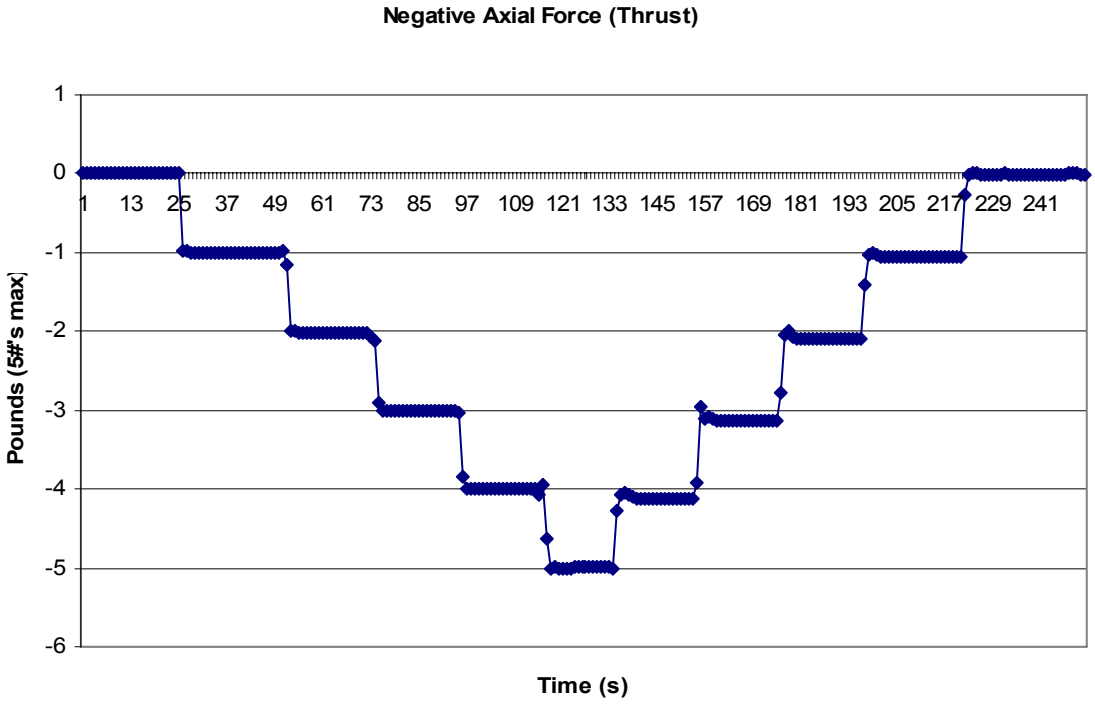

Figure 71. Axial force Calibration Plot

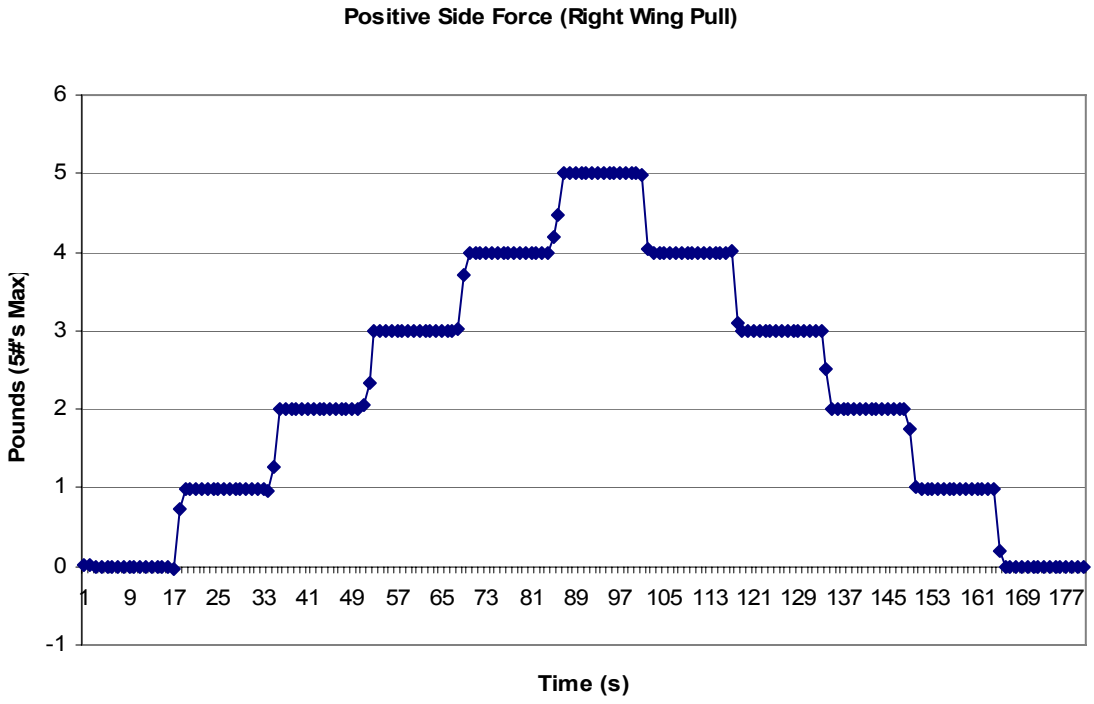

Figure 72. Positive Side Force Calibration Plot

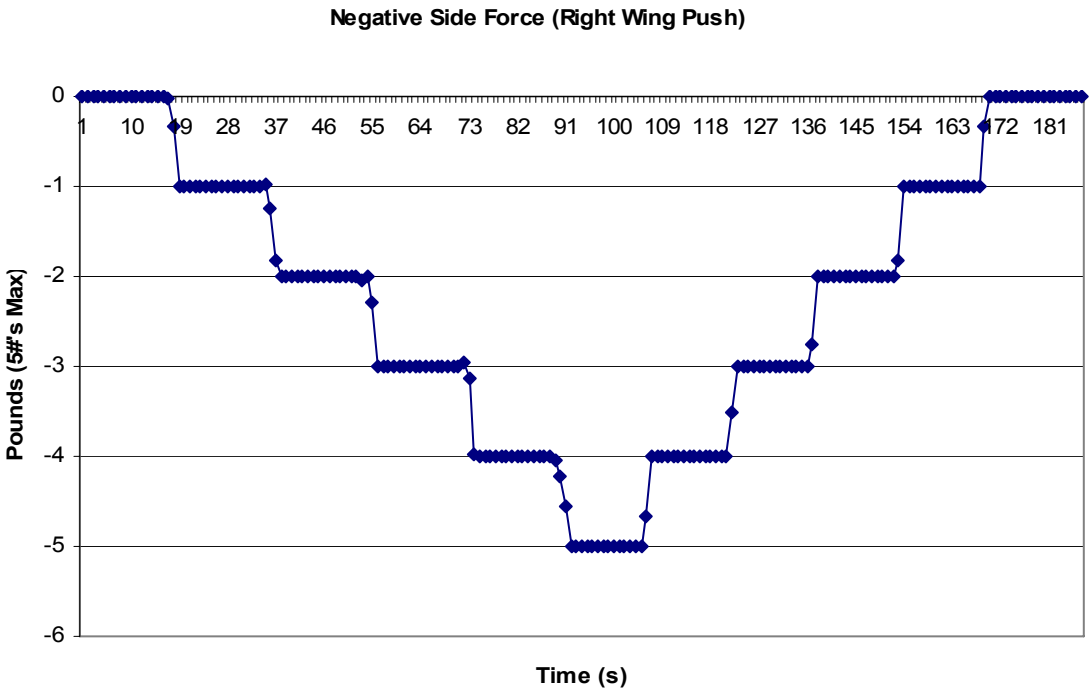

Figure 73. Negative Side Force Calibration Plot

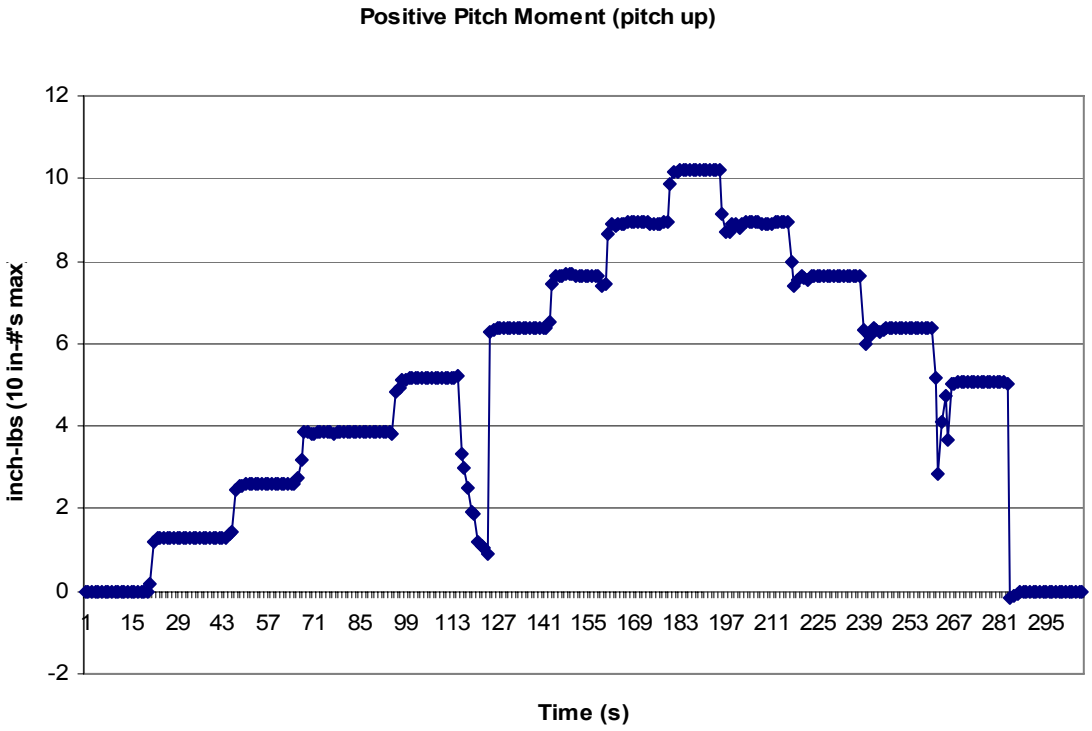

Figure 74. Positive Pitch Moment Calibration Plot

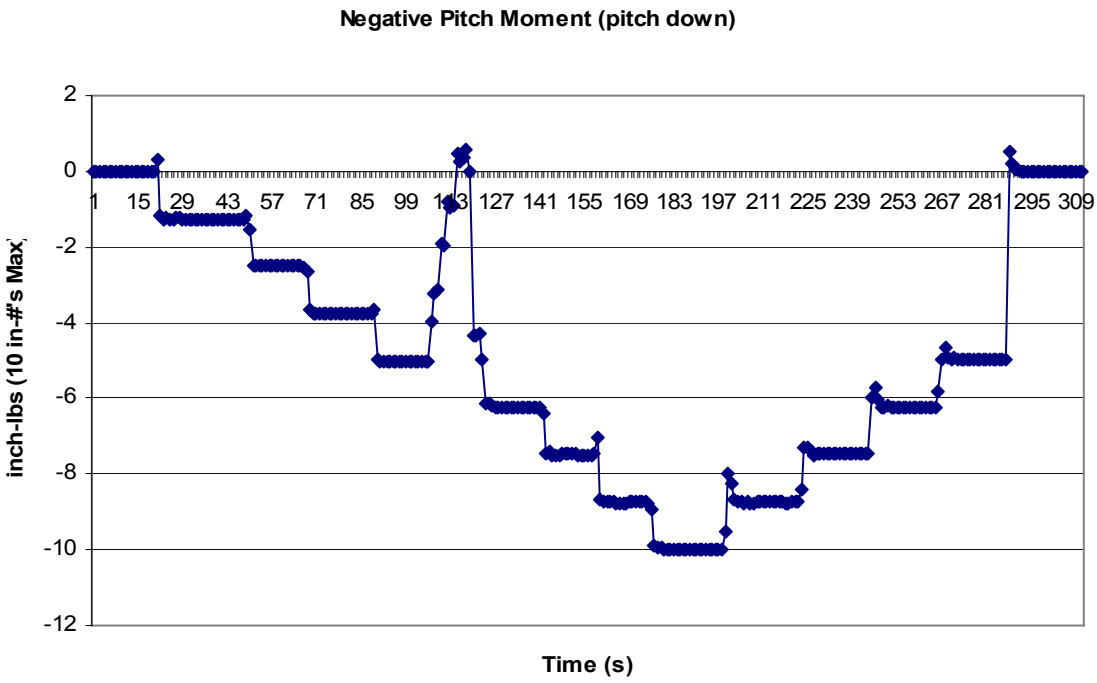

Figure 75. Negative Pitch Moment Calibration Plot

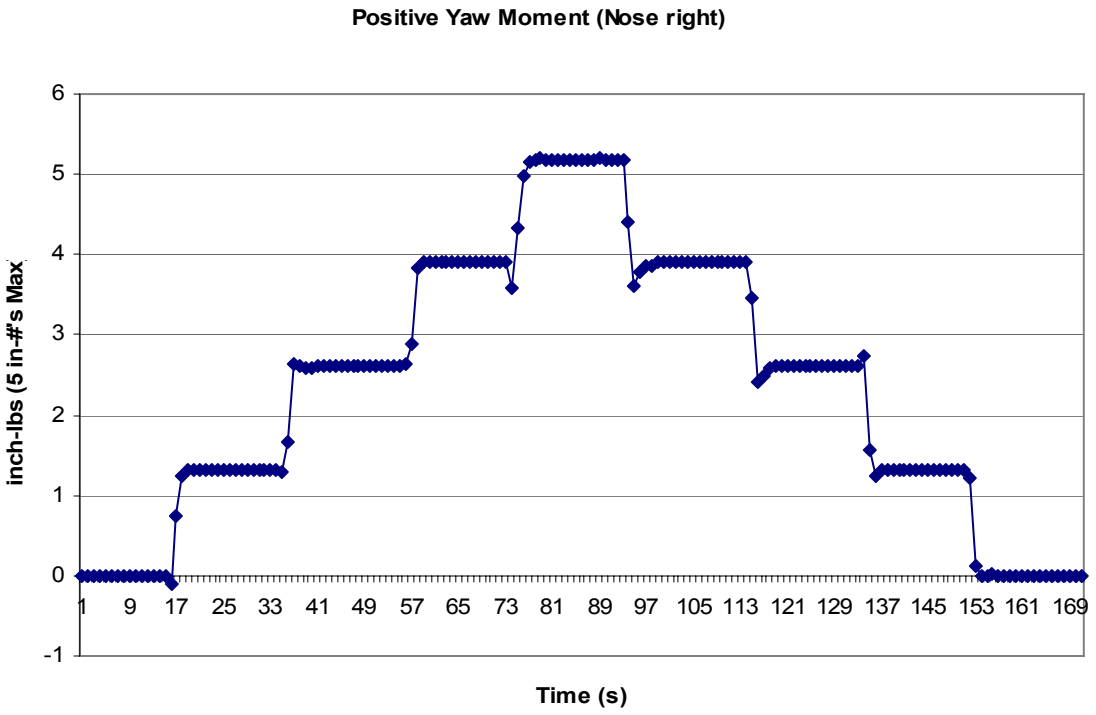

Figure 76. Positive Yaw Moment Calibration Plot

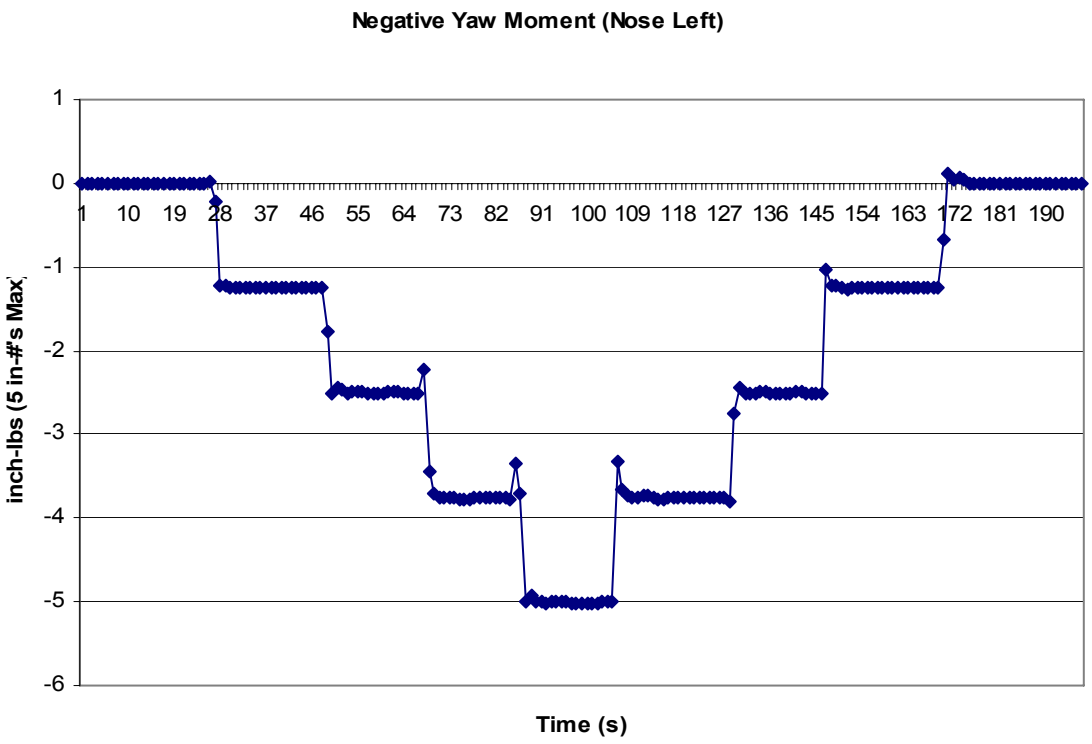

Figure 77. Negative Yaw Moment Calibration Plot

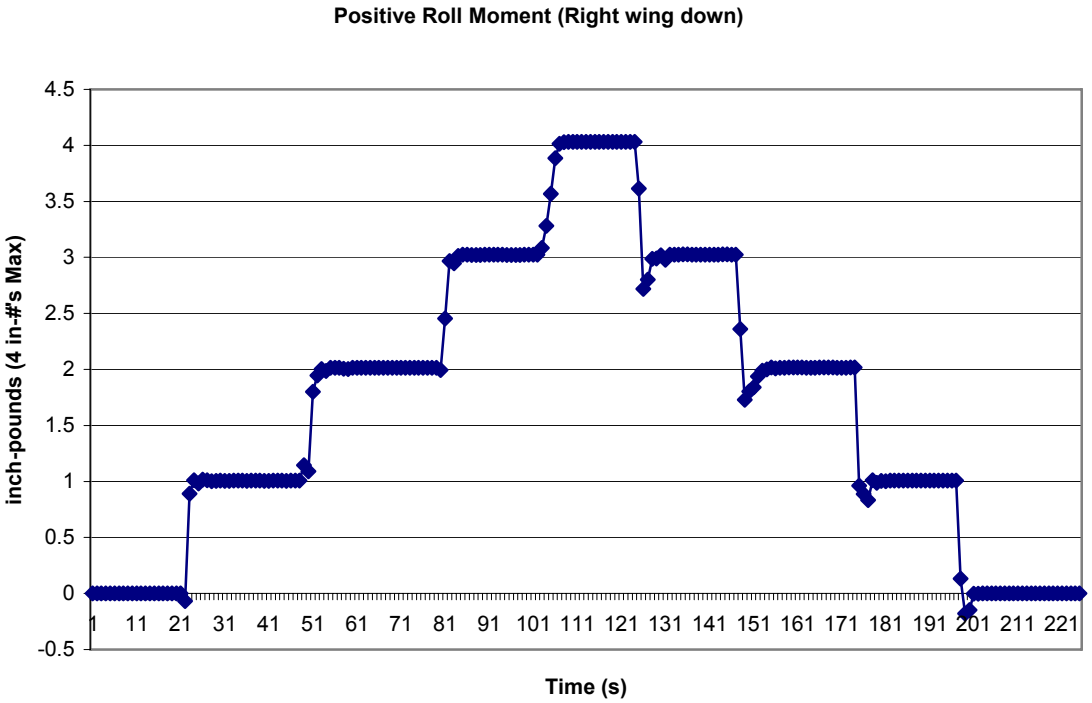

Figure 78. Positive Roll Moment Calibration Plot

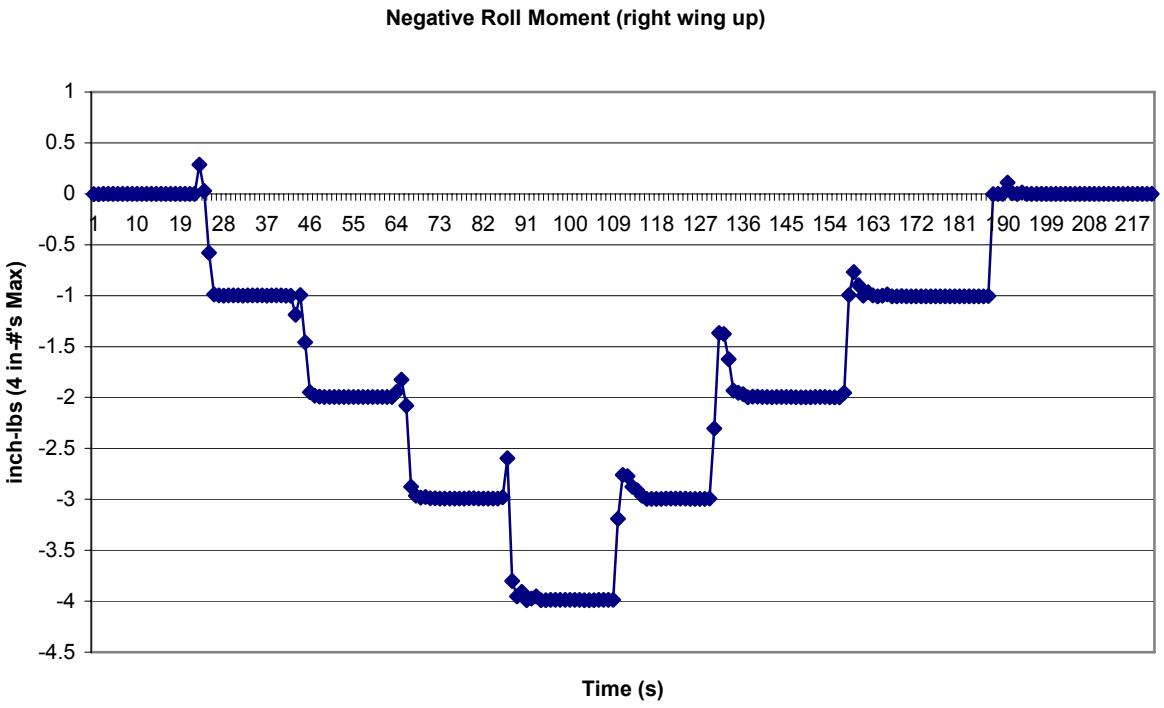

Figure 79. Negative Roll Moment Calibration Plot

Appendix C Additional Plots

Plots in this appendix are not referenced in the text. These plots are included to better show stabilizer effect on the MAV/rotatable tail combination. Figures 80 to 83 show similar trends as discussed for C_L plots in the text. Figure 83 departs slightly from trends by showing an increase in lift at $\delta_e = 55^o$. Change in tail deflection due to wind is most likely the cause.

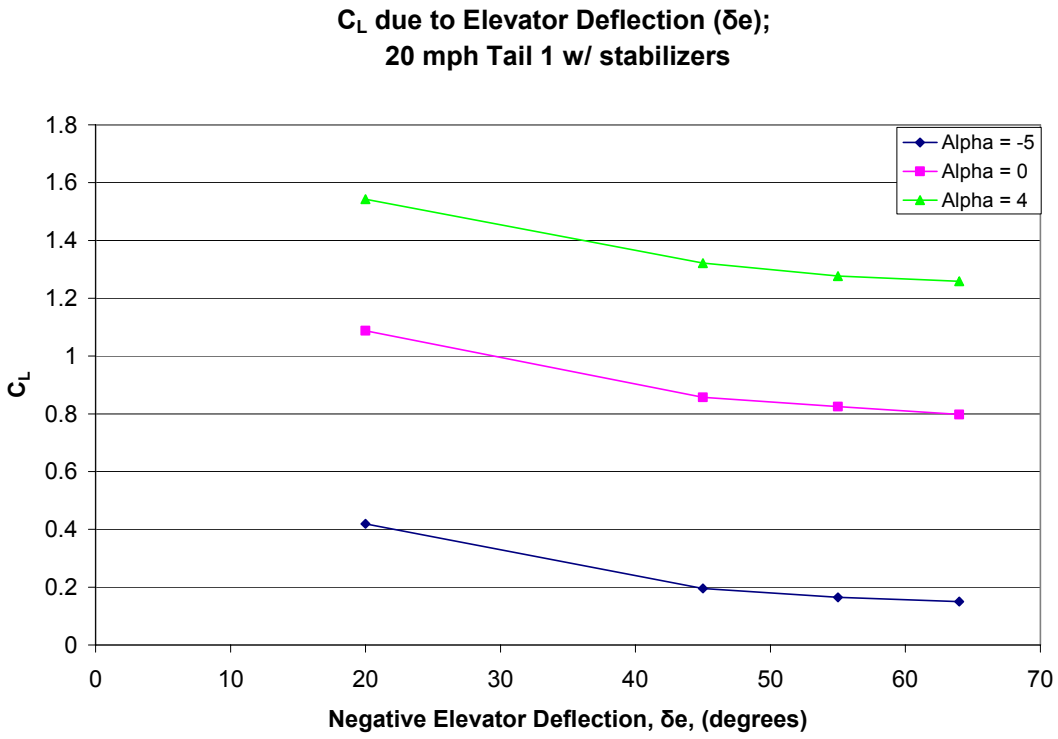

Figure 80. C_L vs. δ_e, 20 mph, Tail 1 w/stabilizers

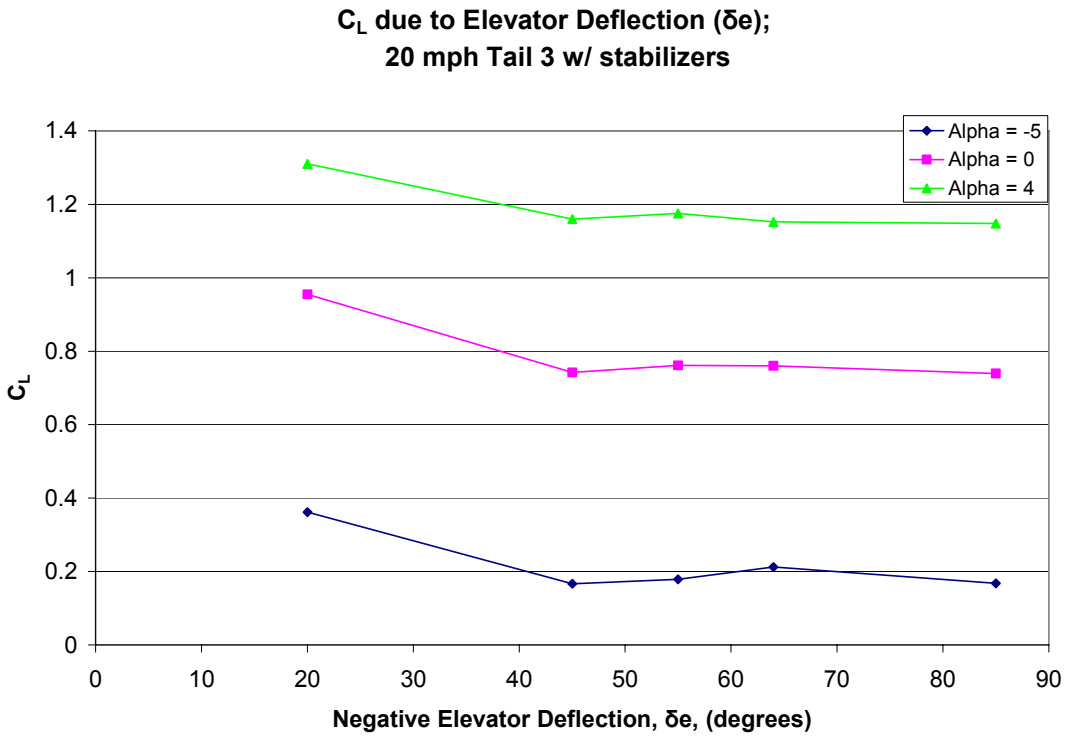

Figure 81. C_L vs. δ_e, 20 mph, Tail 3 w/stabilizers

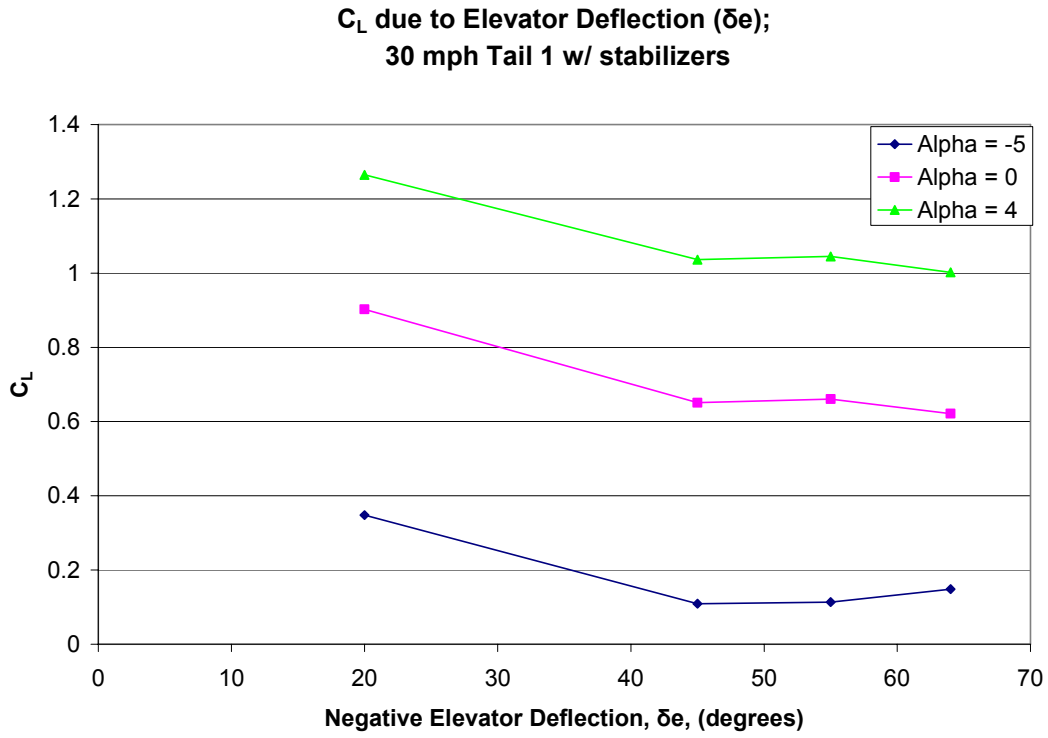

Figure 82. C_L vs. δ_e, 30 mph, Tail 1 w/stabilizers

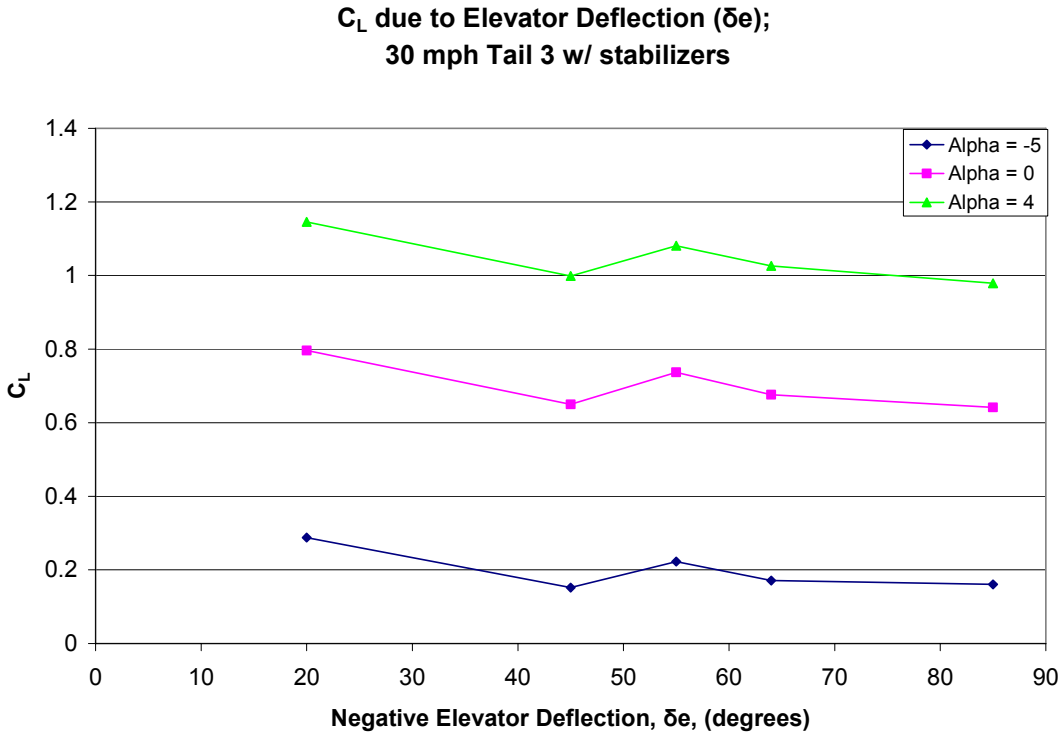

Figure 83. C_L vs. δ_e, 30 mph, Tail 3 w/stabilizers

Figure 84 through 87 are the C_D plots for various flight conditions and tail configurations. Drag generally increased for all plots at δ_e became more negative. Figure 86 and Figure 87 again show a decrease in drag at $\delta_e = 55^o$. This corresponds to the increase in lift seen in the C_L plots for the same condition.

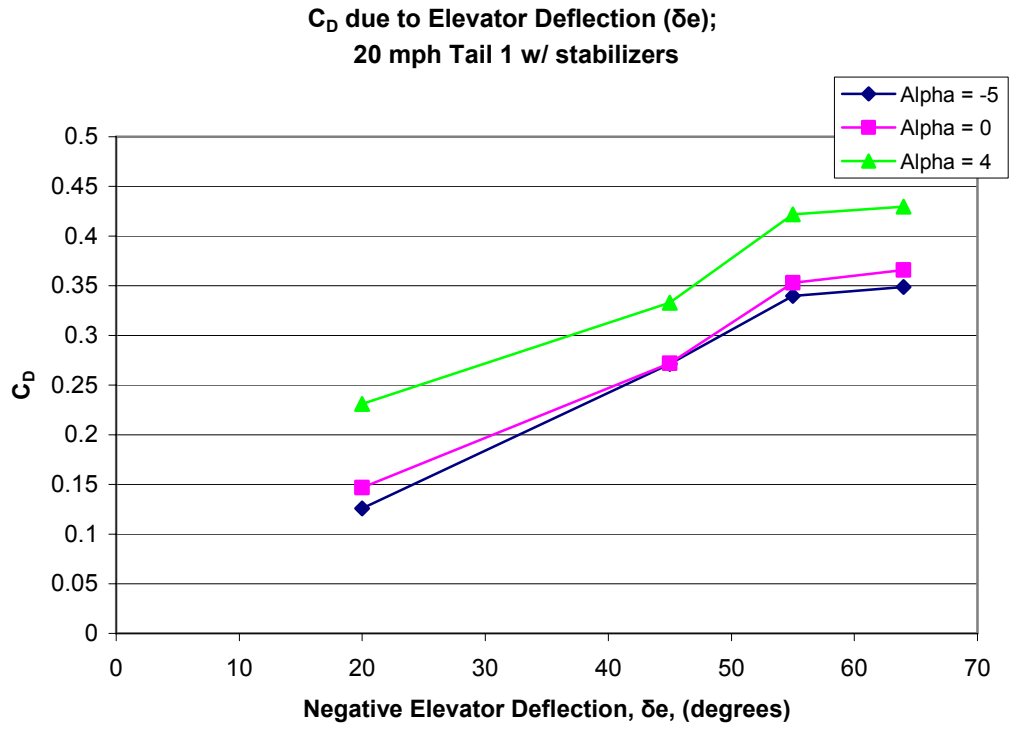

Figure 84. C_D vs. δ_e, 20 mph, Tail 1 w/stabilizers

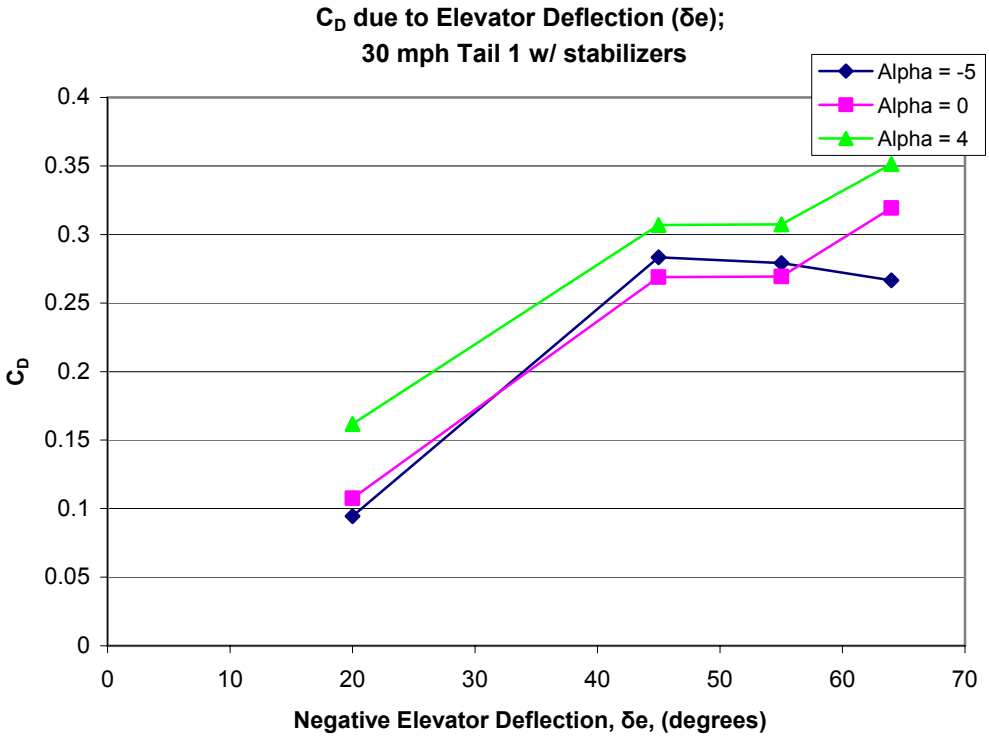

Figure 85. C_D vs. δ_e, 30 mph, Tail 1 w/stabilizers

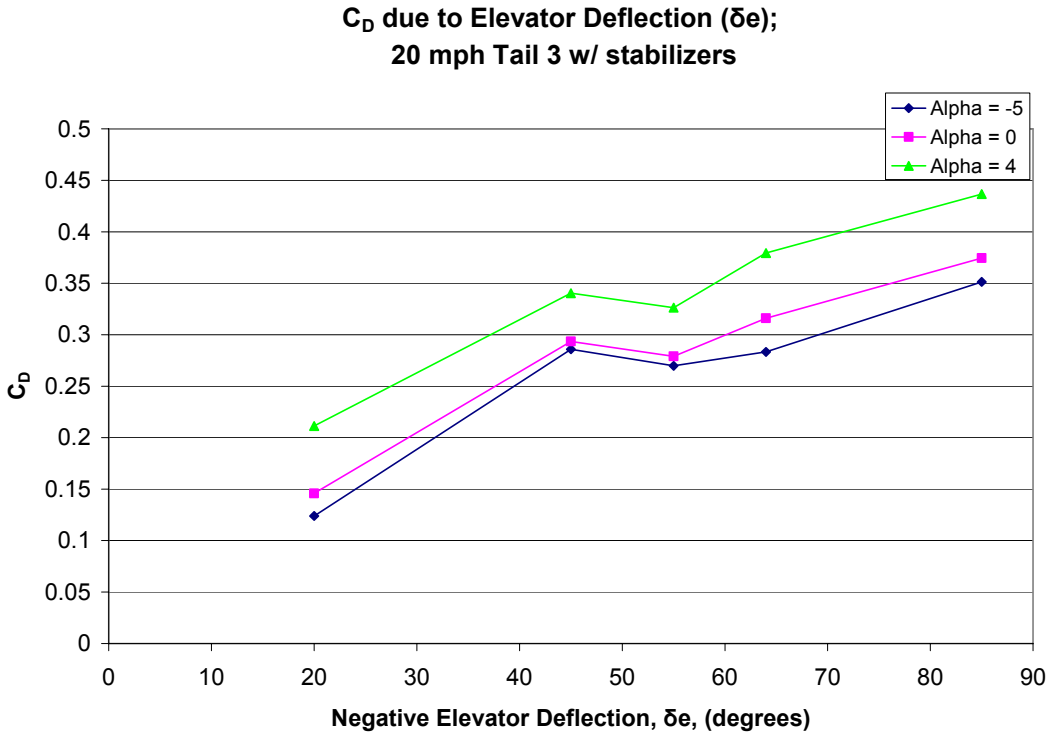

Figure 86. C_D vs. δ_e, 20 mph, Tail 3 w/stabilizers

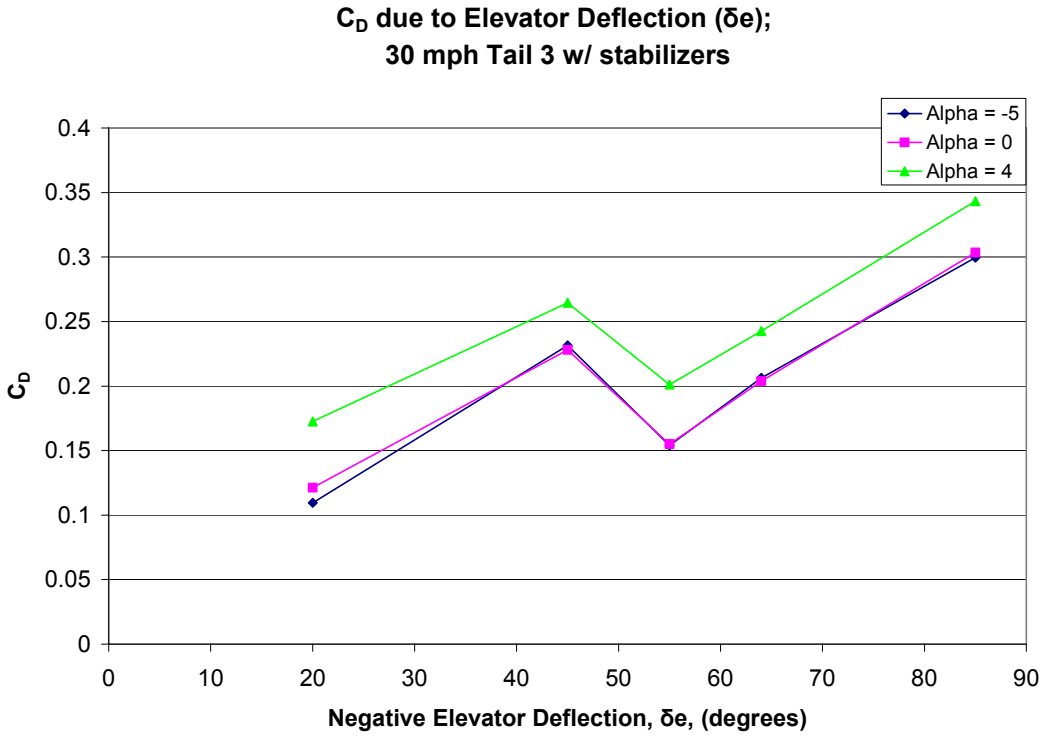

Figure 87. C_D vs. δ_e, 30 mph, Tail 3 w/stabilizers

Figure 88 through 92 are C_m plots for the various configurations. Figure 88 shows a direct comparison of one flight condition for both configurations. The stabilizer weight is seen to reduce the pitching moment for most of the range of δ_e, though the shift in CG was somewhat compensated for in the data reduction program. A sharp drop in C_m is seen in Figure 90 and Figure 91 at $\delta_e = 55^o$. This anomaly corresponds with similar anomalies in the C_L and C_D plots above. Similarly the anomaly corresponds with trends in the text that were related to a flat plate at incidence. For the conditions in Figure 91 the largest Cm value is at $\delta_e = 45^o$ corresponding with the largest C_{normal} seen in the flat plate. The drop off after $\delta_e = 45^o$ in Figure 91 is similar to the drop in C_{normal} at the same angular condition.

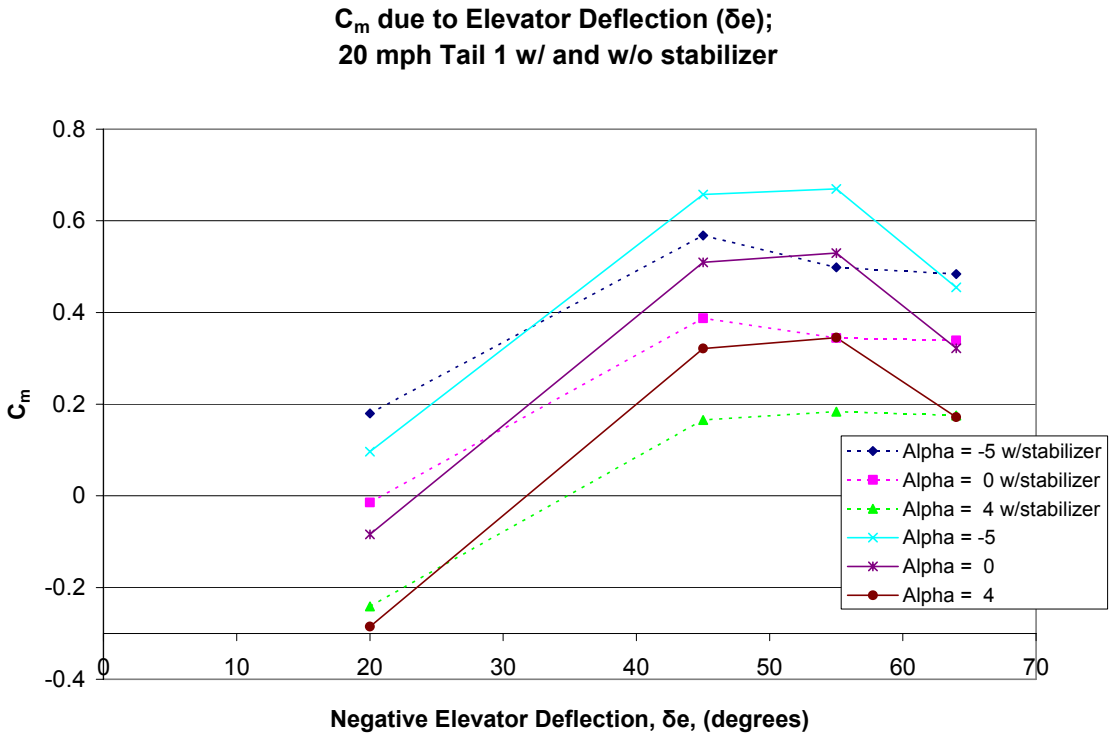

Figure 88. C_m vs. δ_e, 20 mph, Tail 1 w/ & w/o stabilizer

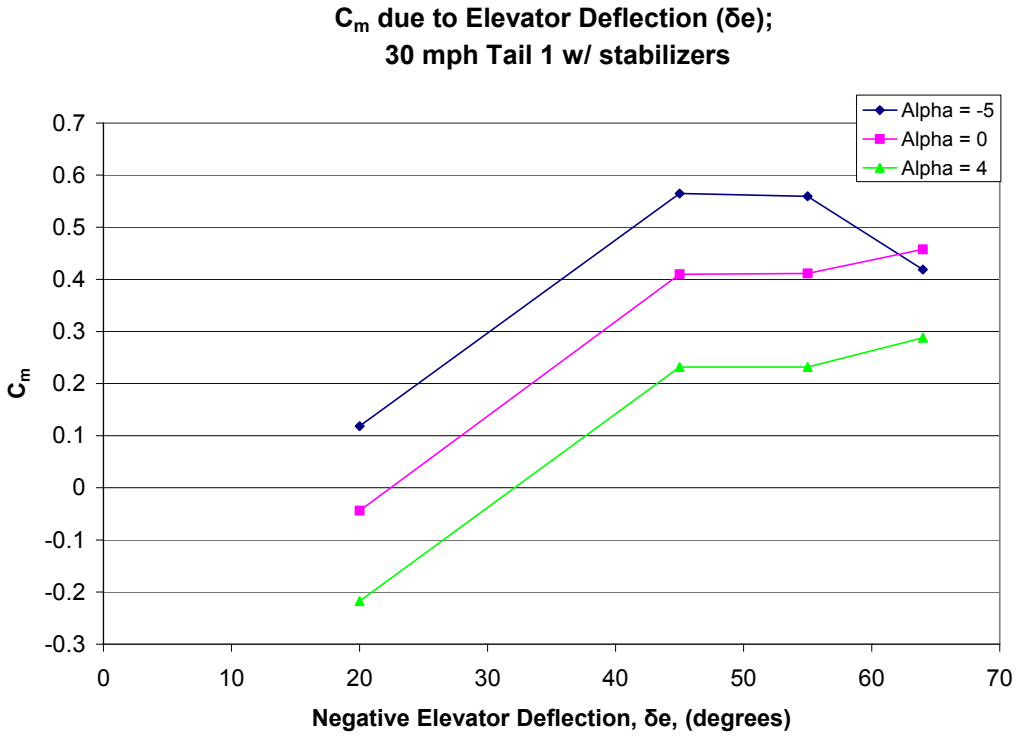

Figure 89. C_m vs. δ_e, 30 mph, Tail 1 w/stabilizers

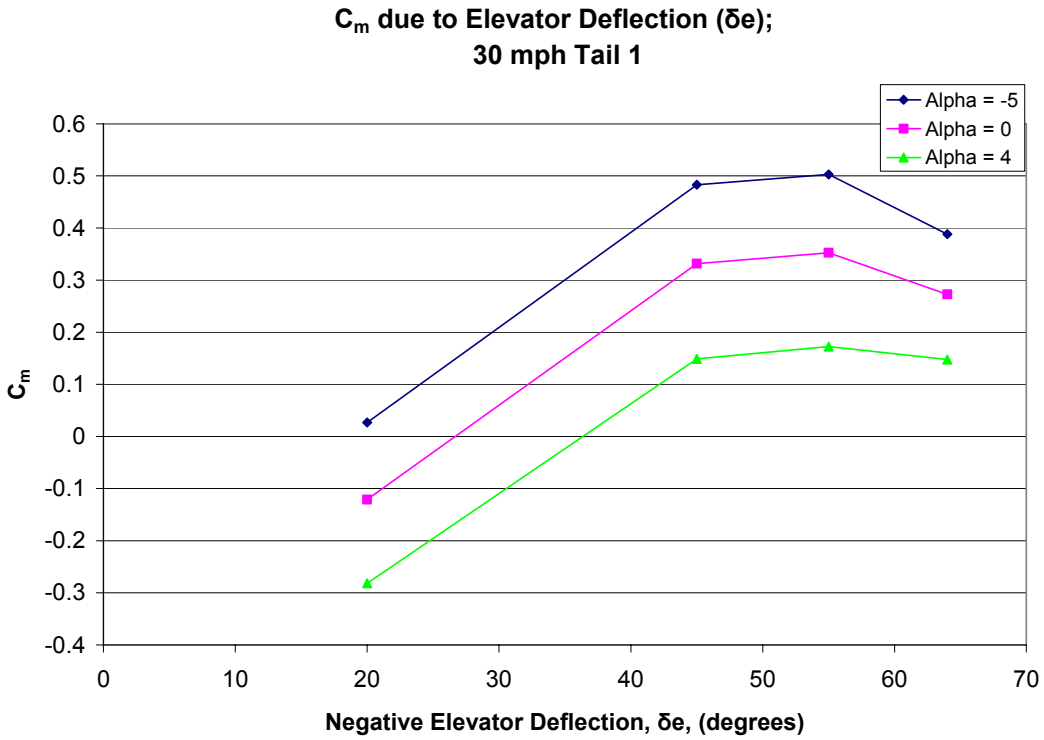

Figure 90. C_m vs. δ_e, 30 mph, Tail 1

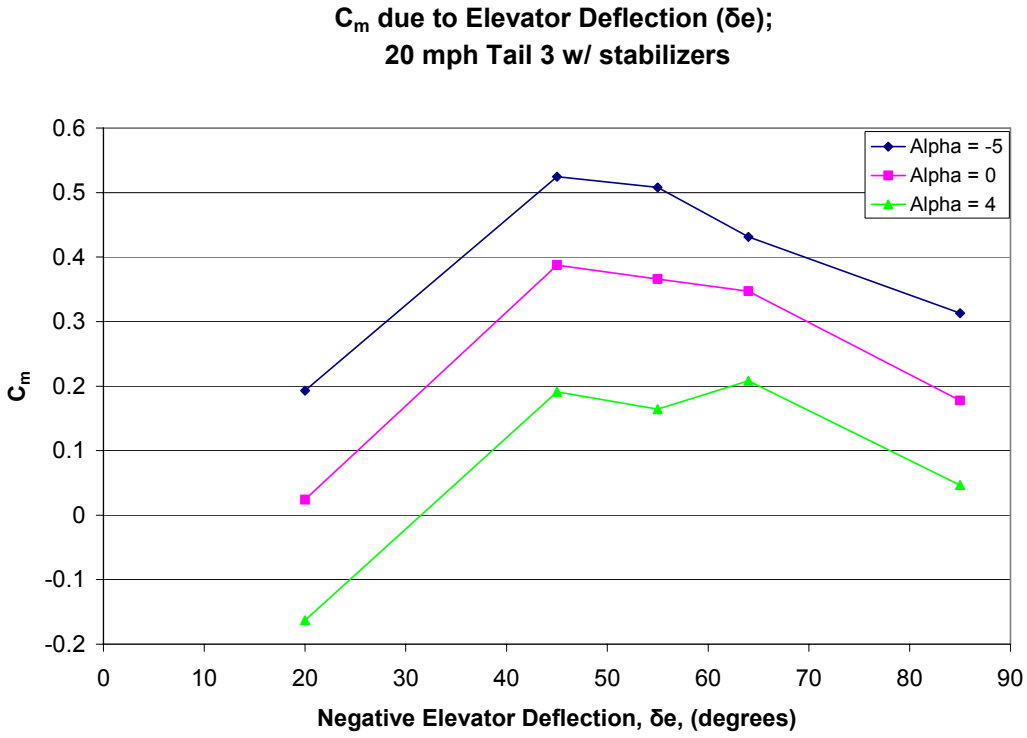

Figure 91. C_m vs. δ_e, 20 mph, Tail 3 w/stabilizers

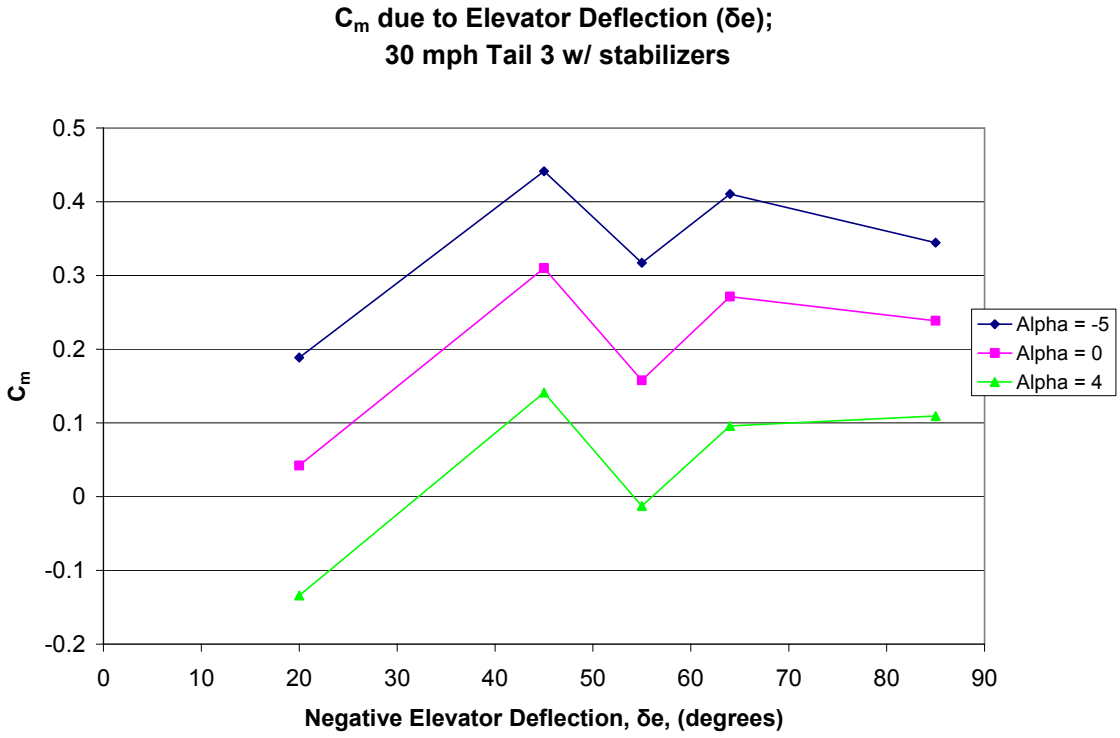

Figure 92. C_m vs. δ_e, 30 mph, Tail 3 w/stabilizers

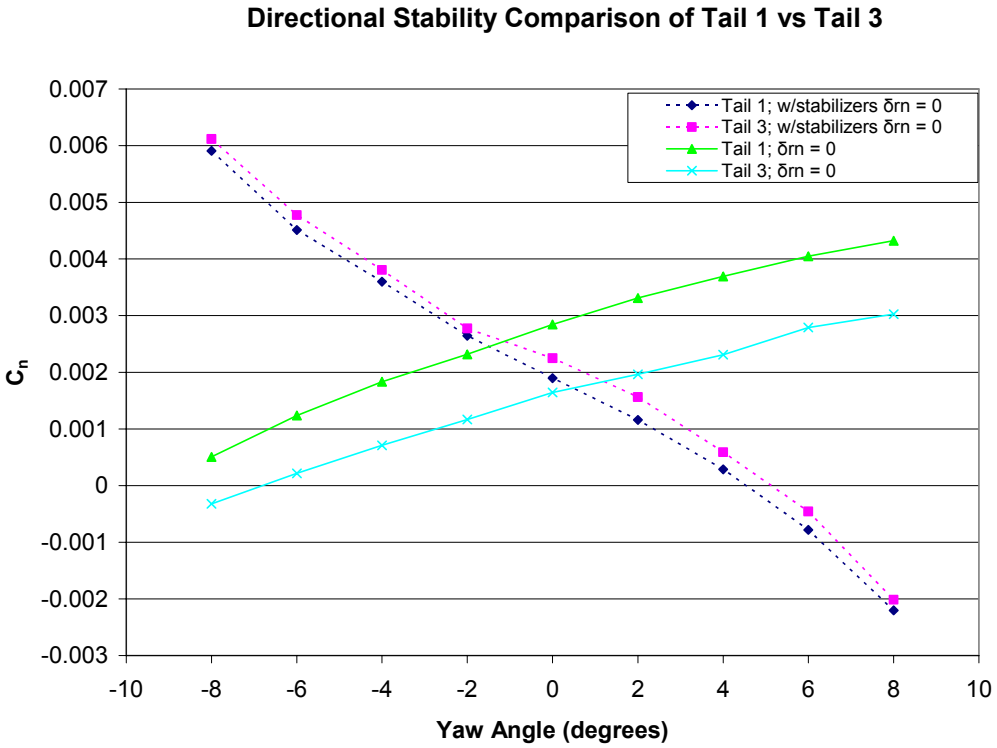

Figure 93. Directional Stability of Tail 1 vs. Tail 3

Figure 93 shows that the stabilizer improved stability. $C_{n\psi}$ should be negative for stability. The slopes of the stabilizer plots in this figure are negative while without stabilizer the slope is positive.

Appendix D MATLAB® Code for Data Reduction

```
%*********************************************************************
%********** Lt. Gebbie & Capt Anthony DeLuca **********************
%* Adapted for the Balance AFIT 1 and rotary tails by Lt. Rivera Parga %***********
%******* re-adapted for angled balance mount by ENS Troy Leveron **********
%********** Calculation of Lift, Drag, Moments ************************
%********** FLEX WING, Prop OFF, ALPHA SWEEPS *****************
%This Code will transfer measured Forces and Moments on the AFIT 1 balance to Wind
%(earth) centered frame of reference by correcting for tare effects, balance
%interactions, and wind tunnel irregularities, then gives a file with all the
%corrected data
clear;
clc;
close all;
format long
%#########################################################################
% INPUT DECK
%FIRST FILL THE FOLLOWING INFORMATION
Masskg=0.415; % Mass of the UAV in KGS
T_room = mean([72.3]) + 459.67; %deg R **Changed for each day of testing*
P_barro = mean([29.06]) * 0.4911541; %Psi ****Changed for each day of testing****
% Added 24 April to allow easier change of input tare and data files
load tarefile.txt;                  %tarefile
TareFile = tarefile(:,1:9);
load datafile.txt;                   %datafile
DataFile = datafile(:,1:9);

%Offset distances from the Mounting Block to the Model C.G. (inches)
Y_cmb = -(0.05); %inches
X_cmb = 0.71; %inches
Z_cmb = -1.31; %inches
% Requeried for the Solid body blockage corrections due to wing and fuselage
Body_Volume = ((9.42962435*(2/16))+(0)+ (0.9375)+...
(3.5*((2.75+1.35)/2)*((1.95+1.32)/2))...
+(5.25*3.0*((1.95+1.45)/2))) / 12^3;
%(ft^3): Tail+vertical stabilizers (Tail 2)+ Connector+Prop-to-Wing+Wing Front-to-
Wing Back
% Requeried for the Pitching Moment Correction
l_t = 9/12; % ft = length from tail MAC to aircraft CG
Span_t =(4+(6/16)) / 12; % ft = horizontal span
Tail_Area = (9.42962435) / 144; % ft^2 = horizontal tail area
% BEFORE CONTINUING IT IS NECCESARY TO CHANGE THE NAME:
% INPUT DATA FILE AND INPUT DATA TARE FILE
% THE OUTPUT DATA FILE
```

```
%#########################################################################
%I. Polynomial Curve fit of Chord Dimensions to Spanwise length to get an
% Equation defining thet Chord anywhere along the span.
%#########################################################################
Span_Location = [0 2.62 (2.62*2) (2.62*3) (2.62*4)]; %in
Chord_Dist = [1/2 59/16 5 89/16 6]; %in
c1 = polyfit(Span_Location,Chord_Dist,2);
Chord1 = polyval(c1,Span_Location);
c2 = polyfit(Span_Location,Chord_Dist,3);
Chord2 = polyval(c2,Span_Location);
c3 = polyfit(Span_Location,Chord_Dist,4);
Chord3 = polyval(c3,Span_Location);
figure(1)
plot(Span_Location,Chord_Dist,'x',Span_Location,Chord1,'- .',Span_Location,Chord2,'o-
.',Span_Location,Chord3,'*-');
%4th order chord equation as a function of the span (b) or C(y) integrated
%from 0 to b/2 to calculate 1/2 of the wing area.
chord_eqn = inline('-0.00044213367831*b.^4+0.01737585355753*b.^3-
0.25190354097469*b.^2+1.76526717557252*b+0.50');
Wing_Area = (2 * quad(chord_eqn,0,4*2.62)) / 144; %ft^2
%#########################################################################
%II. Room Conditions and Model Specifics :
% UNITS are in Ft, Sec, lbm, Psf, Rankine, fps
%#########################################################################
Mass = (Masskg * 1000) * 0.0022046; %lbm (flex MAV with batteries)
Gas_Const = 1716; %ft-lbf/Slug-R
Density = (P_barro * 144)/(1716 * T_room); %lbm/ft^3 or lbf-s^2/ft^4
Root_Chord = 6 * (1/12); %ft
Span = 24 / 12; %ft
Aspect_Ratio = Span^2 / Wing_Area;
Viscosity = .372e-6; %slug/ft-s
Speed_of_Sound = sqrt(1.4 * T_room * Gas_Const); %fps
%#########################################################################
%III. Solid body blockage corrections due to wing and fuselage
%#########################################################################
K_1 = 0.9;
K_3 = 0.93;
delta = 0.1125;
Tau_1 = 0.83125;
X_Section = (31/12)*(44/12); %ft^2
Wing_Volume = Wing_Area * (.006/12); %ft^3
Epsilon_sb_w = (K_1*Tau_1*Wing_Volume) / X_Section^(3/2);
Epsilon_sb_b = (K_3*Tau_1*Body_Volume) / X_Section^(3/2);
Epsilon_tot = Epsilon_sb_w + Epsilon_sb_b;
%#########################################################################
% III. Load the static tare data for the alpha sweep w/o the wind,
```

```
% separate each force from the file, and fit a 4th order poly
% as an x-y plot (AoA vs.Force) for each of the 6 force sensors.
%#########################################################################

%load tare1.txt;                % Raw tare data file to be read in; commented to reflect
change above
FILE=TareFile(:,1:9);            %
j=1;
k=1;
L=length(FILE);

for i=1:L                        %Run for all data points # of rows
   if i~=L                       %if current row is not last row, go to next
      NEXT=i+1;                     %set next equal to the value of the next row
      VALUE2=FILE(NEXT,1);          %set value2 as next row column 1
   else if i==L                  %unless the it is the last value
      VALUE2=50;                    %value2 set to 50 to end the sequence
   end
   end
   A(j,:)=FILE(i,:);             %set row j of A equal to row i of FILE
   VALUE1=FILE(i,1);                %set value1 equal to row i column 1 of FILE
   if VALUE1==VALUE2                %if value1 equals value2, go to next row
      j=j+1;
   else if VALUE1~=VALUE2           %if value1 and value2 are different check
      if length(A(:,1))<5           %if less than 20 values, ignored due to angle change
         j=1;
         clear A;
      else if length(A(:,1))>5      %if more than 20 values
            C=length(A(:,1));          %find length of A
            for m=1:9               %Average all rows of the like values in A
               B(k,m)=mean(A(4:C,m));    %disregarding first 10 for vibrations
            end
            j=1;
            k=k+1;
            clear A
      end
      end

   end
   end
end

if B(k-1,1)<B((k-2),1)
   B=B(1:(k-2),:)
end
```

```
tare=[B];

%_____________________________________End of inserted code
[row,col] = size(tare);for k = 1:row;
theta_tare(k,:,:) = tare(k,1).* (pi/180);
NF_tare(k,:,:) = tare(k,4);
PM_tare(k,:,:) = tare(k,5);
SF_tare(k,:,:) = tare(k,7);
YM_tare(k,:,:) = tare(k,8);
AF_tare(k,:,:) = tare(k,6);
RM_tare(k,:,:) = tare(k,9);
end
NF_poly = polyfit(theta_tare,NF_tare,4);
PM_poly = polyfit(theta_tare,PM_tare,4);
SF_poly = polyfit(theta_tare,SF_tare,4);
YM_poly = polyfit(theta_tare,YM_tare,4);
AF_poly = polyfit(theta_tare,AF_tare,4);
RM_poly = polyfit(theta_tare,RM_tare,4);
%##########################################################################
%IV. Load the specific test run files,
%##########################################################################
clear ('AA','B','C','L')
%_____________________________________________
%load data1.txt;                % Raw data file to be read in commented
                                % to reflect change made above
FILE=DataFile(:,:);             %
j=1;
k=1;
L=length(FILE);

for i=1:L                       %Run for all data points # of rows
   if i~=L                      %if current row is not last row, go to next
      NEXT=i+1;                 %set next equal to the value of the next row
      VALUE2=FILE(NEXT,1);   %set value2 as next row column 1; changed 1 to 2 for beta runs
   else if i==L                 %unless the it is the last value
      VALUE2=50;                %value2 set to 50 to end the sequence
   end
   end
   A(j,:)=FILE(i,:);            %set row j of A equal to row i of FILE
   VALUE1=FILE(i,1);            %set value1 equal to row i column 1 of FILE; change 1 to 2 for beta
   if VALUE1==VALUE2            %if value1 equals value2, go to next row
      j=j+1;
   else if VALUE1~=VALUE2       %if value1 and value2 are different check
      if length(A(:,1))<5       %if less than 20 values, ignored due to angle change;
                                %change to 2 for beta
         j=1;
         clear A;
      else if length(A(:,1))>5  %if more than 20 values;  change 1 to 2 for beta runs
            C=length(A(:,1));   %find length of A;  change 1 to 2 for beta runs
            for m=1:9           %Average all rows of the like values in A
               B(k,m)=mean(A(4:C,m));  %disregarding first 10 for vibrations
```

```
            end
            j=1;
            k=k+1;
            clear A
        end
        end
    end
    end
end

if B(k-1,1)<B((k-2),1)  %change 1 in ",1)" to 2 for beta runs
    B=B(1:(k-2),:)
end

sample_data=[B];

%_____________________________________End of inserted code
 %_____________________________________End of inserted code
[row2,col2] = size(sample_data);
for i = 1:row2;
%Angles of the model during test runs (Roll, Pitch {AoA}, Yaw {Beta}):
phi = 0;
theta(i,:) = sample_data(i,1) .* (pi/180); %radians
si(i,:) = sample_data(i,2) .* (pi/180); %radians
Wind_Speed(i,:) = sample_data(i,3) .* (5280/3600); %fps
%Flight Parameters (Re#, Ma#, Dynamic Pressure):
q = (.5 * Density) .* Wind_Speed.^2; %lbf/ft^2
q_Corrected = q .* (1 + Epsilon_tot)^2; %lbf/ft^2
Wind_Speed_Corrected = Wind_Speed .* (1 + Epsilon_tot); %fps
Mach_Number = Wind_Speed_Corrected ./ Speed_of_Sound; %NonDimensional
Reynolds_Number = ((Density * Root_Chord) .* Wind_Speed_Corrected) ./ Viscosity;
%NonDimensional
Flight_Parameters = [Mach_Number Reynolds_Number q_Corrected];
%individual forces and moments for each sensor:
NF_test(i,:,:) = sample_data(i,4);
PM_test(i,:,:) = sample_data(i,5);
SF_test(i,:,:) = sample_data(i,7);
YM_test(i,:,:) = sample_data(i,8);
AF_test(i,:,:) = sample_data(i,6);
RM_test(i,:,:) = sample_data(i,9);

%##########################################################################
%V. Subtract the effect of the static
% weight with the tare polynomials above
%##########################################################################
%Evaluating the actual test theta angle (AoA) in the tare polynomial to
%determine the tare values for the angles tested in each run.
NF_eval = polyval(NF_poly,theta);
PM_eval = polyval(PM_poly,theta);
```

```
SF_eval = polyval(SF_poly,theta);
YM_eval = polyval(YM_poly,theta);
AF_eval = polyval(AF_poly,theta);
RM_eval = polyval(RM_poly,theta);
%The Time-Averaged (raw) forces and momentums NF,AF,SF,PM,YM AND RM
measured in the wind
%tunnel (body axis) with the tare effect of the weight subtracted off.
NF_resolved = NF_test - (NF_eval);
PM_resolved = PM_test - (PM_eval);
SF_resolved = SF_test - (SF_eval);
YM_resolved = YM_test - (YM_eval);
AF_resolved = AF_test - (AF_eval);
RM_resolved = RM_test - (RM_eval);
Forces_minus_tare = [NF_resolved, AF_resolved, PM_resolved, RM_resolved,
YM_resolved, SF_resolved]';
%#########################################################################
%VI. CORRECT FORCES AND MOMENTS FOR BALANCE INTERATIONS (body
axis)
%#########################################################################
%USING THE REDUCTION EQUATIONS
%LET US SET A MAXIMUN NUMBER OF INTERATIONS (FOR AVOIDING AN
INFINIT LOOP)
MAXIT=100;
%SET THE LIMIT FOR THE DIFFERENCE BETWEEN INTERATIONS(CRITERIA
FOR FINISH THE INTERATIONS)
LIMIT= 10E-14;
%MATCHING EACH NAME WITH THE DATA
MNF=NF_resolved(i);
MAF=AF_resolved(i);
MPM=PM_resolved(i);
MRM=RM_resolved(i);
MYM=YM_resolved(i);
MSF=SF_resolved(i);
%INPUT OF THE CONSTANTS VALUES FROM THE MATRIX FOR
SENSITIVITIES AND INTERATIONS
K=[0 -1.3567E-03 -3.8021E-03 -4.2814E-03 -1.6966E-03 1.7567E-03 ...
5.3167E-05 -1.3867E-04 -5.5629E-05 3.5181E-05 1.0601E-05 -2.5271E-04...
5.6693E-05 -1.9537E-04 1.7908E-05 -3.6606E-05 -4.9934E-05 4.1205E-05...
2.5648E-05 -1.9289E-05 8.9661E-05 -1.9594E-05 -4.9859E-04 -1.1599E-03...
5.7163E-05 8.9798E-05 -7.8591E-05 9.3187E-03 0 -3.8421E-03 3.5740E-03...
9.7714E-05 -2.7776E-03 -1.3552E-04 5.1538E-04 2.2082E-04 -1.2706E-05...
-2.3637E-05 1.3686E-05 1.1085E-04 -3.6557E-06 4.9876E-06 8.1085E-06...
3.7381E-05 1.2791E-04 -9.4527E-06 -2.3083E-06 -1.2046E-06 7.8161E-04...
-1.1997E-03 -3.0560E-05 -6.6202E-05 3.7227E-04 -2.1469E-04 4.8386E-03...
-3.7387E-03 0 -1.8479E-02 3.9077E-03 9.9165E-04 -1.4825E-05 -1.4830E-06...
6.0845E-05 8.0667E-05 1.8547E-05 -5.0212E-05 1.0539E-04 -2.2676E-04...
```

```
4.3793E-05 -1.0456E-05 -8.1186E-06 -2.1653E-05 -3.3070E-05 1.7280E-05...
-7.4509E-05 -3.4399E-05 -8.2999E-04 -6.7962E-04 4.0521E-05 -5.1604E-05...
9.1132E-06 -5.7360E-03 -2.2213E-04 9.9131E-04 0 -9.5790E-03 6.7114E-03...
3.6824E-05 1.0056E-04 -3.7105E-05 -9.0295E-05 -7.4580E-05 1.4814E-04...
7.2634E-05 -8.4778E-06 6.3486E-05 5.6328E-05 -1.3617E-04 2.2196E-05...
1.3606E-05 -3.6689E-05 8.3283E-05 1.1865E-04 1.8544E-05 -1.9831E-05...
1.7894E-05 -6.8164E-05 -7.0892E-05 1.2378E-03 1.6961E-03 -6.5102E-03...
-9.3202E-03 0 5.1349E-03 1.3612E-05 -1.3175E-04 7.2442E-06 5.6705E-04...
-1.4723E-05 -4.8656E-05 -1.4282E-04 5.9711E-05 5.9046E-05 -3.6490E-04...
7.4881E-05 5.4601E-06 1.0129E-03 -1.3867E-04 8.1617E-05 6.6053E-05...
-1.3417E-05 9.0025E-05 -4.5362E-05 -4.4672E-06 9.5087E-05 -3.4077E-02...
7.9142E-04 1.6667E-03 -6.6512E-03 8.1538E-03 0 -1.4185E-05 7.3209E-05...
-2.5849E-05 1.2325E-03 -4.1696E-05 4.6266E-05 8.6146E-05 2.1436E-05...
5.0874E-05 -3.2738E-04 2.2218E-04 8.6478E-06 7.3395E-04 -4.1453E-05...
3.5719E-05 2.5313E-05 1.5182E-04 3.6007E-05 -2.8844E-05 8.9741E-05...
-7.3257E-05];
%COMPUTE THE UNCORRECTED FORCES AND MOMENTS BY
%CONSIDERING THAT THE PRIME SENSITIVITY CONSTANTS ARE ALREADY
APLIED:
NF1=MNF;
AF1=MAF;
PM1=MPM;
RM1=MRM;
195
YM1=MYM;
SF1=MSF;
%FOR THE FIRST INTERACTION LET US INIZIALICE THE VALUES OF FORCES
AND
%MOMENTS WITH THE VALUES OF THE UNCORRECTED FORCES AND
MOMENTS
NF(1)=NF1;
AF(1)=AF1;
PM(1)=PM1;
RM(1)=RM1;
YM(1)=YM1;
SF(1)=SF1;
%DOING THE INTERACTION EQUATIONS:
for n=2:MAXIT;
NF(n)=NF1-((K(2)*AF(n-1))+(K(3)*PM(n-1))+(K(4)*RM(n-1))+(K(5)*YM(n-
1))+(K(6)*SF(n-1))+(K(7)*NF(n-1)^2)+...
(K(8)*(NF(n-1)*AF(n-1)))+(K(9)*(NF(n-1)*PM(n-1)))+(K(10)*(NF(n-1)*RM(n-
1)))+(K(11)*(NF(n-1)*YM(n-1)))+...
(K(12)*(NF(n-1)*SF(n-1)))+(K(13)*(AF(n-1)^2))+(K(14)*(AF(n-1)*PM(n-
1)))+(K(15)*(AF(n-1)*RM(n-1)))+...
(K(16)*(AF(n-1)*YM(n-1)))+(K(17)*(AF(n-1)*SF(n-1)))+(K(18)*(PM(n-
1)^2))+(K(19)*(PM(n-1)*RM(n-1)))+...
```

(K(20)*(PM(n-1)*YM(n-1)))+(K(21)*(PM(n-1)*SF(n-1)))+(K(22)*(RM(n-1)^2))+(K(23)*(RM(n-1)*YM(n-1)))+...
(K(24)*(RM(n-1)*SF(n-1)))+(K(25)*(YM(n-1)^2))+(K(26)*(YM(n-1)*SF(n-1)))+(K(27)*(SF(n-1)^2)));
AF(n)=AF1-((K(28)*NF(n-1))+(K(30)*PM(n-1))+(K(31)*RM(n-1))+(K(32)*YM(n-1))+(K(33)*SF(n-1))+(K(34)*NF(n-1)^2)+...
(K(35)*(NF(n-1)*AF(n-1)))+(K(36)*(NF(n-1)*PM(n-1)))+(K(37)*(NF(n-1)*RM(n-1)))+(K(38)*(NF(n-1)*YM(n-1)))+...
(K(39)*(NF(n-1)*SF(n-1)))+(K(40)*(AF(n-1)^2))+(K(41)*(AF(n-1)*PM(n-1)))+(K(42)*(AF(n-1)*RM(n-1)))+...
(K(43)*(AF(n-1)*YM(n-1)))+(K(44)*(AF(n-1)*SF(n-1)))+(K(45)*(PM(n-1)^2))+(K(46)*(PM(n-1)*RM(n-1)))+...
(K(47)*(PM(n-1)*YM(n-1)))+(K(48)*(PM(n-1)*SF(n-1)))+(K(49)*(RM(n-1)^2))+(K(50)*(RM(n-1)*YM(n-1)))+...
(K(51)*(RM(n-1)*SF(n-1)))+(K(52)*(YM(n-1)^2))+(K(53)*(YM(n-1)*SF(n-1)))+(K(54)*(SF(n-1)^2)));
PM(n)=PM1-((K(55)*NF(n-1))+(K(56)*AF(n-1))+(K(58)*RM(n-1))+(K(59)*YM(n-1))+(K(60)*SF(n-1))+(K(61)*NF(n-1)^2)+...
(K(62)*(NF(n-1)*AF(n-1)))+(K(63)*(NF(n-1)*PM(n-1)))+(K(64)*(NF(n-1)*RM(n-1)))+(K(65)*(NF(n-1)*YM(n-1)))+...
(K(66)*(NF(n-1)*SF(n-1)))+(K(67)*(AF(n-1)^2))+(K(68)*(AF(n-1)*PM(n-1)))+(K(69)*(AF(n-1)*RM(n-1)))+...
(K(70)*(AF(n-1)*YM(n-1)))+(K(71)*(AF(n-1)*SF(n-1)))+(K(72)*(PM(n-1)^2))+(K(73)*(PM(n-1)*RM(n-1)))+...
(K(74)*(PM(n-1)*YM(n-1)))+(K(75)*(PM(n-1)*SF(n-1)))+(K(76)*(RM(n-1)^2))+(K(77)*(RM(n-1)*YM(n-1)))+...
(K(78)*(RM(n-1)*SF(n-1)))+(K(79)*(YM(n-1)^2))+(K(80)*(YM(n-1)*SF(n-1)))+(K(81)*(SF(n-1)^2)));
RM(n)=RM1-((K(82)*NF(n-1))+(K(83)*AF(n-1))+(K(84)*PM(n-1))+(K(86)*YM(n-1))+(K(87)*SF(n-1))+(K(88)*NF(n-1)^2)+...
(K(89)*(NF(n-1)*AF(n-1)))+(K(90)*(NF(n-1)*PM(n-1)))+(K(91)*(NF(n-1)*RM(n-1)))+(K(92)*(NF(n-1)*YM(n-1)))+...
(K(93)*(NF(n-1)*SF(n-1)))+(K(94)*(AF(n-1)^2))+(K(95)*(AF(n-1)*PM(n-1)))+(K(96)*(AF(n-1)*RM(n-1)))+...
(K(97)*(AF(n-1)*YM(n-1)))+(K(98)*(AF(n-1)*SF(n-1)))+(K(99)*(PM(n-1)^2))+(K(100)*(PM(n-1)*RM(n-1)))+...
(K(101)*(PM(n-1)*YM(n-1)))+(K(102)*(PM(n-1)*SF(n-1)))+(K(103)*(RM(n-1)^2))+(K(104)*(RM(n-1)*YM(n-1)))+...
(K(105)*(RM(n-1)*SF(n-1)))+(K(106)*(YM(n-1)^2))+(K(107)*(YM(n-1)*SF(n-1)))+(K(108)*(SF(n-1)^2)));
YM(n)=YM1-((K(109)*NF(n-1))+(K(110)*AF(n-1))+(K(111)*PM(n-1))+(K(112)*RM(n-1))+(K(114)*SF(n-1))+(K(115)*NF(n-1)^2)+...
(K(116)*(NF(n-1)*AF(n-1)))+(K(117)*(NF(n-1)*PM(n-1)))+(K(118)*(NF(n-1)*RM(n-1)))+(K(119)*(NF(n-1)*YM(n-1)))+...
(K(120)*(NF(n-1)*SF(n-1)))+(K(121)*(AF(n-1)^2))+(K(122)*(AF(n-1)*PM(n-1)))+(K(123)*(AF(n-1)*RM(n-1)))+...

```
(K(124)*(AF(n-1)*YM(n-1)))+(K(125)*(AF(n-1)*SF(n-1)))+(K(126)*(PM(n-
1)^2))+(K(127)*(PM(n-1)*RM(n-1)))+...
(K(128)*(PM(n-1)*YM(n-1)))+(K(129)*(PM(n-1)*SF(n-1)))+(K(130)*(RM(n-
1)^2))+(K(131)*(RM(n-1)*YM(n-1)))+...
(K(132)*(RM(n-1)*SF(n-1)))+(K(133)*(YM(n-1)^2))+(K(134)*(YM(n-1)*SF(n-
1)))+(K(135)*(SF(n-1)^2)));
SF(n)=SF1-((K(136)*NF(n-1))+(K(137)*AF(n-1))+(K(138)*PM(n-1))+(K(139)*RM(n-
1))+(K(140)*YM(n-1))+(K(142)*NF(n-1)^2)+...
(K(143)*(NF(n-1)*AF(n-1)))+(K(144)*(NF(n-1)*PM(n-1)))+(K(145)*(NF(n-
1)*RM(n-1)))+(K(146)*(NF(n-1)*YM(n-1)))+...
(K(147)*(NF(n-1)*SF(n-1)))+(K(148)*(AF(n-1)^2))+(K(149)*(AF(n-1)*PM(n-
1)))+(K(150)*(AF(n-1)*RM(n-1)))+...
 (K(151)*(AF(n-1)*YM(n-1)))+(K(152)*(AF(n-1)*SF(n-1)))+(K(153)*(PM(n-
1)^2))+(K(154)*(PM(n-1)*RM(n-1)))+...
(K(155)*(PM(n-1)*YM(n-1)))+(K(156)*(PM(n-1)*SF(n-1)))+(K(157)*(RM(n-
1)^2))+(K(158)*(RM(n-1)*YM(n-1)))+...
(K(159)*(RM(n-1)*SF(n-1)))+(K(160)*(YM(n-1)^2))+(K(161)*(YM(n-1)*SF(n-
1)))+(K(162)*(SF(n-1)^2)));
% SET THE LIMIT FOR THE DIFFERENCE BETWEEN INTERATIONS(CRITERIA
FOR FINISH THE INTERATIONS)
DIFFNF(n)=abs(NF(n)-NF(n-1));
DIFFAF(n)=abs(AF(n)-AF(n-1));
DIFFPM(n)=abs(PM(n)-PM(n-1));
DIFFRM(n)=abs(RM(n)-RM(n-1));
DIFFYM(n)=abs(YM(n)-YM(n-1));
DIFFSF(n)=abs(SF(n)-SF(n-1));
if DIFFNF(n)&DIFFAF(n)&DIFFPM(n)&DIFFRM(n)&DIFFYM(n)&DIFFSF(n) <
LIMIT
break
end
end
%disp('THE FINAL VALUES ARE (NF,AF,PM,RM,YM,SF):')
Corrected_Data(:,i)= [NF(n);AF(n);PM(n);RM(n);YM(n);SF(n)];
%disp('THE FINAL DIFFERENCE BETWEEN INTERATIONS ARE(FOR
%NF,AF,PM,RM,YM,SF) :')
%FINAL_DIFFERENCE=[DIFFNF(n),DIFFAF(n),DIFFPM(n),DIFFRM(n),DIFFYM(n),
%DIFFSF(n)]
%disp('THE NUMBER OF INTERATIONS USED WAS:')
%%%%%%%%%%%%%%%%%%%%%%%%%%%%%%%%%%%%%%%%%%%%%%%%%%%%%%%%%%%%%%%%%%%%%%%
%VII. Calculation of the Axial, Side, & Normal Forces from the corrected balance
% forces in the Body Axis reference frame
%%%%%%%%%%%%%%%%%%%%%%%%%%%%%%%%%%%%%%%%%%%%%%%%%%%%%%%%%%%%%%%%%%%%%%%
Forces_b(:,i) = [Corrected_Data(2,i); Corrected_Data(6,i); Corrected_Data(1,i)];
%Calculation of the Drag, Side, & Lift Forces in the Wind Axis reference frame
Forces_w = [Forces_b(1,:).*cos(theta').*cos(si')+Forces_b(2,:).*sin(si')+Forces_b(3,:).
*sin(theta').*cos(si'); -Forces_b(1,:).*sin(si').*cos(theta')+
Forces_b(2,:).*cos(si') -Forces_b(3,:).*sin(theta').*sin(si');
```

```
-Forces_b(1,:).*sin(theta')+Forces_b(3,:).*cos(theta')];

%First entry is the moments calculated by the balance or direct calculation
%in the Body Reference Frame. Balance measures Roll (l), Yaw is about the
%z-axis (n), and Pitch is about the y-axis (m). Distances from strain
%gages to C.G. are in INCHES. Moments are in-lbf
m = Corrected_Data(3,i);
n = Corrected_Data(5,i);
l = Corrected_Data(4,i);
Moments_b(:,i) = [l; m; n];
%Second entry is the conversion from the "Balance Centeric" moments to the
%Wind Reference monments with respect to the Balance Center (bc)
Moments_w_bc = [Moments_b(1,:).*cos(theta').*cos(si')-Moments_b(2,:).
*sin(si')+Moments_b(3,:).*sin(theta').*cos(si');
Moments_b(1,:).*sin(si').*cos(theta')+Moments_b(2,:).*cos(si')+
Moments_b(3,:).*sin(theta').*sin(si');
-Moments_b(1,:).*sin(theta')+Moments_b(3,:).*cos(theta')];
%Finally, the balance centered moments are converted to moments about the
%Model's Center of Mass (cm) or Center of Gravity (CG)
cgdist=sqrt((X_cmb)^2+(Z_cmb)^2); %Obtaining the direct distance between the
center of the balance and the center of mass
w=atan(-Z_cmb/X_cmb); %Obtaining the angle between cgdist and the x axes at zero
angle of attack
X_cm(i,:)= cos(theta(i,:)+w)*cos(si(i,:))*(cgdist);
Y_cm(i,:) = Y_cmb + X_cm(i,:)*tan(si(i,:));
Z_cm(i,:)= -sin(theta(i,:)+w)*(cgdist);
Moments_w_cg_u = [Moments_w_bc(1,:) + Z_cm(i,:)*Forces_w(2,:) + Forces_w(3,:)*
Y_cm;
Moments_w_bc(2,:) - Forces_w(3,:)* X_cm(i,:) + Forces_w(1,:)*
Z_cm(i,:);
Moments_w_bc(3,:) - Forces_w(1,:)* Y_cm - Forces_w(2,:)*
X_cm(i,:)];
%##########################################################################
%VIII. Calculation of the actual Lift and Drag no dimensional Coefficients, uncorrected
for tunnel effects, (Cl and Cd)
%##########################################################################
C_D_u = Forces_w(1,:) ./ (q_Corrected' .* Wing_Area);
C_Y_u = Forces_w(2,:) ./ (q_Corrected' .* Wing_Area);
C_L_u = Forces_w(3,:) ./ (q_Corrected' .* Wing_Area);
Coefficients = [C_L_u; C_D_u; C_Y_u]';
Ave_Cl = mean(Coefficients(:,1));
Ave_Cd = mean(Coefficients(:,2));
end
%##########################################################################
%IX Drag Coefficient Correction
%##########################################################################
```

```
C_D_o = min(Coefficients(:,2));
C_L_u_sqrd = Coefficients(:,1).^2;
Delta_C_D_w = ((delta * Wing_Area) / X_Section) .* C_L_u_sqrd;
C_D_Corrected = C_D_u' + Delta_C_D_w;
%#########################################################################
%X. Angle of Attack due to upwash Correction
%#########################################################################
alpha_before = sample_data(:,1);
alpha = [alpha_before]-[5]  %changed 18 Apr for mounting block angle
Delta_alpha_w = ((delta * Wing_Area) / X_Section) .* (57.3 * C_L_u);
alpha_Corrected = alpha + Delta_alpha_w';
%#########################################################################
%XI. Pitching Moment Correction
%#########################################################################
tau2 = 0.65;
c_bar = (mean([6, 5+9/16, 5, 3+11/16, 0.5])) / 12; % ft = Mean Chord of wing
V_bar = (Tail_Area * l_t) / (Wing_Area * c_bar); % Horizontal tail volume ratio
eta_t = 1.0;
epsilon_o = 0;
i_t = pi/4; % radians
i_w = 0;
Aspect_Ratio_t = Span_t^2 / Tail_Area;
D_epslion_D_alpha = ((2 .* C_L_u) ./ (pi* Aspect_Ratio))';
epsilon = epsilon_o + (D_epslion_D_alpha .* alpha_Corrected );
alpha_t = alpha_Corrected - i_w - epsilon + i_t;
C_L_alpha_t = ((0.1* Aspect_Ratio) / (Aspect_Ratio_t +2)) * 0.8;
D_Cm_cg_t_D_alpha_t = -C_L_alpha_t* V_bar * eta_t;
Delta_C_m_cg_t = ((D_Cm_cg_t_D_alpha_t) * (delta*tau2) * (Wing_Area /
X_Section) .* (C_L_u * 57.3))';

Cl_w_cg = Moments_w_cg_u(1,:) ./ (q_Corrected' .* (Wing_Area * Span*12));
Cm_w_cg_u = Moments_w_cg_u(2,:) ./ (q_Corrected' .* (Wing_Area * c_bar*12));
Cn_w_cg = Moments_w_cg_u(3,:) ./ (q_Corrected' .* (Wing_Area * Span*12));
Cm_w_cg_corrected = Cm_w_cg_u - Delta_C_m_cg_t';
Corrected_Moment_Coefficients = [Cl_w_cg' Cm_w_cg_corrected' Cn_w_cg'];
%OBTAINING THE MOMENTS COEFFICIENTS CORRECTED ABOUT THE
CENTER OF THE
%BALANCE
Cl_w_bc = Moments_w_bc(1,:) ./ (q_Corrected' .* (Wing_Area * Span*12));
Cm_w_bc_u = Moments_w_bc(2,:) ./ (q_Corrected' .* (Wing_Area * c_bar*12));
Cn_w_bc = Moments_w_bc(3,:) ./ (q_Corrected' .* (Wing_Area * Span*12));
Cm_w_bc_corrected = Cm_w_bc_u - Delta_C_m_cg_t';
Corrected_Moment_Coefficients_bc = [Cl_w_bc' Cm_w_bc_corrected' Cn_w_bc'];
%#########################################################################
%XII. OUTPUT VARIABLES FORMATING
%#########################################################################
alpha = sample_data(:,1);
```

```
fprintf('   Mach Number Reynolds Number Dynamic Pressure(Psf)\r')
Flight_Parameters
fprintf(' \r');
fprintf(' Loads are in lbf and arranged [D S L] across the top and increments of alpha down the
side \r')
Forces_w'
fprintf(' \r')
fprintf(' Moments are in in-lbf and arranged [L M N] down the side and increments of alpha along
the top \r')
Moments_w_cg_u
fprintf(' \r')
fprintf('      Cl_u          Cd_u           CY_u \r');
Coefficients
fprintf(' \r')
fprintf('    Del_CD_w       CD_u     CD_Corrected \r');
Compare_CD = [Delta_C_D_w C_D_u' C_D_Corrected]
fprintf(' \r')
fprintf('    Del_alpha_w    alpha_g     alpha_Corrected \r');
Compare_alpha = [Delta_alpha_w' alpha alpha_Corrected ]
fprintf(' \r')
fprintf('    Cl_cg_wind    Cm_cg_corrected_w     Cn_cg_wind \r');
Corrected_Moment_Coefficients
fprintf(' \r')
fprintf('      M#          Re#          q_c          Uoo       alpha_c       C_L       C_D_c      Cl_cg_w
Cm_cg_c_w    Cn_cg_w       C_Y\r');
YY=[Flight_Parameters (Wind_Speed_Corrected .* (3600/5280)) alpha_Corrected C_L_u'
C_D_Corrected Corrected_Moment_Coefficients C_Y_u']%pressure]
%XX=['M#' 'Re#' 'q_c'  'Uoo' 'alpha_c' 'C_L' 'C_D_c' 'Cl_cg_w' 'Cm_cg_c_w' 'Cn_cg_w \r'];

%ZZ=[XX; YY];
wk1write('output.xls',YY,2,0)


Max_Cl = max(Coefficients(:,1));

% LET US SAVE TOTAL DATA IN A EXTERNAL FILE

%dlmwrite('TEST TOTAL DATA T2 DE M9 DRN 20',TOTAL_DATA,'\t')
```

Bibliography

Al-Bahi, Ali. M. "Investigation of the Flow Field Past an Airfoil-Spoiler Configuration". AIAA paper 1996-0552.

Barlow, Jewel B., William H. Rae, Jr., Alan Pope. *Low-Speed Wind Tunnel Testing*. (3rd Edition). New York: John Wiley and Sons, 1999.

Biber, Kasim, Ol, M., and Tillman, C. "Some Examples of Airfoil Design For Future Unmanned Air Vehicle Concepts," *42nd AIAA Aerospace Sciences Meeting and Exhibit.* AIAA Paper 2004-1050, Istanbul, Turkey 34870 and Air Force Research Laboratory, Air Vehicles Directorate, Aeronautical Sciences Division, WPAFB OH. 5-8 January 2004.

Carmichael, B.H., "Low Reynolds Number Airfoil Survey," NASA CR-165803, 1981.

Gad-el_Hak, Mohamed. "Micro-Air-Vehicles: Can they be Controlled Better," *Journal of Aircraft*, Vol. 38:419-429 (May-June 2001).

Hoerner, Sighard F. *Fluid dynamic Drag*. Midland Park, New Jersey, 1965.

Horton-Smith, Clifford. *The Flight of Birds.* H.F & G. Witherby, Ltd. London, 1938.

Ifju, P.G., D.A. Jenkins, S. Ettinger, Y. Lian, W. Shyy, and M. R. Waszak. "Flexible-Wing-Based Micro Air Vehicles," *40th AIAA Aerospace Sciences Meeting and Exhibit.* AIAA Paper 2002-0705, Reno, Nevada, 14-17 January 2002.

Launius, Roger, D. *Innovation and the Development of Flight*. College Station: Texas A&M University Press, 1999.

Milius, S. "Tests Hint Bird Tails Are Misunderstood," *Science News*, July 14,2001.

Nechyba, Michael and Peter Ifju. "Towards Autonomous Flight of Micro Air Vehicles (MAVs): Vision-Guided Flight Stability and Control," Informational Briefing-Audience Unknown, Department of Electrical and Computer Engineering and Department of Aerospace and Mechanical Science, University of Florida, Gainesville Florida, 2002.

Nickel, K.l and Wohlfahrt, M., *Tailless Aircraft in Theory and Practice*. AIAA Education Series.American Institute of Aeronautics and Astronautics; London, Englan: E. Arnold, 1994.

Parga, Jose R. Rivera. "Wind Tunnel Investigation of the Static Stability and Control Effectiveness of a Rotary Tail in a Portable UAV," Thesis, Department of Aeronautics and Astronautics, Air Force Institute of Technology, Wright-Patterson AFT, OH, 2004.

Penn State. Online. *Stress, Strain, and Strain Gages*. Pennsylvania State University, 1 May 2004 http://www.me.psu.edu/me82/Learning/Strain/strain.html.

Perkins, Courtland D. and Robert E. Hage. *Airplane Performance Stability and Control.* John Wiley & Sons, Inc. New York, 1958.

Rayner, Jeremy M.V. "Form and Function in Avian Flight", *Current Ornithology,* Vol. 5, pp. 1-65, 1988.

Taylor Michael J.H. and David Mondey. *Milestones of Flight*. London: Jane's Publishing Company Limited, 1983

Storer, John H. *The Flight of Birds Analyzed Through Slow-Motion Photography.* Cranbrook Institute of Science, Bloomfield Hills, Michigan, c1948.

Warrick, D.R., M. W. Bundle, and K. P. Dial. "Bird Maneuvering Flight: Blurred Bodies, Clear Heads" From the symposium on *Stability and Maneuverability* at Annual Meeting of the Society for Integrative and Comparative Biology, Chicago, Illinois, 3 January 2001.

Waszak, Martin R and Luther N. Jenkins. "Stability and Control Properties of an Aeroelastic Fixed Wing Micro Aerial Vehicle," *AIAA Atmospheric Flight Mechanics Conference.* AIAA Paper 2001-4005, Montreal Canada, 6-9 August 2001.

Vita

Ensign Troy Andre Leveron spent the early years of his life exploring the hills of southern Indiana. He graduated from Forest Park Junior-Senior High School in Ferdinand, Indiana in 1999. The following academic year he attended Purdue University. In 2000 he received an appointment to the United States Naval Academy. He graduated USNA with a Bachelor of Science in Naval Architecture in May 2004. Also, in May 2004, he received orders to report to Air Force Institute of Technology, Wright Patterson AFB, OH. In July of 2005 he will report to Pensacola, Florida to begin Naval Aviation flight training.

REPORT DOCUMENTATION PAGE

Form Approved
OMB No. 074-0188

1. REPORT DATE *(DD-MM-YYYY)*	2. REPORT TYPE	3. DATES COVERED *(From – To)*
13-06-2005	**Master's Thesis**	JUN 2004 – JUN 2005

4. TITLE AND SUBTITLE

Characterization of a Rotary Flat Tail as a Spoiler and Parametric Analysis of Improving Directional Stability in a Portable UAV

5a. CONTRACT NUMBER

5b. GRANT NUMBER

5c. PROGRAM ELEMENT NUMBER

6. AUTHOR(S)

Leveron, Troy A., Ensign, USNR

5d. PROJECT NUMBER

5e. TASK NUMBER

5f. WORK UNIT NUMBER

7. PERFORMING ORGANIZATION NAMES(S) AND ADDRESS(S)

Air Force Institute of Technology
Graduate School of Engineering and Management (AFIT/EN)
2950 Hobson Way
WPAFB OH 45433-7765

8. PERFORMING ORGANIZATION REPORT NUMBER

AFIT/GAE/ENY/05-J06

9. SPONSORING/MONITORING AGENCY NAME(S) AND ADDRESS(ES)

AFRL/MNAV
Capt. Ian Bautista
Eglin AFB, FL 32542

10. SPONSOR/MONITOR'S ACRONYM(S)

11. SPONSOR/MONITOR'S REPORT NUMBER(S)

12. DISTRIBUTION/AVAILABILITY STATEMENT

APPROVED FOR PUBLIC RELEASE; DISTRIBUTION UNLIMITED.

13. SUPPLEMENTARY NOTES

14. ABSTRACT

The United States Air Force Research Lab, Munitions Directorate, Flight Vehicles, Integration Branch (AFRL/MNAV), has developed a flexible wing micro air vehicle (MAV) to be used with special tactics groups. In keeping with the requirement that this MAV be compact, previous research developed a rotatable tail mechanism which resulted in tail movement similar to that of a bird's tail. In this study the design of this tail was modified to produce a more storable vehicle. The redesign also allowed the tail to deflect upward to large angles, enabling the tail to be used as a spoiler. The aerodynamic affects of adding a vertical stabilizer mechanism to improve the stability of the vehicle and rotatable tail combination was also quantified. Data from these tests confirmed the tail is a plausible method to reduce lift and increase drag, consistent with proper spoiler function. A wide range of angles were used to demonstrate that forces and moments from the flat tail were similar to those of traditional rudder. Directional stability was improved by the stabilizer, and recommendations for further improvements are given.

15. SUBJECT TERMS

Micro Air Vehicles, Rotatable Tail, Flexible Wing, Wind Tunnel Testing

16. SECURITY CLASSIFICATION OF:			17. LIMITATION OF ABSTRACT	18. NUMBER OF PAGES	19a. NAME OF RESPONSIBLE PERSON
a. REPORT					Dr. Mark Reeder (ENY)
U	**U**	**U**	**UU**	125	19b. TELEPHONE NUMBER *(Include area code)*
					937-785-3636 x4530 mark.reeder@afit.edu

Standard Form 298 (Rev. 8-98)
Prescribed by ANSI Std. Z39-18

Form Approved
OMB No. 074-0188